CONTACT ANGLE MEASUREMENTS ON FINE COAL PARTICLES

BY

YING BIN HE

B.A.Sc., Heilongjiang Institute of
Mining & Tech., P.R.C, 1982

A THESIS SUBMITTED IN PARTIAL FULFILLMENT OF

THE REQUIREMENTS FOR THE DEGREE OF

MASTER OF APPLIED SCIENCE

in

THE FACULTY OF GRADUATE STUDIES

(Department of Mining and Mineral Process Engineering)

We accept this thesis as conforming

to the required standard

THE UNIVERSITY OF BRITISH COLUMBIA

August 1989

In presenting this thesis in partial fulfilment of the requirements for an advanced degree at the University of British Columbia, I agree that the Library shall make it freely available for reference and study. I further agree that permission for extensive copying of this thesis for scholarly purposes may be granted by the head of my department or by his or her representatives. It is understood that copying or publication of this thesis for financial gain shall not be allowed without my written permission.

Department of Mining and Mineral Process Engineering

The University of British Columbia
Vancouver, Canada

Date Oct. 13, 1989

ABSTRACT

This study investigates the techniques of contact angle measurement on fine coal particles. Two techniques, one direct and one indirect, have been investigated and modified.

In the direct contact angle measurement technique, high pressure is employed to compress the coal powder into a pellet and the artificial surface of the pellet is employed in the contact angle measurements. The contact angle versus time and versus drop size on the pellet surface are examined. In addition, the pellet properties and factors affecting the pellet properties are also studied. A pellet surface model and a method for contact angle correction are proposed.

In the indirect measurement, the contact angle is calculated from the penetration rate. The method is modified to employ high pressures to produce highly compact columns. The holding glass tube traditionally used for the column of powder is, therefore, no longer needed. The change in penetration behaviour of the liquid within such columns is investigated. The properties of the columns and the impact of the pressure applied in their formation on the rate of liquid penetration as well as other phenomena are studied. A contact angle calculation procedure is also proposed.

TABLE OF CONTENTS

LIST OF TABLES

LIST OF FIGURES

ACKNOWLEDGEMENT

The author wishes to express his deepest gratitude to Dr. Janusz S. Laskowski under whose kind direction and guidance this work was undertaken.

The technical assistance provided by Mrs. S. Finora, and Mr. F. Schmidiger is gratefully acknowledged.

The author also wishes to express his gratitude to Professor A.L Mular for his valuable teaching in some very interesting and useful courses, and to all the fellow students in Dept. of Mining and Mineral Process Engineering (UBC), especially to Mrs. Maria Holuzko for many valuable discussions; to Mr. K. Lund and Mr. B. Klein for proof reading this thesis.

My special thanks are given to my wife, Ying Wang, for encouraging me with understanding, care, and enduring love, and for sharing in the happiness and hardships of the past years.

CHAPTER 1

INTRODUCTION

The hydrophilic-hydrophobic characteristic of a solid plays a predominant role in diverse technological processes such as froth flotation, lithographic printing, detergency, textile manufacturing, cell adhesion and the thrombo-resistance of bio-materials, etc. One of the most common methods for determining the hydrophobicity of a solid surface has been through the contact angle measurements.

Some materials on which the contact angles are to be measured, are not available in sizes large enough to be polished to accommodate the sessile drops. In the case of coal, additional problems arise because coal is a mixture of the degradation products of plants and of mineral matter. Wide variations in their genesis, composition, and hydrophobicity make coal highly heterogeneous.

In order to accomplish meaningful contact angle measurements, two techniques have been studied. One is the Compressed Pellet Method - a direct contact angle

measurement technique; another is the Rate of Penetration Method - an indirect technique. In both cases, a very fine original sample was utilized.

For direct contact angle measurement (compressed pellet method), it is desirable to obtain a flat surface which should be macroscopically homogeneous as compared with the dimension of the sessile drop and representative of the entire coal sample tested. The coal powder was compressed under high pressure into pellets of 25.4 mm diameter (one inch) and 5 to 8 mm height. The contact angles were directly measured on the pellet upper surface. The feasibility of this technique and a variety of factors influencing the contact angle measurement on pellet surface were investigated.

The measured contact angles were considered the apparent ones. A pellet surface model and contact angle correction method were tentatively proposed to convert the measured contact angle values to the true contact angle values.

This technique has the advantage of being quick and direct. However, when the contact angle values are very small, the liquid from the sessile drop starts to penetrate into the pellet and equilibrium can not be established.

Contact angles have also been measured indirectly from the rate of penetration The technique was modified in this work by making the columns using a machine-controlled high pressure press. This made possible to overcome problems in the traditional method resulting from the poor reproducibility in column physical properties, data scattering etc.. The effects of column-making pressure on the liquid penetration rate and column properties were studied. A new calibration method was proposed.

Since in the direct method only those particles which form the pellet surface participate in the measurement, while all particles in the column have an effect on the penetration rate, the latter technique is statistically more reliable. Its accuracy and reproducibility are higher than the direct method.

CHAPTER 2

LITERATURE REVIEW

The wettability of a solid surface is very important in many technological processes. The contact angle of liquid on the solid surface is the most commonly used parameter in the wettability study process. The contact angles are usually measured on flat surfaces, and less frequently on particulate solids <Good, 1979>.

The surface characterization and contact angle measurement on finely divided particulate solid surfaces has become more and more important and has developed into a new field for study. A variety of techniques have emerged in the last twenty years. Some relevant basic theories and recently developed modifications will be briefly reviewed in the following sections.

2.1 GENERAL CONCEPTS

2.1.1 Contact Angle On An Ideal Surface

The contact angle is, intrinsically, a macroscopic property and a useful measure of solid wettability. On an idealized smooth, homogeneous, nondeformable surface, the free liquid drop takes the shape which minimizes the free energy of the system. The equilibrium contact angle formed by liquid on the idealized surface is a unique quantity <Neumann and Good, 1972>.

The contact angle was first linked to surface energy by Thomas Young <1855>. It was demonstrated by Gibbs, <1928> that minimizing the free energy requires the minimization of the sum

$$\gamma_{lv}A_{lv} + \gamma_{sv}A_{sv} + \gamma_{sl}A_{sl} \qquad 2.1.1$$

where γ is a surface or interfacial tension, A is an area, and the subscripts lv, sv, and sl refer to liquid/vapour, solid/ vapour and solid/liquid interfaces, respectively. The minimization yields the following equation

$$\gamma_{lg}\cos\theta = \gamma_{sg} - \gamma_{sl} \qquad 2.1.2$$

where θ is the contact angle. This equation is known as Young's equation. Figure 2.1.1 illustrates the classical three-phase line of contact between water, vapour, and a smooth nondeformable solid surface. The angle which a drop assumes on the solid surface is the result of a balance between the forces at air/liquid γ_{lg}, liquid/solid γ_{sl}, and air/solid γ_{sl} interface as shown in the above equation and Figure 2.1.1.

2.1.2 Contact Angle Hysteresis

For a real liquid/solid system, a number of stable contact angles can be assumed, in apparent contradiction to the Young equation. Two relatively reproducible angles are the largest and the smallest. These are called the advancing angle, θ_a, and the receding angle, θ_r, respectively. Their names are derived from the fact that the advancing angle is measured when the periphery of a drop advances over a surface, and the receding angle is measured by pulling it back. The difference $\theta_a - \theta_e$ is termed the contact angle hysteresis.

Two major factors which are attributed to the hysteresis are surface heterogeneity and roughness. Detailed review of both will follow in the next two sections.

The symbols θ_e and θ_y stand for the equilibrium contact angle, and Young contact angle, respectively. θ_y obeys Young's equation on a smooth, homogeneous surface of specific composition and structure, while θ_e may exist on heterogeneous or rough surfaces and it may not conform to Young's equation. Commonly, θ_e is obtained from experiment.

2.1.3 Heterogeneity And The Cassie Equation

One of the major causes of hysteresis is the heterogeneous nature of solid surfaces <Johnson and Dettre, 1964>. The surface consists of varying chemical compositions. They may be present as a distinct phase or as an adsorbed film which can not be identifiable as a phase.

Figure 2.1.2. shows two regions of a solid surface mosaic. The local contact angle will depend on the surface energy of the region with which the liquid is in contact. The islands in Fig.2.1.2(a) represent high-contact-angle regions on the surface. As a drop periphery advances over such a surface, the edge of the liquid tends to stop at the boundaries of the islands. It was suggested <Pease, 1945> that advancing angles should be associated with the intrinsic angle of the high-contact-angle regions of surfaces. Similarly, receding angles should be associated

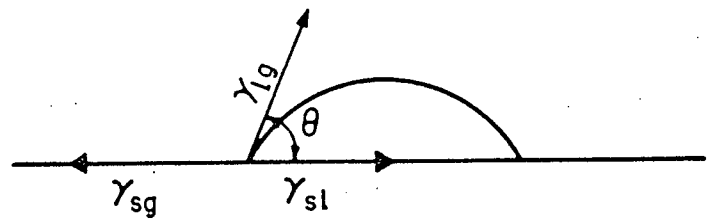

Figure 2.1.1 Equilibrium contact angle formed by water vapour(gas), and solid phases.

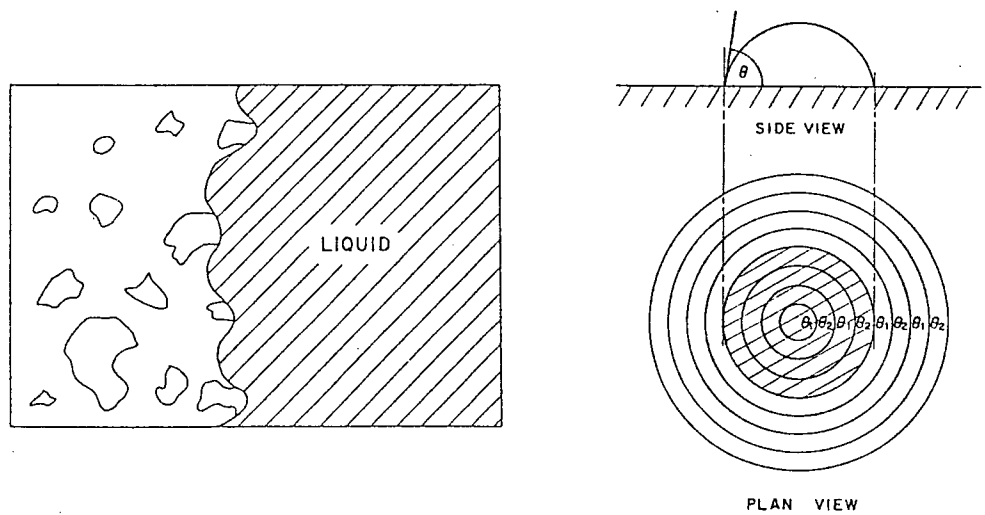

(a) A general model; (b) An idealized model

Figure 2.1.2 Models of heterogeneous surfaces

with the low-contact-angle areas.

Cassie <Cassie, 1948> suggested that the equilibrium contact angle of a smooth micro-heterogeneous surface consisting of a "patchwork" arrangement of two homogeneous elements could be described by

$$\cos\theta = \sigma_1 \cdot \cos\theta_1 + \sigma_2 \cdot \cos\theta_2 \qquad 2.1.4$$

where σ_1 is the fraction of the surface characterized by contact angle θ_1, and σ_2 is the fraction having angle θ_2

$$\sigma_1 + \sigma_2 = 1 \qquad 2.1.5$$

When the number of elements is more than two, this equation can be generalized as

$$\cos\theta = \Sigma\ \sigma_i \cdot \cos\theta_i \qquad 2.1.6$$

Embodied in this equation is the assumption that the two components occur as discrete, uniformly distributed patches at the surface which are small compared to the area of the drop or bubble used to measure the contact angle. The Cassie equation has been confirmed experimentally and used in various situations <Cassie and Baxter, 1944; Oliver et al., 1977; Lamb and Furlong, 1977; and Blake and Ralston, 1985>. Johnson and Dettre <1964> analyzed an idealized model

consisting of concentric circular regions of alternating intrinsic contact angle θ_1 and θ_2 as shown in Figure 2.1.2 (b).

The results reveal that as the vibrational state of the liquid becomes greater, or as the sizes of the heterogeneities on the surface become smaller, the contact angles tend to be closer to that predicted by Cassie's equation. The random heterogeneity of a real surface permits more meta-stable configuration and smaller energy barriers. The wettability behaviour of a real surface should still be quantitatively similar to that of the concentric circular model. This has been experimentally verified <Dettre and Johnson 1964; Crawford and Koopal, 1987>.

For the composite surface with pores as in the case of pellet, the region of pores can be considered as a composite consisting of air, and the Cassie equation can still be applied.

2.1.4 Roughness And The Wenzel Equation

The contact angles of a liquid with the solid are directly dependent on the macroscopic geometry of the solid. Wenzel<1936> developed a relation between the macroscopic roughness of a solid surface and the contact angle:

$$\cos\theta' = r \cdot \cos\theta \qquad 2.1.7$$

where θ' is the measured or apparent contact angle, θ is the true contact angle, and r is the surface roughness coefficient. The simplest parameter for describing roughness is the roughness ratio

$$r = A/a \qquad 2.1.8$$

where A is the true surface area and a is the apparent or envelope area on a plane parallel to the apparent surface.

Certain idealized configuration have been studied by Johnson and Dettre <1964>, and Eick et al.<1975>. The model chosen by Johnson and Dettre (Figure 2.1.3) consisted of a drop of liquid on a surface of concentric grooves which were large with respect to molecular dimensions, but small compared with macroscopic laboratory apparatus. The analysis of this idealized surface showed that roughness leads to a large number of meta-stable configurations. Each meta-stable state was separated from an adjacent state by an energy barrier. The heights of the energy barriers were approximately directly proportional to the height of the asperities and independent of their separation.

There are, however, significant differences between

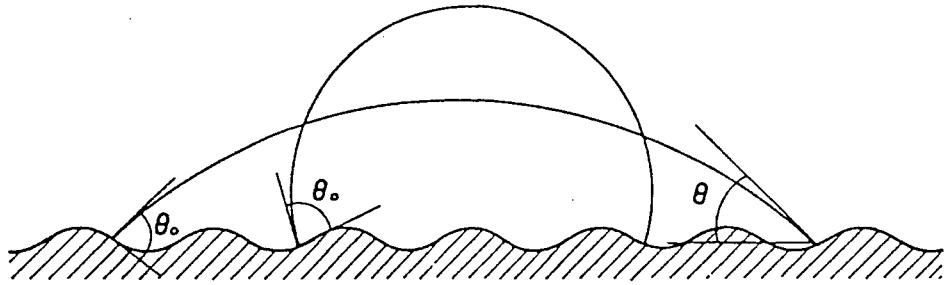

Figure 2.1.3 A model of idealized rough surface (Johnson and Dettre<1964>)

the idealized model of rough surface and real surfaces. From a thermodynamic standpoint, going from a circular groove model to a random hill-and-valley model introduces more meta-stable states and lowers the energy barriers between them. Huh and Mason<1977> modified Wenzel's original roughness equation to account for the case of random surface roughness by introducing a surface textile factor Ψ

$$\cos\theta' = (r + (r-1)\Psi)\cdot\cos\theta \qquad 2.1.9$$

Concentric grooves and radial grooves would present two possible textures for which r could be the same but the influence on θ be quite different. For a roughness in which the height follows a Gaussian distribution, it was found that when the drop size is large compared to the roughness, $\Psi \to 0$.

Objections have been raised from time to time concerning Wenzel's equation. Because the angle depends on the geometry in the immediate vicinity of the periphery of the drop, Wenzel's description is not useful if the surface is non-uniformly rough.

One of the most recent criticisms was raised by Bracke et al.<1988>. They demonstrated by means of the calculus of variations that even on rough surfaces the Young equation still applies. They, however, claimed that the Wenzel equation relies on a false assumption. Contact angle hysteresis, i.e. the difference in the apparent advancing and receding angles, for homogeneous rough solid substrate is due to the local slope of the solid at the three phase of contact-line. The thermodynamic Young angle is the arithmetic mean between these advancing and receding angle values.

2.1.5 Composite Configuration And The Cassie-Baxter Equation

Liquids with high intrinsic angles may not be able to penetrate into cracks and crevices of very rough or porous surfaces. These incompletely penetrated surfaces are called composite. An idealized composite is shown in Figure 2.1.4.

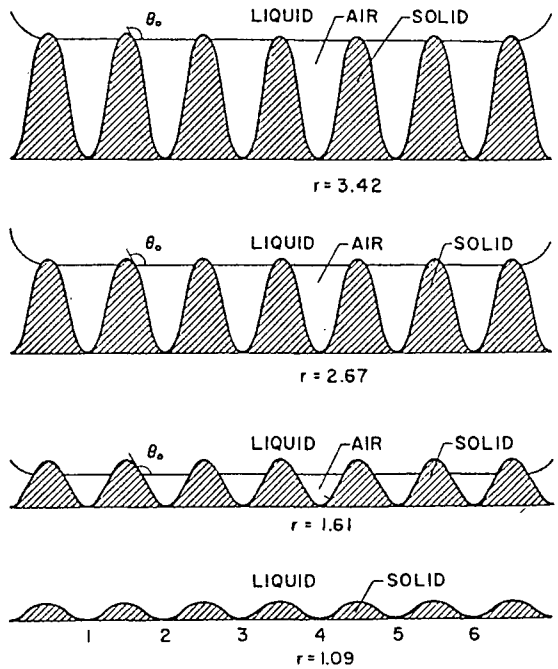

Figure 2.1.4 An illustration of composite configuration (Johnson and Dettre)

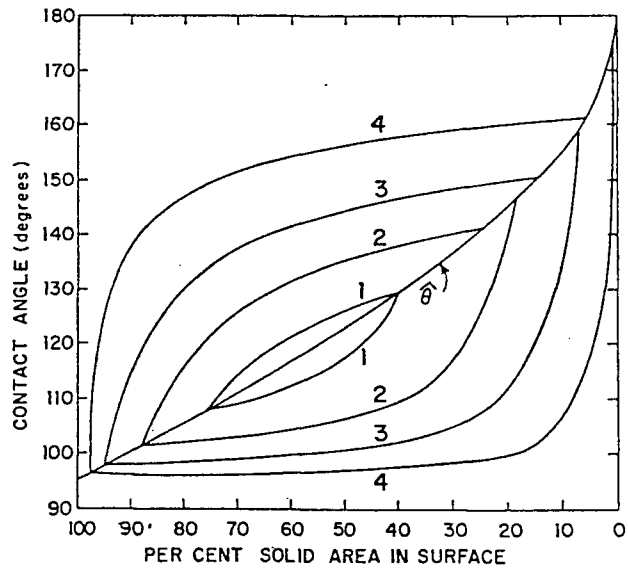

Figure 2.1.5 Contact angle hysteresis on a model porous surface (Cassie and Baxter)

Cassie and Baxter<1944> have derived an equation for composite interfaces

$$\cos\theta = \sigma_1 \cdot \cos\theta_0 - \sigma_2 \qquad 2.1.10$$

where $\sigma_1 = A_{s1}/A$, $\sigma_2 = A_{1g}/A$, A is apparent surface area, A_{s1} is contact area of liquid with solid, and A_{1g} is the free liquid-air interface under the drop.

A composite interface is obviously a particular example of a heterogeneous surface. By assuming that region 2 consists of air (θ=180°), the Cassie equation (2.1.4) reduces to equation 2.1.10. Particularly, this equation reduces to Wenzel equation when σ_2=0.

A family of contact angle curves is shown in Figure 2.1.5 for the model porous surfaces. It shows how contact angle and contact angle hysteresis vary with the percentage of the solid area in surface. The centre line is calculated from Cassie's equation. The curves above Cassie's curve represent possible advancing angles and those below represent corresponding receding angles on surfaces of different roughness with less rough surface being close to the centre line. The receding angle depends strongly on the wettability of the solid portion of a surface and is insensitive to surface porosity.

2.2 CONTACT ANGLE MEASUREMENTS

Some major techniques that have been used for the measurement of contact angles are reviewed. In general, the techniques of contact angle measurements can be divided into two major categories; the direct contact angle measurement from which the angle value is directly obtained, and the indirect contact angle measurements from which the value of contact angle is calculated.

2.2.1 Direct Contact Angle Measurements

2.2.1.1 Sessile Drop and Air Bubble

Of all the methods which were developed, the sessile and pendent drop method, and the adhesion air bubble method are the most general experimental techniques<Neumann and Good, 1979>. The method of measuring contact angles involving direct measurement on the profile of a sessile liquid drop or, alternatively, of the adhering air bubble, is the most commonly employed technique.

The contact angle is determined by directly constructing a tangent to the profile at the point of

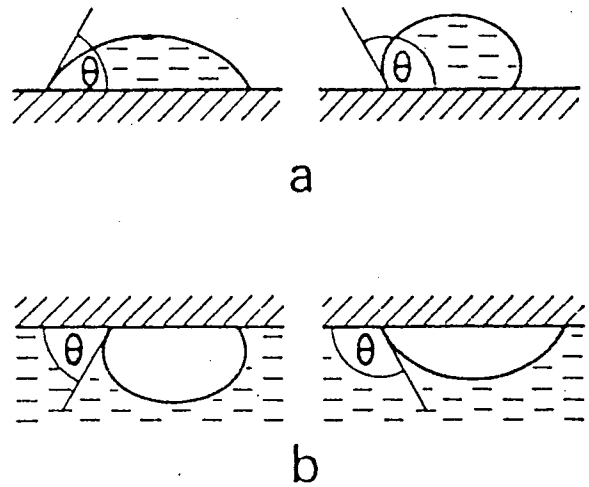

Figure 2.2.1 Constructing a tangent to the profile
a. sessile drop method; b. adhering air bubble method

contact of the three phases (Figure 2.2.1). The angle can be measured directly by using a telescope fitted with a goniometer eyepiece, or on a projected image or photograph of the drop profile. An accuracy of ±2° for these methods is generally claimed.

2.2.1.2 Tilted Plate Method

The tilted plate method was devised by Adams and Jessop <1925>. The principle of the method is illustrated in Figure 2.2.2. A solid plate is partially immersed in the liquid which will form a concaved or convex meniscus near the plate. The plate is tilted until the curved meniscus disappears. The most important advantage of the tilted plate method is the simplicity of the apparatus.

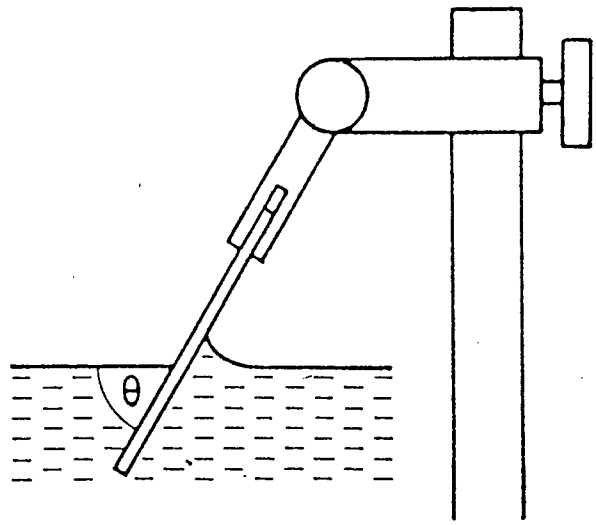

Figure 2.2.2 Tilted plate method for contact angle measurement

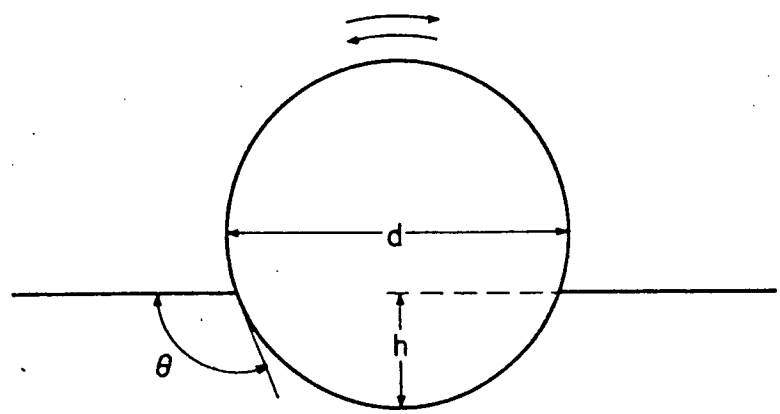

Figure 2.2.3 Cylindrical rod method for contact angle measurement

2.2.1.3 Cylindrical Rod Method

As a modification of the tilted plate method, cylindrical rod method encloses, in a glass cell, a cylinder which can be rotated. The level of the liquid around a partially immersed horizontal cylinder can be adjusted until it touches the cylinder without any curvature. Figure 2.2.3 shows a cross section of the cylinder immersed in liquid. The contact angle is calculated from the equation

$$\cos\theta = 2h/d - 1 \qquad 2.2.1$$

where d is the diameter of the cylinder and h is the height of the liquid surface above the bottom of the cylinder.

2.2.1.4 Compressed pellet method

The surface of compressed pellet is usually macroscopically glossy and smooth, especially when the particle size of powder is fine or the pellet-making pressure is high. It was demonstrated thermodynamically <Shuttleworth and Bailey, 1948> that the contact angle on a porous surface will be higher than on a smooth surface even if the composition is the same. This can be explaned by Cassie-Baxter equation 2.1.10.

It was concluded <Neumann and Good, 1979> that contact angles measured on compressed pellets, although they may reach a limiting value (i.e., they do not change further if the compressing pressure is increased above certain value), are determined by microscopic roughness and porosity.

An attempt was made by Kossen and Heertjes <1965> to modify the preparation of the compressed pellet to allow contact angle measurement in cases where liquid penetrates the compressed powder. It was observed that presoaking the pellet with the measuring liquid could produce solid surfaces on which drops placed to measure the contact angles are quite stable.

The contact angles on solids were calculated by Kossen and Heertjes <1965> from the observed angle using Cassie's method, which relates the contact angle measurement on a heterogeneous solid surface to the intrinsic contact angles. The implicit assumption was that the exposed surfaces of particles were (a) perfectly flat and (b) oriented parallel to the overall surface of the compacted pellet. Doubt has been raised by Neumann and Good (1979) concerning the validity of this assumption.

2.2.2 Indirect Contact Angle Measurements

2.2.2.1 The Wilhelmy Method

As shown in Figure 2.2.4, if a smooth, vertical plate is brought into contact with a liquid, the liquid will exert a downward force on the plate

$$f = P \cdot \gamma_{lv} \cdot \cos\theta - V \cdot \Delta\rho \cdot g \qquad 2.2.2$$

where P is the perimeter of the plate, V is the volume displaced, $\Delta\rho$ is the difference in density between the two fluids (air and the liquid).

To calculate θ, the plate is slowly lowered into the liquid and f is plotted against time. Prior to the establishment of contact between the plate and the liquid, the recorder indicate constant weight (line AB). Immediately after contact, the recorder jumps from B to C due to the capillary rise of the liquid at the plate (see Figure 2.2.4.b). As the immersion continues, the weight on the balance decreases again (line CD). If the average contact angle along the line of contact does not remain constant during the immersion, the chart line will not be straight but contorted around line CD. From the length of the line BC, the force in equation above is obtained

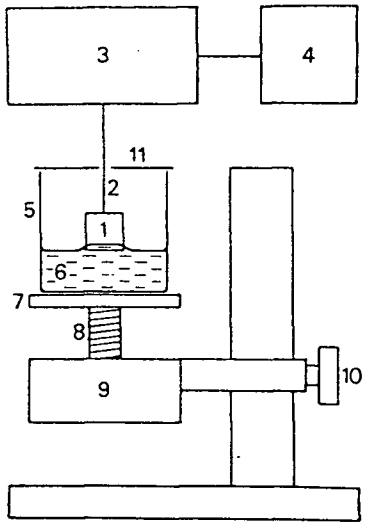

(a) Device for Wilhelmy technique

1.measuring device, 2.glass fibre or rod, 3.electrobalance, 4.recorder, 5.measuring cell, 6.liquid, 7.movable platform, 8.screw or gear mechanism to raise or lower the platform, 9.motor, 10.clamp and support, 11.lid.

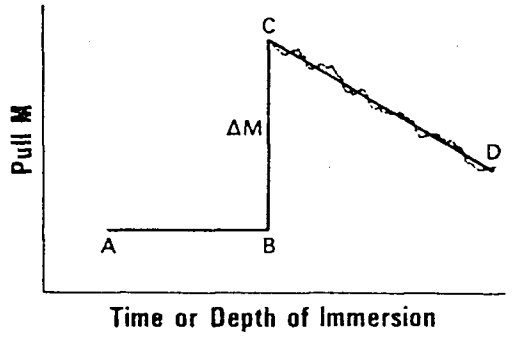

(b) Weight of the plate as a method function of the depth of immersion

Figure 2.2.4 Wilhelmy method

$$f = \Delta M \cdot g \qquad 2.2.3$$

where ΔM is in grams.

In this method, the measurement of a contact angle is reduced to the measurement of a weight, which can be performed with much higher accuracy than the direct reading of an angle with a goniometer.

The disadvantages of this method are that the perimeter of the plate must be strictly constant, and each part of the plate must have the same composition and morphology. In measurements that extend over appreciable time intervals, swelling or dissolution of the solid may become a problem.

2.2.2.2 The Capillary Rise at a Vertical Plate

As a variant of Wilhelmy method, the capillary rise at a vertical plate method only needs the capillary rise h at the vertical surface to be measured (Figure 2.2.5). For infinitely wide plate, an integration of the Laplace equation yields

$$\sin\theta = 1 - \Delta\rho gh / 2\gamma_{lv} \qquad 2.2.4$$

where $\Delta\rho$ is density difference between the two fluids. For practical purposes, plates that are about 2 cm wide satisfy the theoretical requirement of "infinite" width. If g, $\Delta\rho$, and γ_{lv} are known, the task of determining a contact angle is reduced to measuring the capillary rise, which may be determined optically with a cathetometer. This technique has been broadly used and found particularly effective for measuring contact angles as a function of rate of advance and retreat.

2.2.2.3 Interference Microscopy

The principle of this method is illustrated in Figure 2.2.6. Destructive interference (dark fringes) will occur when the optical path difference between adjacent interfering beams is given by

$$t = \lambda/2\mu \qquad 2.2.5$$

where μ is the refractive index of the liquid and λ the wavelength. From the geometry in Figure 2.2.6, we have

$$\theta = \arctan(t/x) \qquad 2.2.6$$

where x is the distance between dark fringes. Combining

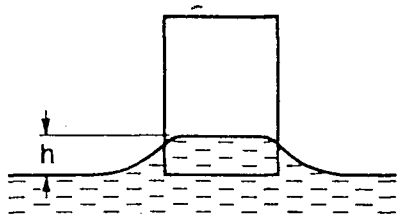

Figure 2.2.5 Capillary rise at vertical plate

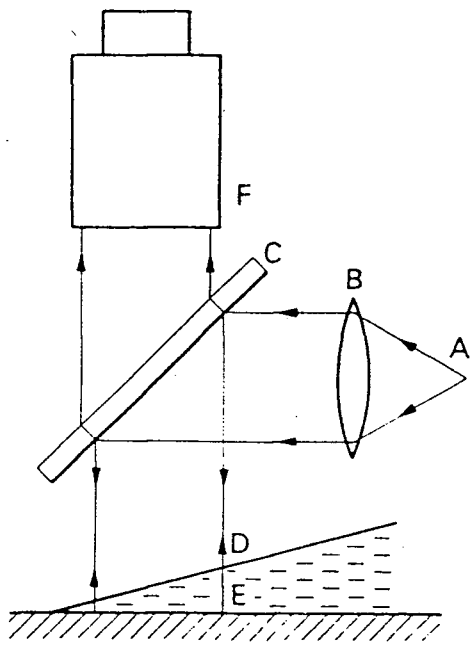

Figure 2.2.6 Interference Microscope Method

A.light source, B.lens, C.half-silvered glass mirror,
D.liquid-vapour interface, E.substrate-liquid interface,
F.microscope.

above two equations yields

$$\theta = \arctan(\lambda/2\mu x) \qquad 2.2.7$$

This method can only be used for small contact angle measurements. It uses a very small amount of liquid.

2.2.2.4 Capillary Rise Method

Given the height of liquid rise (or depression) in a capillary tube, the contact angle can be calculated from the equation

$$\cos\theta = hr\rho g/2\gamma_{lv} \qquad 2.2.8$$

where h is the liquid height, r is the capillary radius, ρ is liquid density. Advancing or receding angles are obtained after lowering or raising the liquid level in the tube.

The method requires that the solid be available as a transparent capillary tube, or as a coating within a capillary. It is restricted to small tubes which are so narrow that the meniscus may be considered to be spherical. For wide tubes, in which the meniscus is not spherical, a correction must be applied to account for deviation from sphericity.

2.2.2.5 Rate of Penetration

In the method, the liquid is allowed to rise unopposed through a column of powder in a glass tube <Crowl and Wooldridge, 1967; Bruil and van Aarsten, 1974>. Statistically, the rate of penetration method is more accurate than direct contact angle measurement. The theory of this technique was developed by a generalization of the law that governs penetration into capillaries given by Washburn equation

$$h^2 = \frac{K \cdot \gamma \cdot t \cdot \cos\theta}{2\mu} \qquad 2.2.9$$

where γ is the surface tension of liquid, μ is the liquid viscosity, and K is a constant for a given packing of podwer and it can be called tortuosity constant. Detailed discusion on this equation is given in Section 7.2.1.

The experimental procedure commonly adopted <Studebaker and Snow, 1955; Crowl and Wooldridge, 1967; Bruil and van Aarsten, 1974> is as follows; a known weight of the dried powder is placed in a glass tube of about 0.8 cm i.d. with an attached scale, and consolidated by manual tapping. The lower end of the tube is closed with a glass or

paper filter supported by a small plug of cotton wool. The column is placed vertically in the wetting liquid and the time at which wetting started is recorded. By means of a lamp the position of the liquid level is periodically recorded.

Statistically, the rate of penetration method is more accurate than direct contact angle measurement. The rate of penetration is obtained from a flow of liquid through capillaries surrounded by a large number of particles, while the contact angle measurement is carried out for one spot (usually the angle is measured on various places on the specimen, and the average value is calculated).

The problem associated with present experimental technique, as claimed by Good and Lin <1976>, is that the data measured generally exhibit a large statistical scatter.

2.3 OTHER TECHNIQUES

In addition to the direct and indirect contact angle measurements, there are many other techniques developed to characterize the wettability of particulate solid surfaces. They all use other parameters than contact angle as the indicators and usually reflect some aspects of solid surface properties.

2.3.1 Hydrophilicity Index

Solid surface properties are governed by their surface compositions. The surface of a coal particle can be considered consisting of, at molecular and macro-size levels, three main kinds of components: i) naturally hydrophobic un-oxidized patches (HO), ii) oxygen bearing, hydrophilic coal patches (HL), and iii) mineral matter. If the mineral matter is neglected, the wettability of pure coal surface is controlled by the relative abundances of various functional groups on its surface. In respect to these properties, the concept of hydrophilicity index has been formulated by Ye et al.<1987> using FTIR spectroscopy <Painter, 1983; Yuh and Wolf, 1983;84; Jin et al., 1987> to analyze the ratio of the surface hydrophilic group content (hydroxyl and carboxyl groups) to the content of surface

hydrophobic groups (aliphatic and aromatic CH groups),

$$\text{Hydrophilicity Index} = \frac{\Sigma\ k_i\ (HL)_i}{\Sigma\ k_j\ (HO)_j} \qquad 2.3.1$$

where $(HL)_i$ is a measure of the hydrophilic functional group i content, and $(HO)_j$ a measure of the hydrophobic functional group j content at coal surface, respectively. k_i and k_j are corresponding coefficients.

Since, aliphatic and aromatic CH groups are the only hydrophobic functional groups and hydroxylic and carboxylic groups are the only hydrophilic groups, the hydrophilicity index can be simplified by substituting the corresponding values of the absorption intensities of the functional groups. It was claimed <Ye et al., 1987> that this index, as determined from FTIR spectra, provides a rather good measure of hydrophobicity / hydrophilicity balance at a coal surface.

2.3.2 Induction Time

Induction time was first introduced by Sven-Nillson in 1934. It is defined as the minimum time required for the disjoining water film between a particle and a bubble to drain to such a thickness that rupture of the water film

takes place. Therefore hydrophobic particles possess shorter induction time; while the induction time for hydrophilic solids would be longer.

The induction time method has been used by many researchers <Eigeles and Volova, 1960; Laskowski and Iskra, 1970; Lekki and Laskowski, 1971; Blake and Kitechener, 1972; Ye et al., 1986; Yordan and Yoon, 1988>. The factors influencing the induction time, such as flotation reagents, pH, temperature, inorganic salts, have been studied by many workers <Laskowski, 1974; Yordan and Yoon, 1986>.

The basic procedure of this technique is that a layer of particles to be tested is formed in a rectangular optical cell. The cell, containing approximately 20 ml of the reagent solution, is then placed on the moving stage of a microscope. An air bubble approximately 2 mm in diameter is formed at the tip of a glass capillary tube using a micro-syringe. By lowering the glass capillary tube, the bubble is kept in touch with the particle layer for a preset contact time period. Then, the capillary tube is returned to the original position separating the air-solid contact.

The bubble is examined through the microscope to see if any particles are picked up by the bubble. If the contact time is too short, no particles attach to the bubble. The experiment is repeated changing the contact time

incrementally. In this way, the minimum contact time, for which at least one particle is actually picked up in five out of ten contacts, was determined. This contact time is taken as the induction time.

Contact angle measurements show whether the adhesion is thermodynamically possible, but cannot describe the dynamic nature of the particle-to-bubble attachment. Induction time can provide kinetic information. Both the thermodynamic and kinetic criteria must be fulfilled for the flotation to be possible.

2.3.3 Heat of Immersion

Heat of immersion is the negative of the heat evolved per square centimetre (or per gram) of powder immersed in a liquid. It has been shown<Good and Girifalco, 1958> that the heat of immersion is related to the contact angle and its temperature derivative

$$\Delta H = \gamma_{lv} \cdot d(\cos\theta)/d(\ln T) - e_{lv} \cdot \cos\theta \qquad 2.3.2$$

where e_{lv} is the total surface energy of the liquid

$$e_{lv} = \gamma_{lv} + d\gamma_{lv}/d(\ln T) \qquad 2.3.3$$

In this method, the calorimeter is first calibrated by passing a known current through a precision resistor for a given time. The sample powder (150-200 mg) is weighed to the nearest tenth milligram and placed in small, cylindrical glass tubes with break-off tips. The tubes were evacuated at a pressure of approximately 1 mPa for 15 min and then sealed under vacuum. The evacuated and sealed sample tubes are placed inside stainless-steel vessels containing about 3 cm^3 of the wetting liquid. The whole assembly is lowered into the micro calorimeter which is maintained at a constant temperature and allowed to attain thermal equilibrium. After steady-state had been established, the break-off tips of each tube is broken by remote mechanical action. The liberated heat is detected and recorded by electronic integration of the detector signal.

Heat of immersion can provide information on hydrophobicity of solid surfaces; the energies of interaction for system in cases of spreading wetting or zero contact angle <Zettlemoyer, 1964>. In addition, it can determine the average polarity of solid surfaces, heterogeneities on solid surfaces, wetting by surfactants, and thermodynamics of the specific interaction of molecules from solution onto solid surfaces <Zettlemoyer, 1965>.

Initially, this method was mainly employed in the area of inorganic minerals<Zettlemoyer, 1964 and 1965;

Cochrane and Hendriksen, 1967; Taylor, 1967> which were basically hydrophilic in nature and to a lesser extent to hydrophobic materials<Cokill et al., 1967>. Application of this method to coal had been studied by Glanville and Wightman<1980>. Heat of immersion was proved to be one of the valuable methods for investigation.

2.3.4 Rate of Immersion

The immersion time measurement was initiated by Walker et al.<1952> to test surface active agents. The procedure consists of dropping coal particles individually, from approximately 1 cm, on the surface of progressively more dilute solutions until a dilution was found at which the particles were not instantaneously wetted.

This procedure has been adopted and modified <Garhsva et al., 1978; Marmur, et al., 1986; Fuerstenau et al. 1986> to testing the wettability of mineral surfaces and employed by many others<Glanville and Wightman, 1980; Laskowski, 1986>.

In one of the modified procedures <Garbsva et al., 1976>, 150 mg of the powdered narrow-sized material is gently placed on the surface of a mixture of solvents with different percentages of water in a number of 16x150 mm

Pyrex test tubes without stirring. The time taken for 3/4 of the material to sink is determined and is plotted against the percentage of water. At certain concentrations of water, immersion time abruptly increases. For a given solid, the change in slope occurs at a constant surface tension (Figure 2.3.1(a)). This value is called the critical surface tension; and it is typical for each solid.

Because of heterogeneity of powder as well as contact angle hysteresis, some researchers <Marmur et al., 1986> tend to use more parameters to characterize solid surface properties. Data has been presented in terms of the highest concentration of alcohol at which all the particles float and the lowest concentration of alcohol at which all the particles sink.

In Figure 2.3.1 (b), the lowest ethanol (methanol) concentration, at which all the particles sink, is termed the "Total Sinking Concentration" (TSC). The highest ethanol (methanol) concentration, at which all the particles float, is termed "Total Float Concentrate" (TFC). It was claimed <Marmur et al.,1986> that this method of characterization of the wettability of particles is more sensitive to the surface energy than contact angle measurements. A small difference in the contact angle and surface energy for various surface can be associated with large differences in the TFC or TSC values.

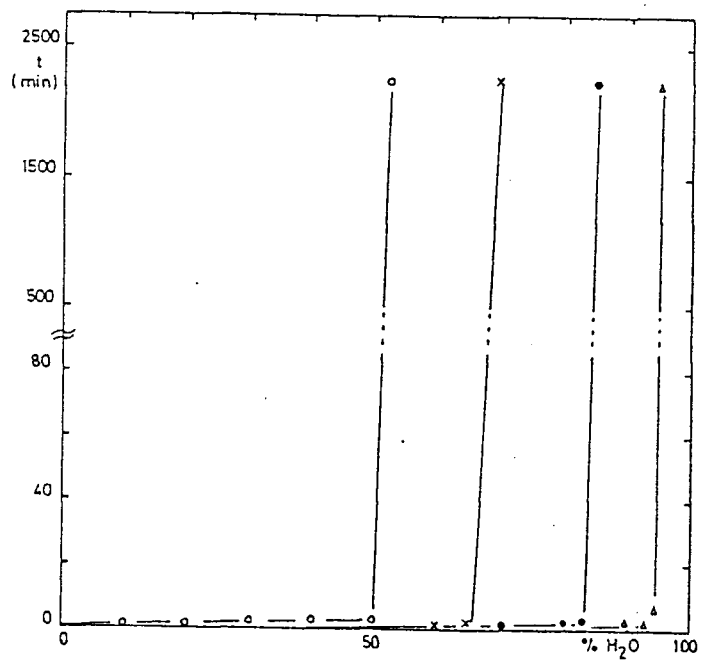

a. Immersion times of methylated quartz powder in different water/alcohol mixtures as a function of concentration of water. o methanol/water; x ethanol/water; ● propanol/water; Δ butanol/water (Garbsva et al.)

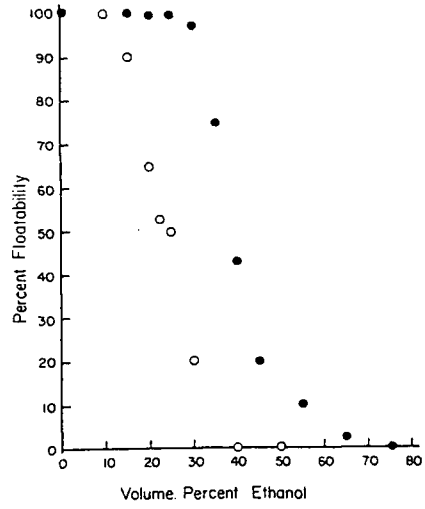

FIG. 2. Floatability of PMMA-coated glass beads on ethanol–water mixtures: (●) 74.1 μm, (○) 127 μm.

b. floatability of the polymethylmethacrylate (PMMA)-coated beads on Ethanol-water mixtures: (●) 74.1 μm, (o) 127 μm. (Marmur et al.)

Figure 2.3.1 Rate of immersion technique

2.3.5 Film Flotation

Another modification of the Walker technique is referred as film flotation (developed by Fuerstenau and Williams <1987>). This method uses a set of three parameters to describe surface properties. A monolayer of tested fine particles (about 0.06 to 0.3 gram in the case of coal) is placed on the surface of a solution in a shallow vessel of 25 mm diameter and 20 or 30 mm depth. The closely sized solid either remains on the liquid surface or is immediately imbibed; and splits into lyophobic and lyophilic (imbibed) fractions. The surface tension of the liquid is varied by the addition of methanol to triply distilled water.

The percentage of particles not imbibed by the liquid is plotted as a function of the surface tension of the liquid in Figure 2.3.2. They approximately conform to the quasi-Gausian distributions. Two of the three parameters describing the wettability and heterogeneity of powder can be obtained from Figure 2.3.3 (a), the surface tension of the solution that wets all particles, γ_c^{min}, and the surface tension of the solution in which none of the particles are wetted, γ_c^{max}; and (b) the mass fraction of the particles plotted against the surface tension of the imbibing solution allows calculation of the third parameter - the standard deviation σ. σ is a measure of the heterogeneity of the

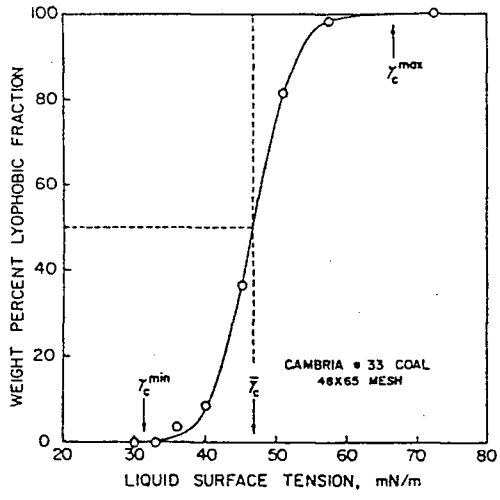

(a)

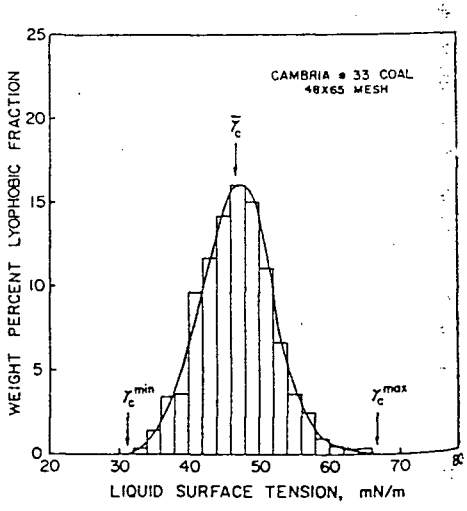

(b)

Figure 2.3.2 Film flotation (Fuerstenau and William)

(a) Accumulative percentage of material floating
(b) Frequency histogram

material.

Three factors: the size distribution, variation in surface energies and contact angle hysteresis can be the reasons for difference between the TSC (total sinking concentration) and the TFC (total float concentration) in Rate of Immersion, or between γ_c^{min} and γ_c^{max} in Film Flotation. Study by Marmur et al. <1986> shows that the effect of size distribution is negligible while variation in surface energy has a major effect.

2.3.6 Critical Surface Tension of Flotation

The concept of Critical Surface Tension, γ_c, developed by Zisman <1964>, is the surface tension of the wetting liquid that would just spread on the substrate to give complete wetting. A convenient way of illustrating the concept is the adhesion tension diagram, $\gamma_{lv}\cos\theta$ versus γ_{lv}, as shown in Figure 2.3.3(a). On such a diagram, the measured contact angles give a straight line, which may be represented by the equation

$$\gamma_{lv}\cos\theta = \beta\cdot\gamma_{lv} + (1-\beta)\gamma_c \qquad 2.3.3$$

Hornsby and Leja<1980, 83, and 84> extended Zisman's concept of critical surface tension to dynamic flotation

conditions <Gaudin, 1957; Tomlinson and Fleming, 1963; Reay and Ratcliff, 1973; Lekki and Laskowski, 1971; Blake and Kitchener, 1972; Laskowski, 1974; Jameson et al., 1977> and distinguished critical surface tension of adhesion, γ_{ca}; critical surface tension of particle-bubble stability, γ_{cs}; and critical surface tension of floatability, γ_{cf}.

The critical surface tension of adhesion, γ_{ca}, is the minimum surface tension of liquid in contact with the tested solid for which the adhesion of air bubble from the liquid onto the solid is possible. Apparently it is determined by solid surface properties, and should be greater than critical surface tension, γ_c. Hydrophobic particles of the same size d but $\gamma'_{ca}<\gamma''_{ca}$, may be separated into fractions in a solution of γ_c if $\gamma'_{ca}<\gamma_c<\gamma''_{ca}$.

However for particles with the same surface properties, γ_{ca}, but with different sizes, smaller particles may be floatable whereas the large size particle are non-floatable. This is due to the kinetic effect of particle size. On this account, the critical surface tension of stability γ_{cs} was introduced. Obviously for particles with same γ_{ca}, the larger the particle size is, the greater the γ_{cs} value will be. Two particles of sizes d'<d" would have the relevant $\theta'_{cs}<\theta''_{cs}$ and $\gamma'_{cs}<\gamma''_{cs}$. As shown in Figure 2.3.3(b), if a solution of γ_c was used and $\gamma'_{cs}<\gamma_{lv}<\gamma''_{cs}$, the smaller-size particles would be floated whereas the

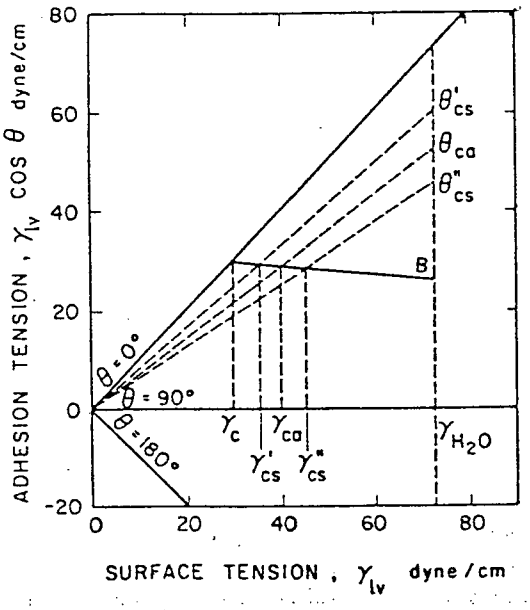

a. Adhesion tension diagram illustrating the concept of critical surface tension of adhesion, γ_{ca}, for a low energy solid with wettability line B in aqueous solutions of a short chain n-alcohol (Hornsby and Leja).

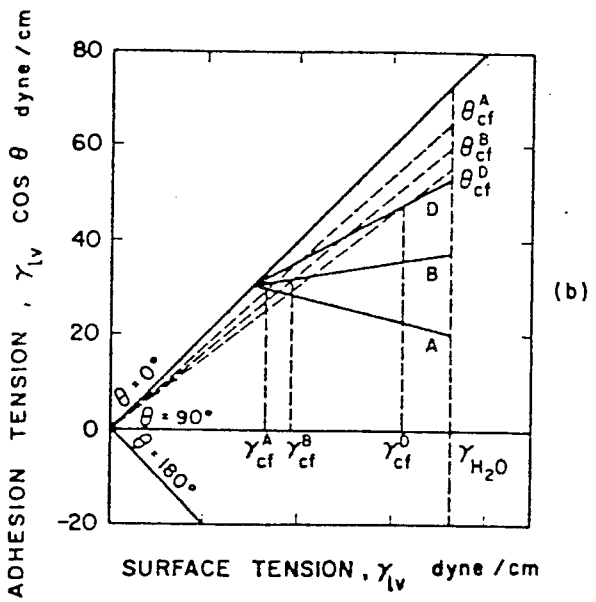

$$\theta^A_{cf} < \theta^B_{cf} < \theta^D_{cf}$$

b. Adhesion tension diagram illustrating possible differences in critical surface tension of floatability for three low energy solids of different wettability in aqueous solutions of a short chain n-alcohol (Hornsby and Leja).

Figure 2.3.3 Critical surface tension of flotation

larger-size particle would be non-floatable. This means that wettability and floatability are not necessarily synonymous under certain circumstances.

All above factors are included in a general term called critical surface tension of floatability γ_{cf}. According to this concept a particle will be floatable if its γ_{cf} is smaller than the liquid-vapour surface tension γ_{lv} (Figure 2.3.3(b))

The concept of critical surface tension of floatability indicates that a significant difference in γ_{cf} values may exist between two inherently hydrophobic solids if the slope of their wettability lines are significantly different, although there may be little or no difference in γ_c value. Such a difference would provide a selective floatability region, where separation of the two solids by flotation should be theoretically possible.

The concept of critical surface tension of flotation has been employed by others <Kelebek and Smith, 1985; Kelebek, 1987> in characterization and flotation of inherently hydrophobic minerals.

2.3.7 Other Techniques

In addition to above mentioned techniques, a variety of other techniques have also been developed. Among them are partition between kerosene and water <Adams-Viola et al., 1981>, salt flotation <Laskowski, 1965 and 1974; Yoon and Sabey, 1989> et al. They will not be discussed here.

CHAPTER 3

COAL

3.1 INTRODUCTION

The materials used in surface wettability studies, such as Teflon and Quartz, are commonly homogeneous. Measures can be taken to acquire a very clean, smooth, and chemically consistent surface for contact angle measurements. Fairly reproducible results can be obtained. Nonetheless, contact angle measurements on coal <Vargha-Butler, et al. 1986> show that this is not true for coal. Coal has a very complex composition and heterogeneous surface. Some of the coal properties are unique and deserve detailed summary.

3.1.1 Classification

Coal is first classified by rank. The coal rank indicates the extent to which coalification process has occurred and is arranged in an ascending order of carbon content as shown in Table 3.1.1. The highest rank coal is graphite, which is the final product of the coalification process; the lowest one is woody material peat, followed by

lignite.

Table 3.1.1 Coals Arranged in an Ascending Order of Carbon Content

	Coal Rank				
	Peat	lignite	Sub bituminous	Bituminous	Anthracite
%C	60	70	75	80	93
%O	35	25	20	15	3
Calorific value MC/kg	28	30	31	32.5	36.5

The properties of the coal within each rank depend, to some extent, on the nature of the various components in the original organic accumulation; specifically they depend on both the forms of vegetation and the degree of degradation prior to burial. The components, called macerals, are analogous to the different mineral constituents found in inorganic sediments. They are organic minerals, characterized by their botanic structure rather than their crystallographic properties. They are optically homogeneous aggregates of organic substances, possessing distinctive physical and chemical properties <Winans and Crelling, 1984>.

Macerals are classified in three groups <Stach, 1982>:

I. Vitrinite,

II. Exinite,

III. Inertinite.

Coal macerals rarely occur by themselves; they are more usually associated with other maceral groups. Such associations are called micro-lithotypes. They are mainly: vitrite, liptite, inertite, clarite, vitrinertite, durite, and trimacerite.

These micro-lithotypes further combine to form the mass of a banded bituminous coal. These combined ingredients are visible to the eye and are known as lithotypes. They are:

I. fusain (charcoal-like fragments - soft lithotype)

II. durain (dull hard coal type - the hardest lithotype)

III. clarain
IV. vitrain > together the equivalent of bright coal type

These four banded ingredients differ in their specific gravity, ash content, chemical composition, hardness, and coking properties as well as in their wetting properties.

3.1.2 Chemical Composition

Change in coal rank is reflected by a steady change in chemical composition and calorific value. Coal is not a mineral of constant composition, but an organo-clastic sedimentary rock composed essentially of lithified plant debris. It has substantially different properties from inorganic minerals. Due to its extraordinarily complex carbon chemistry, these macerals cannot be represented by any uniquely defined chemical structure.

Pure coal is the combustible organic mineral, which is a highly cross-linked polymer, consisting of a number of stable fragments connected by relatively week cross-links <VanKrevelen, 1961>. The remaining components, which have no heating value, are regarded as impurity minerals including shale, kaolin, sulphates, carbonates, and chlorides.

Coal is a polymeric solid, i.e. it consists of many high molecular weight molecules. It contains mainly carbon, hydrogen and oxygen along with small quantities of sulphur and nitrogen. The molecular models proposed are based on ultimate elemental analysis and large amount of other information such as variety of spectroscopic analyses, functional group analysis, molecular weight determinations, statistical constitution analysis etc.. The molecular model

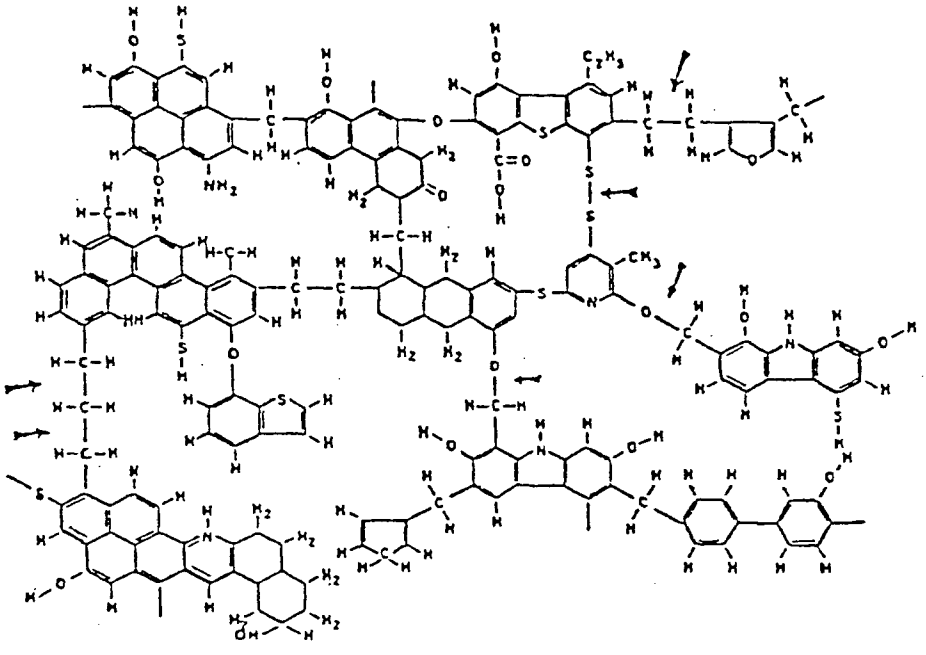

Figure 3.1.1 A molecular model of coal proposed by Wiser (1975)

of Wiser<1975> is given in Figure 3.1.1. The arrows in the model indicate the week points of the structure. This model also includes various functional groups found in coals. Most functional groups contain oxygen and appear as phenolic, hydroxylic, carbonylic, and carboxylic functional groups. The rest of the oxygen is thought to link aromatic nuclei or to be present in a fused polynuclear skeleton.

Mineral matter is an important part of coal composition. It is termed, in its widest sense, as all of the inorganic components found in coal as mineral phases as well as the elements in coal that are considered inorganic <Mraw et al., 1983>. Mineral matter plays an important role in all coal utilization processes.

3.2 HOMOGENIZATION

As stated above, coal is a very heterogeneous organic rock comprised of inorganic minerals and organic macerals. It would be interesting to isolate these individual macerals for coal wettability characterization. However, it is practically impossible to separate them and accumulate enough for characterization. To obtain an accurate picture of the wettability of coal, it has to be separated into less heterogeneous portions. These portions, differing in wettability, need to be characterized separately.

Homogenization of coal is the first step needed for coal surface wettability characterization. Otherwise, studies on such a heterogeneous mixture as a whole may be very misleading.

There are many ways of homogenizing coal. It is the most practicable way to homogenize coal, according to some of its physical or physiochemical properties, such as specific gravity, surface wettability, macro-lithotype, etc., creating fractions which are less heterogeneous.

Since this work is mainly focused on the methodology of the characterization of coal wettability, only the sink-and-float method was employed to prepare fractions for further studies. The coal surface characterization techniques developed in this work can be applied to any coal fractions regardless of the separation method used.

3.3 COALS STUDIED

Coal samples used in this work were from the Line Creek and the Bullmoose (Seam "C") mines.

The Line Creek coal deposit is part of the Upper Elk Coalfield in the East Kootenays, B.C.. It is characterized

as a low sulphur, medium volatile bituminous coal and is a high quality blend coking coal. Some of the characteristic of the Line Creek coal are listed in Table 3.3.1. The proximate analysis of ROM Bullmoose coal is given in Table 3.3.2.

The results of sink-and-float tests for Line Creek and Bullmoose coals are presented in Figures 3.3.1 and 3.3.2, respectively, in which the ash content is plotted against density fraction.

Table 3.3.1 QUALITY CHARACTERISTICS OF LINE CREEK CLEAN COAL

PARAMETER	BASIS	QUANTITY
MOISTURE %	A.D.	
total		6.0 - 8.0
residual		0.4 - 0.6
PROXIMATE %	A.D.	
ash		9.5
volatile		21. - 22.
sulphur		0.3 - 0.4
ULTIMATE %	D.A.F.	
carbon		85.85
hydrogen		4.67
nitrogen		1.10
sulphur		0.37
oxygen		8.01
HARDGROVE GRINDABILITY INDEX		75.0
GROSS CALORIFIC VALUE	KCAL/KG.A.D.	7700

Notes: A.D. stands for Air Dried
D.A.F. stands for Dry Ash Free basis

Table 3.3.2 Proximate Analysis Of ROM Bullmoose Seam "C" Coal Dry Basis

	A.D.	M.A.F.
%Moisture	0.95	
%Volatile	20.37	27.18
%Ash	25.05	
%FIXED C	54.58	72.82

Notes: M.A.F. stands for Moisture and Ash Free basis
A.D. stands for Air Dry basis

SINK-AND-FLOAT TEST OF LINE CREEK COAL

Figure 3.3.1 Ash content versus density fraction

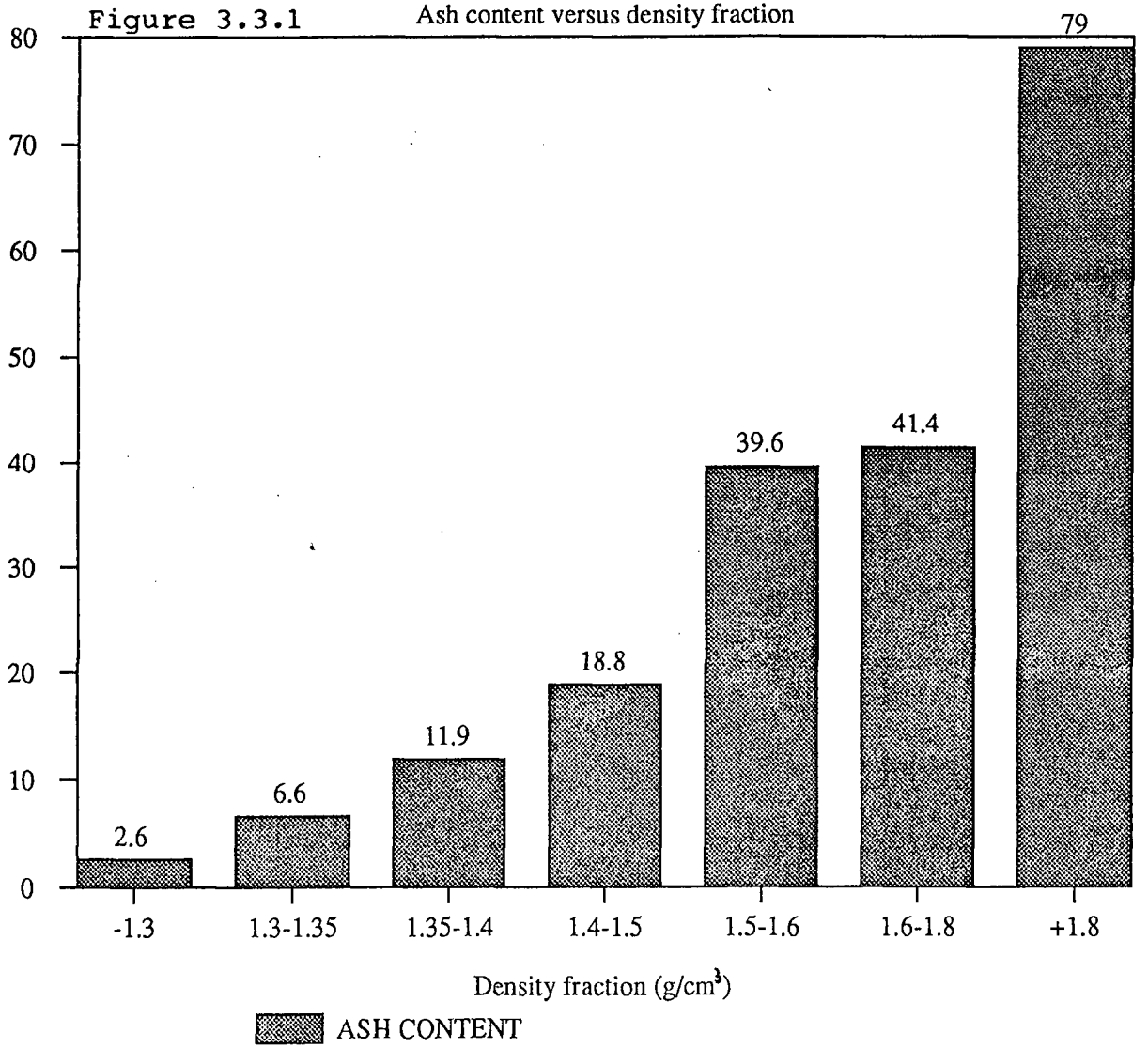

SINK-AND-FLOAT TEST OF BULLMOOSE COAL

Figure 3.3.2 Ash content versus density fraction

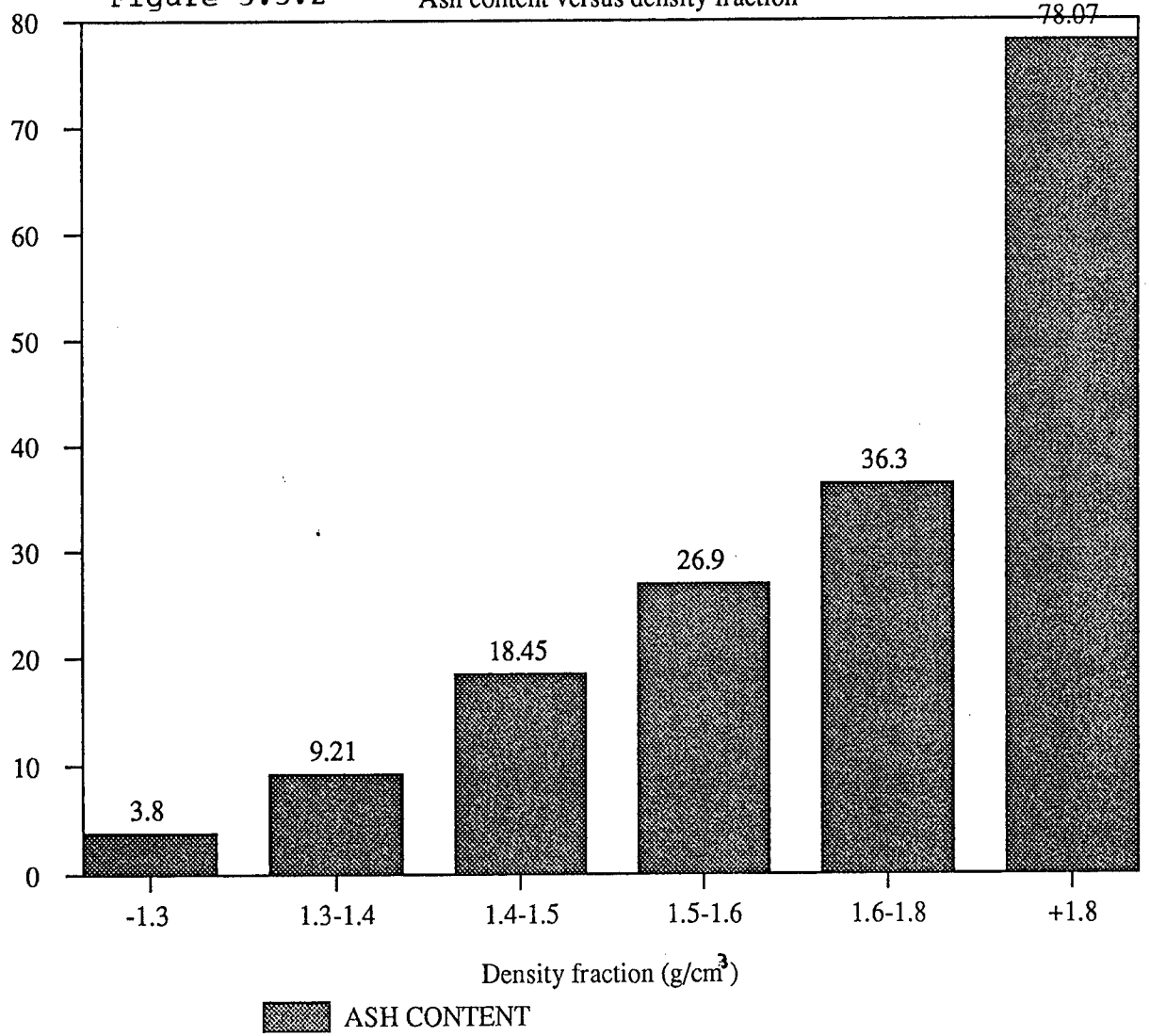

CHAPTER 4

OBJECTIVE

The major objective of the present work is to develope better techniques for contact angle measurements on fine coal particles. Two techniques, one direct and one indirect, have been modified and investigated.

In the direct contact angle measurement technique, the coal powder is compressed under high pressures 20 to 34.5 MPa to form the pellets of 2.54 cm diameter and 0.5-0.8 cm height. The pellet, with its artificial surface, is employed for contact angle measurements. The behaviour of a water drop in contact with the pellet such as the effect of drop size on contact angle, the stability of the sessile drop are examined. In addition, the properties of the pellet and the factors affecting the measurement are also studied. The contact angle measured on the pellet surface is an apparent angle value. A pellet surface model is proposed according to the SEM examination. The apparent contact angle values are corrected using Cassie-Baxter equation to the real angle values.

In the indirect contact angle measurement, the rate

of liquid penetration technique is employed and modified. Pressures ranging from 3.5 to 28 MPa (500 - 4000 psi) are employed to make highly compact columns. The holding glass tube traditionally used for the column of powder is, therefore, no longer needed. The applicability of the Washburn equation to the highly compacted columns for different coal density fractions are studied. The change in penetration behaviour of the liquid within such columns is investigated. The properties of the columns and the impact of the pressure applied in their formation on the rate of liquid penetration as well as other phenomena are also studied.

An assumption is made that for materials having same particle sizes and shapes, their columns, if made at same pressure, possess the same tortuosity constant. Under this assumption, a new calibration method is introduced.

The present work is mainly aimed at methodological development for contact angle measurements on fine coal particles. More work needs to be done to further verify these techniques.

CHAPTER 5

DIRECT CONTACT ANGLE MEASUREMENTS AND EXPERIMENTAL

5.1 INTRODUCTION

Among the direct contact angle measurement methods, the sessile drop technique has many advantages over the adhering air bubble methods. Complications, due to the solubility and swelling, can usually be dealt with more easily with the sessile drop method rather than with the adhering air bubble methods. However, the adhering air bubble method has the advantage of minimizing contamination from airborne substances.

Contact angle measurements are generally performed on coal lumps <Horsley and Smith, 1957, Parekh and Aplan, 1978, Gutierrez-Rodrigues and Aplan, 1984>. Some criteria have been established for the selection of sample specimens for contact angle measurement. The pre-selection of samples (or the area of a coal specimen) likely produces biased results. Although the well-established practice of polishing a coal specimen has the advantage of providing a smooth surface suitable for the measurement, polishing may change the coal surface markedly. Vargha-Butler et al.<1986> have carefully

studied the direct contact angle measurements on polished sections of coal lumps. They indicated that the information obtained from this method is not very reliable because of the heterogeneity.

Coal surfaces are a mosaic with the different elements having varying dimensions. Cracks are often visible on coal surfaces. As indicated by Neumann and Good <1979>, if the dimension of the primary elements is very small relative to the dimension of the sessile drop, the microscopic heterogeneity will not affect the macroscopic contact angle measurements. Therefore, one possible solution to the effect of chemical and mechanical heterogeneity is to crush and grind coal particles to an average diameter of 10 microns. Such a fine powder, though microscopically heterogeneous, may be considered macroscopically homogeneous.

For the surface characterization, it is desirable to work with a flat surface made of a fine powder. Compressing the fine powder under high pressure to form an artificial surface is an obvious solution. The preparation of pellets under high pressure and the determination of the contact angle on the pellet surface are discussed here as well as in the following chapters.

5.2 THEORY AND TECHNIQUES

5.2.1 Background

There are two methods of obtaining the contact angle from the measurement with a sessile drop. One method is to construct a tangent to the drop profile at the three-phase contact line (Figure 2.2.1) and to measure the value of the angle with a goniometer. The another method involves mathematically calculating the contact angle from the profile of the drop <Bashforth and Adams, 1892; Hartland and Hartley, 1976; Malcolm and Paynter, 1981; and Rotenberg et al., 1982>. Depending on the drop size, different equations may be needed.

If a drop size is small enough (10^{-4} ml), so that the drop is indeed a spherical cap, two equations may be employed. One connects the contact angle with the base diameter, D, and height of the drop, h, (Mack, 1936)

$$\frac{2h}{D} = \tan\theta/2 \qquad 5.2.1$$

and the second equation (Johnson and Dettre, 1969) calculates the angle, θ, through the base diameter and the drop volume, v,

$$\frac{D^3}{V} = \frac{24 \sin^3\theta}{\pi(2 - 3\cos\theta + \cos^3\theta)} \qquad 5.2.2$$

The limitations for these two equations are that (1) D and h or v cannot be measured with high accuracy, and (2) the drop must be a spherical cap.

When the drop size is so large that the height of the drop is independent of the drop size, the contact angle can be calculated from:

$$\cos\theta = 1 - \frac{d \cdot g \cdot h^2}{2\gamma} \qquad 5.2.3$$

where h is the limiting height of drop; d the liquid density; g the gravitational acceleration; and γ the liquid surface tension. In order for this equation to apply, the drop must be very large. For water, a drop of one meter in diameter is theoretically required. It is impracticable to produce such a large solid surface to accommodate the liquid drop.

In most cases, the drop volume resides between these two extremities. When the radii of curvature are sufficiently large compared to the thickness of a non-homogeneous film separating two bulk phases, the pressure difference across a curved interface is described by the classical Laplace equation

$$\gamma(1/R_1 + 1/R_2) = \Delta P \qquad 5.2.4$$

where γ is the interfacial tension, R_1 and R_2 represent the two principle radii of curvature, and ΔP is the pressure difference across the interface (see Figure 5.2.1.).

In the absence of external forces, other than gravity, the pressure difference is a linear function of the elevation

$$\Delta P = \Delta P_0 + \Delta\rho \cdot gZ \qquad 5.2.5$$

where ΔP_0 is the pressure difference at a selected datum plane,

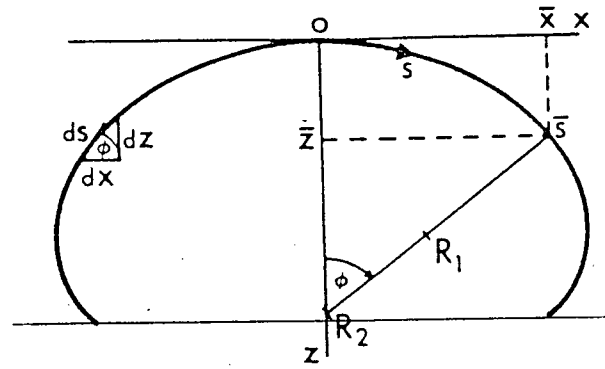

Figure 5.2.1 The definition of the coordinate system for a sessile drop profile

$\Delta\rho$ is the difference in the densities of the two bulk phases, g is the gravitational acceleration and Z is the

vertical height measured from the datum plane.

From the above two equations, Bashforth and Adams <1892> derived the following general equation mathematically describing the sessile drop and sessile bubble interface profile under gravity

$$\gamma(1/R_1 + \sin\Phi/x) = 2\gamma/R_0 + \Delta\rho \cdot \gamma Z \qquad 5.2.6$$

where R_1 turns in the plane of the paper and $R_2=x/\sin\Phi$ rotates in a plane perpendicular to the plane of the paper and about the axis of symmetry; R_0 is the radius of curvature of apex and Φ is the turning angle measured between the tangent to the interface at the point (x,z) and the datum plane.

Many graphical curve fitting techniques have been developed <Malcolm and Paynter, 1981, Rotenberg et al., 1982>. The one developed by Rotenberg, Boruvka, and Neumann employs the strategy to construct an objective function which expresses the error between the observed and the theoretical Laplacian curve, i.e., equation 5.2.6. The objective function is minimized numerically using the method of incremental loading in conjunction with the Newton-Raphson method. Apart from local gravity and densities of liquid and fluid phases, the only input information required to determine the liquid-fluid interfacial tension is the information on the shape of the meniscus and the vertical

coordinate of the three-phase line.

5.2.2 Techniques

The contact angle values were obtained in two ways. They were either directly measured with the use of a goniometer, or the values of the contact angle were calculated from the axisymmetric sessile drop profiles.

5.2.3.1 Direct Measurement

A Ramé-Hart Model 100 contact angle goniometer (see Figure 5.2.2) was utilized in the direct contact angle measurements. It has a stationary telescope. The position of the stage is controlled by graduated micrometer screws, so that the edge of a drop can be moved horizontally and vertically to bring it to the axis of the telescope cross hairs. The micro-syringe for this instrument is mounted so that the needle can be held stationary relative to the stage and moved vertically relative to the stage by a screw. This is a valuable feature for the measurement of advancing and receding contact angles. It is also possible to use the micrometer screws to measure the height and width of a drop. An environmental chamber is provided as an optional attachment used to prevent the liquid evaporation. The

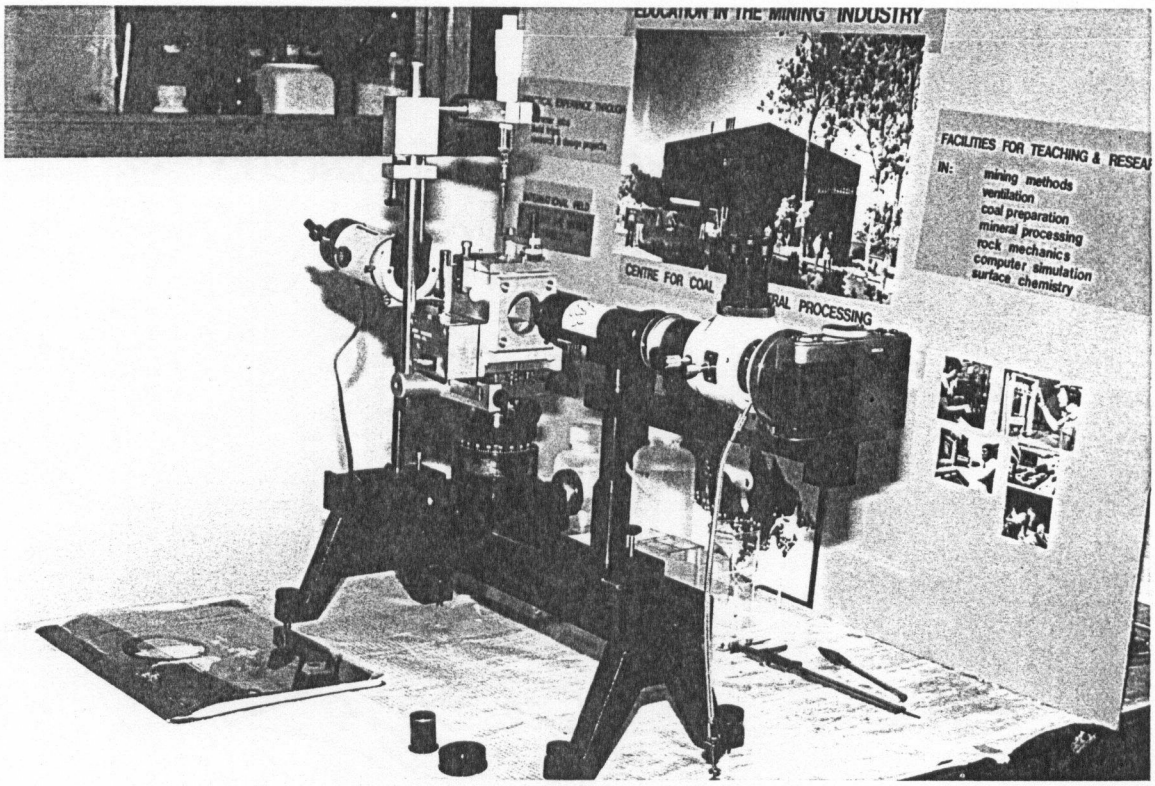

Figure 5.2.2 The set-up of a Rame-Hart model 100 contact angle goniometer

humidity in the chamber was maintained at 100% by filling the sample chamber with distilled water. The temperature was not controlled and varied between 20 and 25 °C. To insure reproducibility, a constant drop size was maintained.

For routine measurements, the pellets were mounted on the horizontal stage in contact with atmosphere. To avoid oxidation, the measurements were made shortly after drop formation. The temperature coefficient of the contact angle is claimed to be small enough so that thermostating is not necessary <Adam, 1964; Neumann and Good, 1979>

To illuminate the drop, a source of light equipped with a filter to minimize heating was fixed behind the drop.

5.2.3.2 Calculation From Axisymmetric Drop Interface

The profile of the sessile drop was photographed through the telescope of the goniometer using a horizontally mounted camera. The pipette of the micro-syringe with known diameter was included in the picture; this served as an accurate scaling reference. The image of the drop profile in the photograph was enlarged approximately 36 times.

The curve fitting technique and corresponding computer program, developed by Rotenberg, Boruvka, and

Neumann (1982) as described in section 5.2.1, was employed. The computer program, already stored in MTS mainframe in UBC, acquires the profile coordinate data on the photograph through a Talos CYBERGRAPH digitizer which was connected to MTS with the Zenith 158 microcomputer acting as a terminal. About 30 to 40 points were generated from each profile for computer processing.

5.3 EXPERIMENTAL AND APPARATUS

5.3.1 Sink-and Float Test

First the coal samples were separated into different density fractions by a sink-and-float procedure. Each fraction was ground to very fine powder in a laboratory rod mill. The size distribution of each ground density fraction sample was characterized using an Elzone size analyzer. The ground samples were sealed in plastic bags and stored in a refrigerator for future use.

In the sink-and-float procedure, aqueous zinc chloride solutions with the following densities: 1.3, 1.35, 1.4, 1.5, 1.6, 1.8 were used. Sinking fractions from each test were transferred to the next liquid of higher density. The floating products were rinsed with fresh water, and air-dried.

5.3.2 Comminution of Coal Samples

The separated coal fractions were pulverized separately using a 195x318 mm laboratory rod mill. The maximum sample size fed to the mill was 300 grams. The mill was used either for one stage grinding or for primary

grinding followed by the secondary grinding which was performed in a mortar grinder.

To study the effect of particle size distribution on the contact angle measurements, the WEKOB mortar grinder was employed to further reduce the size of coal powder. The total volume of ground material in one batch was kept below 150 ml. In the process of mortar grinding, the whole instrument was covered by a plastic bag and purged with nitrogen to prevent oxidation. In addition, the instrument was stopped for a period of five minutes after each two-minute grind to prevent excessive heating.

5.3.3 Particle Size Analysis

Particle size is an important parameter which may affect the pellet porosity and consequently the fractional area of pores on the pellet surface.

The size analysis was conducted using an Electrozone Celloscope (Elzone). In this device, the suspension of fine particles in an electrolyte is drawn through an orifice which also passes an electric current. Each particle, in traversing through the orifice, causes a momentary resistance change proportional to the particle volume. Corresponding to this change, an electrical pulse is

generated. All the electric pulses are processed by a computer to yield particle count and size distribution data.

A dispersing agent (Calgon) and vigorous agitation were required in order to prevent the formation of coal particle aggregation.

The size distribution results are plotted as the relative volume percent against its log size. Three characteristic sizes (in centi-micron) were obtained in this procedure including log mean, mode, and median sizes.

5.3.4 Pellet-Making

The pellet-making is one of the most important steps in the process. The instrument used was MET-A-TEST mounting press as shown in Figure 5.3.1. It has a built-in manual hydraulic gauge and timer with an audible beep at the end of each run. The high pressure was provided by a manual hydraulic pump with a working pressure up to 34.5 MPa (5000 psi). The mould diameter is 25.4 mm (one inch).

After the mold was carefully cleaned by using ethyl alcohol and degreased cotton, 3 grams of coal powder was introduced. The mold was then closed and the pressure was slowly increased by hydraulic pumping. When the pressure

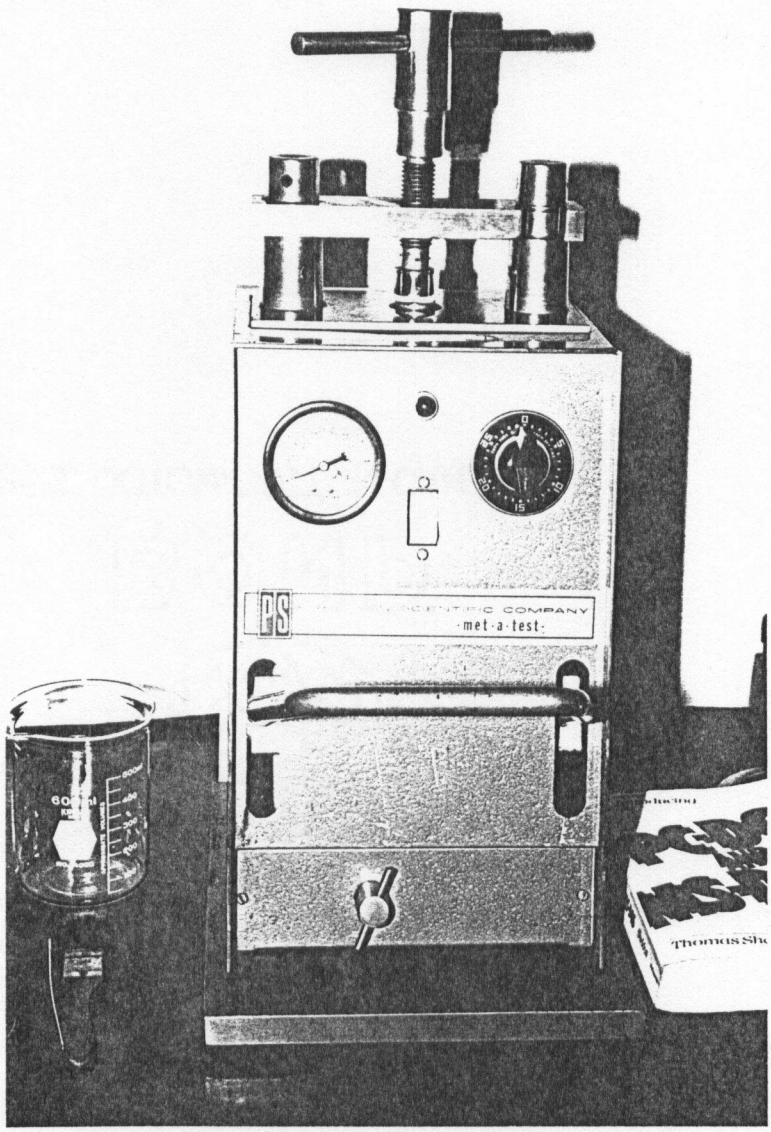

Figure 5.3.1 A MET-A-TEST specimen mounting press

reached a pre-set point, timing was started, which was usually set at 5 minutes. Precautions were taken to control the pressure closely; frequent adjustments were required since the pressure could decline in the pressing process.

The pressure used in making the pellet was varied from 3.45 to 34.5 MPa (500 to 5000 psi) in order to study the effect of pellet-making pressure on the contact angle. Most contact angle measurements were carried out on the pellets prepared at pressures of 27.6 to 34.5 MPa.

5.3.5 The Porosity Measurement

The porosity of a pellet is a very important parameter both in direct contact angle measurement technique (this includes two different methods: direct observation or calculation from the profile of the liquid drop), and in rate of penetration measurement which will be discussed in Chapters 7 and 8. It is determined by the particle size distribution, pellet-making pressure, as well as the inherent porosity of the material itself. In the compressed pellet method, porosity affects the fractional area of air pores on the pellet surface, while in the rate of penetration process, it affects the rate of liquid penetration within a column.

The porosity was determined by saturating the pellet with a certain liquid (kerosene in this case). The weight of the compressed pellet was accurately determined using an analytical balance before and after the saturation process. The weight difference was the weight of the penetrating liquid, the volume of which was assumed to be the volume of the pores in the pellet. The total volume of the pellet could be obtained by accurately measuring its two dimensions - height and diameter using a vernier gauge. The porosity of the pellet can be subsequently calculated from

$$P_o = \frac{(W_1 - W_0)}{\pi \cdot r^2 \cdot h \cdot \rho}$$

where P_o - Porosity

W_1 and W_0 - The pellet weights (gram) before and after penetration (air-dry and saturated pellet)

r - pellet diameter (cm)

h - pellet height (cm)

ρ - the penetrating liquid density (g/cm^3)

5.3.6 Pellet Surface Examination

In order to examine the pellet surface for pores, roughness and possible particle crushing caused by high pressure. The Scanning Electron Microscope (SEM Hitachi S-

570) was used. The magnification employed ranged from 20 to 10000 times. Under such a high magnification, the individual particles and their packing states on the pellet surface could be studied very clearly.

Prior to the surface examination, the pellet surface was coated with carbon. In order to obtain good resolution under very high magnification, the coating process was repeated three times.

The pellet surfaces, at different magnifications, were photographed.

CHAPTER 6

RESULTS AND DISCUSSIONS <I>

The freshly prepared pellet surface was glossy and macroscopically smooth. Surface roughness was not generally considered to be a major effect in contact angle measurements <Nuemann and Good, 1979; Bracke, et al., 1989>. For such a macroscopic process as contact angle measurement, the asperity size on the pellet surface is so small relatively to the liquid drop size that the microscopic events which take place on individual particles as the wetting front passes over them may be masked.

The porosity on pellet surface, though not observable to the naked eyes, could seriously alter the real contact angle. It has been demonstrated thermodynamically <Shuttleworth and Bailey, 1948> that the contact angle on a porous surface will be higher than on a smooth surface that has the same composition. In this work, a model for the pellet surface was proposed and corresponding correction for the contact angle values was introduced.

6.1 CONTACT ANGLE MEASUREMENTS

Practically, all contact angle systems exhibit hysteresis. There are two ways of handling hysteresis. One is to develope a simple method by which reproducible data can be obtained in spite of hysteresis, and to report a single angle for any liquid on a particular solid. This approach was adopted in this work. The second way is to exploit the phenomenon, recognizing that it furnishes additional information about the solid.

As already pointed out, the contact angle data were obtained either by direct reading through goniometer, or by calculating the angle value from the profile of axisymmetric meniscus. Unless otherwise indicated, only advancing contact angles were measured in this work, and the unit of all the angle values in text and figures is degree. The reason for this is that the receding angle is more sensitive to roughness and heterogeneous effects than is the advancing angle <Bartell and Ruch, 1956>. It is easier to get reproducible results for θ_a than for θ_r. Also, θ_a is much easier to measure.

In the process of contact angle measurements, the experimenter can notice, through the goniometer, the clear reflection of the drop profile on the pellet surface. The

reflectivity is obviously a manifestation of surface smoothness. For drops with large contact angle, the drop image may look like an 8-shaped profile having a tip in the middle because of reflection (see Figure 6.1.1). This effect is very useful for determining the three-phase contact line which is vital in contact angle measurement.

Vibration by manual tapping was also tried in the present contact angle measurements with the expectation that it would help to overcome hysteresis energy barrier, and make the advancing contact angle approach the equilibrium contact angle θ_e. Nevertheless, it was found that angles measured in this way were less reproducible than those obtained without the vibration. When vibration was applied, the measured contact angles were located somewhere between the advancing and receding angle. It is probably better, as indicated by Neumann and Good <1979> to insulate against vibration in order to produce reproducible results.

Because of hysteresis, the angles at the left and right sides of the drop may not be equal. This inequality was often observed on the coal pellet surfaces. The observation was rejected if this difference exceeded four degrees.

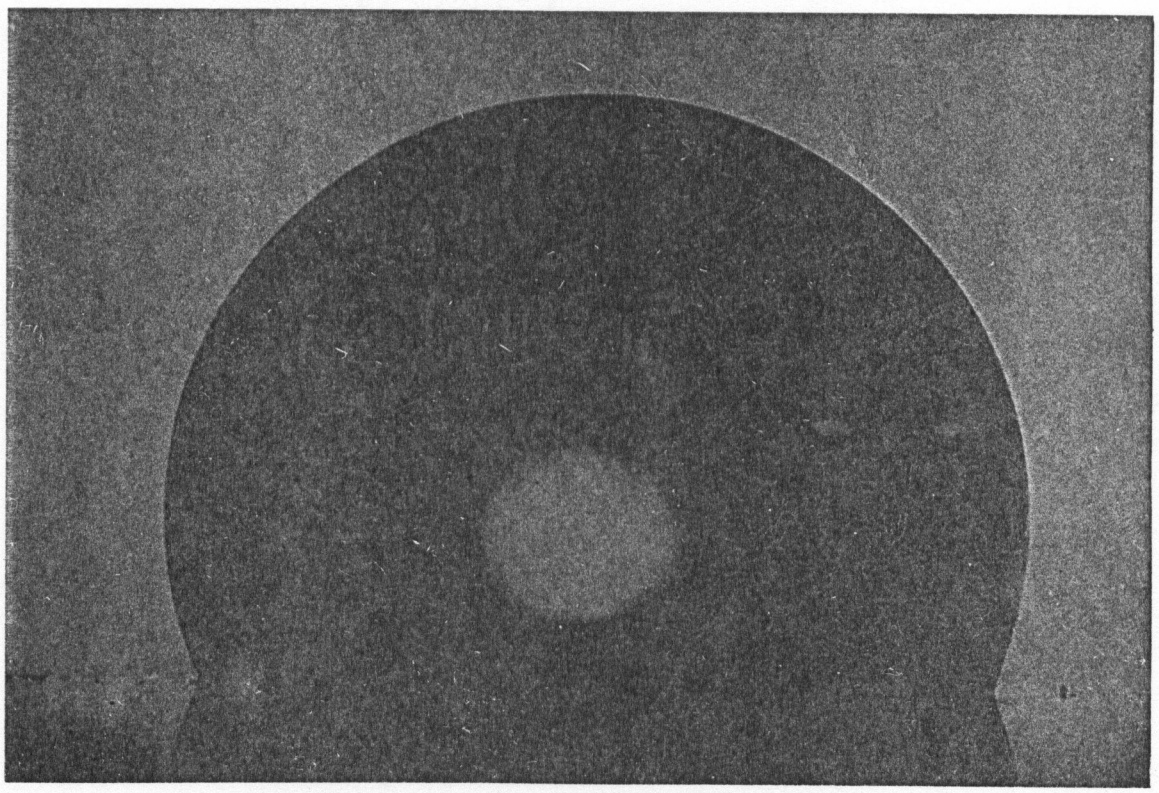

Figure 6.1.1 A sessile drop image observed through the goniometer

6.2 COMPARISON OF THE TWO TECHNIQUES

For each sessile drop, a direct reading was first made with the goniometer by measuring the contact angle value on both sides of the drop. The average of the two angles was taken as the measured contact angle value. A photograph was taken of the same drop right after the direct measurement. From the drop profile in this photograph, the computed angle value was obtained later using the program developed by Rotenberg, Boruvka, and Neumann <1982>.

The comparison was made on the pellets prepared from different density fractions. The direct measured angle was correlated with the computed one for the same sessile drop as shown in Figure 6.2.1. The figure reveals that nearly all of the points fall beneath the line and show fairly large differences.

It appears that the direct measurement gives values lower than the computed angles. One probable reason responsible for this deviation might be the systematic error introduced by either or by both of the procedures. In the section that follows, a series of measurements were conducted to test the reproducibility of the axisymmetric drop technique. Different perturbation effects such as liquid density, scaling factor, positioning of the drop apex

Comparison of the measured & computed

Figure 6.2.1 Contact angles on a pellet (-1.3 LC)

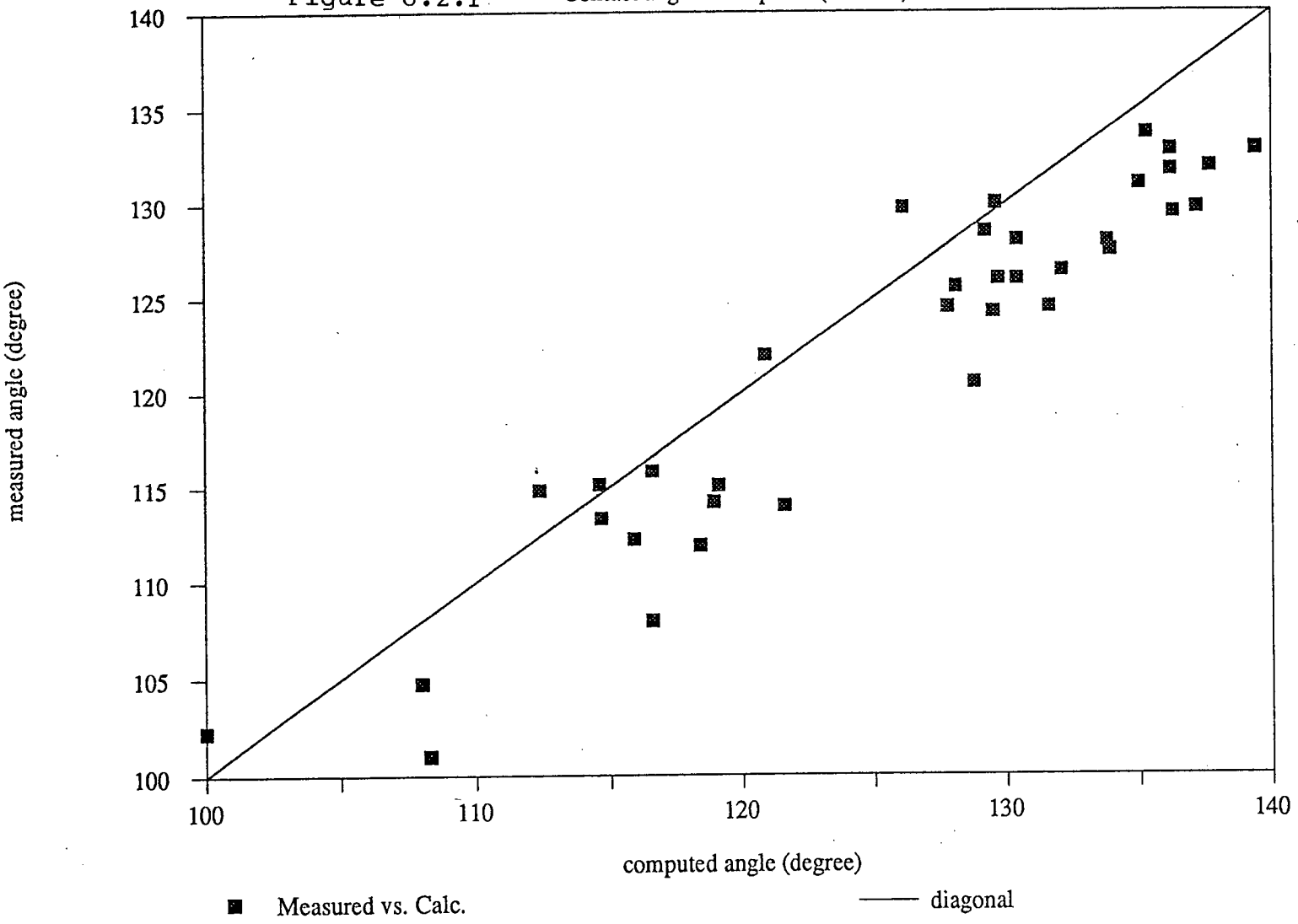

etc., were deliberately introduced into the computer program to examine the consequent deviation. The results showed that the angle deviation in the actual operation could be well confined within 1.5°. This value is much lower than the differences between the two techniques shown in Figure 6.2.1. Therefore, it is very unlikely that the systematic error is introduced by the axisymmetric drop technique.

The accuracy of direct reading through goniometer was also tested by repeated measurements both on the sessile drop and on the photographic profile of the sessile drop. Again, the standard deviation was below 2°. Therefore, the deviation between the two methods can not be attributed to the measurement error. Some other factors must then influence the contact angle measurements.

The hypothesis suggested in the present work is that the deviation between the directly measured and the computed angle values have mainly resulted from the pellet surface heterogeneity, and the sessile drop distortion caused by heterogeneity.

Basically, the pellet surface can be considered to be an uniformly distributed heterogeneous surface. The heterogeneous model proposed by Neumann and Good <1972> in Figure 6.2.2(a) may be employed to illustrate the effect of the surface heterogeneity on the two contact angle measuring

methods. The solid surface in the model consists of parallel strips of two types, on which the liquid assumes different equilibrium contact angles θ_1 and θ_2. The patches on the solid surface would lead to microscopic distortion of the liquid-vapour interface near the solid in order that the edge of the drop may satisfy Young's equation locally. The cross section of Figure 6.2.2 (a) is shown in Figure 6.2.2 (b). The portion of the drop profile (dashed line in the figure) that comes down to the lower-energy patches of the surface is not visible in profile. The visible profile (the solid line) is that part of the liquid surface which is in contact with the high-energy patches of the solid surface. The contortion would extend from the three-phase-contact line upward to the curved liquid surface for some distance and die out merging into a smooth, spheroidal main drop surface. An extrapolation of the main drop surface would fall somewhere between the solid line and the broken line.

In the direct reading through goniometer, what one directly measures through goniometer is the angle of solid line, θ_2, while θ_1 is totally ignored. For the axisymmetric drop method, the data points from the main profile of the sessile drop are fed into digitizer. The contortion near the three-phase contact line might have died out before reaching the main profile. The contact angle thus calculated on the computer should then be the angle assumed by the main profile extrapolated at the three-phase contact line. This

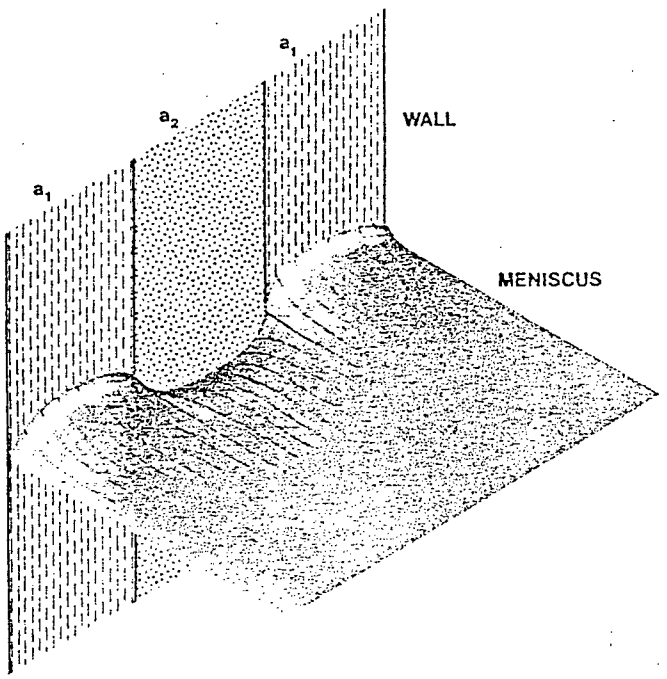

a. An artist's conception of a meniscus in contact with a stripwise heterogeneous wall

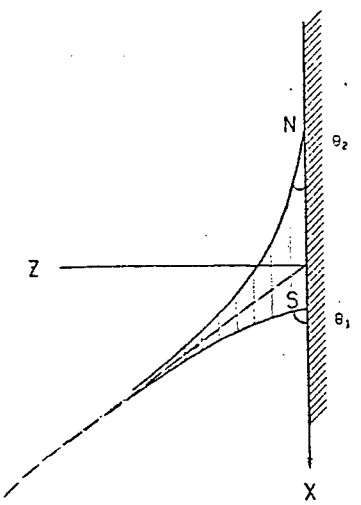

b. A view of cross section in the stripwise direction

Figure 6.2.2 An idealized heterogeneous surface model

angle resides between θ_1 and θ_2 as shown in Figure 6.2.2 (b). So it is always greater measured angle θ_2.

Because the main profile is determined by a cooperative effect of both strips: a_1 and a_2, this contact angle might be considered to be Cassie's angle (confirms to Cassie equation) which reflects the overall surface wettability.

From above discussion, it can be concluded that on a heterogeneous surface: a) the contact angle measured at a three-phase contact line through a goniometer reflects the high energy component, b) Cassie's contact angle cannot be measured at a three phase-contact line but only through the main profile of the sessile drop.

6.3 TESTING THE COMPUTATION METHOD

The direct contact angle measurement is more vulnerable to the effect of heterogeneity and reflects only the wettability of higher energy component. The axisymmetric drop method calculates the angle from the main profile, and reflects the wettability of the overall composites instead of one. It is, therefore, more appropriate to use the axisymmetric drop technique to measure the contact angle on a heterogeneous surface. In this section, different aspects of applying the axisymmetric drop technique are further investigated.

The use of the computer program developed by Rotenberg, Boruvka and Neumann <1983> requires the accurate positioning of the profile baseline (the three-phase contact line) and the positioning of the apex point on the profile. The importance of positioning the baseline was tested by intentionally drifting the baseline from the real one. The results in Figure 6.3.1 show that the calculated angles were greater than the real ones when the baseline was moved upward into the profile, and become smaller when the baseline move downward. Normally the uncertainty in positioning the baseline was in the range of ±0.5 mm, the possible error associated with positioning of the baseline is ±1.25° as shown in Figure 6.3.1. The enlargement of the

drop profile was 34.6. If the scaling factor was larger, the error in the computed angle value associated with the positioning of the baseline would be smaller.

The effect of positioning the apex point was also tested by deliberately moving it away from the real apex point. The results are shown in Figure 6.3.2. As the apex point was removed, along the drop profile, away from the real apex point, the computed value did not show any notable change. The conclusion is that the positioning of the apex point of the drop profile is not important.

The reproducibility of this technique was tested by repeating the measurement on the same photograph. The standard deviation was as small as 0.32°; in comparison with ±2° for the direct contact angle reading obtained using the goniometer.

The use of the computer program also requires the accurate measurement of the two parameters: the enlargement (scaling factor) of the drop profile on photograph, and the liquid density. These measurements are required to compute the contact angle and other quantities such as the liquid surface tension, surface area, and contact radius of the sessile drop. The effects of these factors were further tested by replacing the real scaling factor (34.6) and liquid density (1.0) with some arbitrary values. Results in

The positioning of drop baseline and its effect on computed angle

Figure 6.3.1

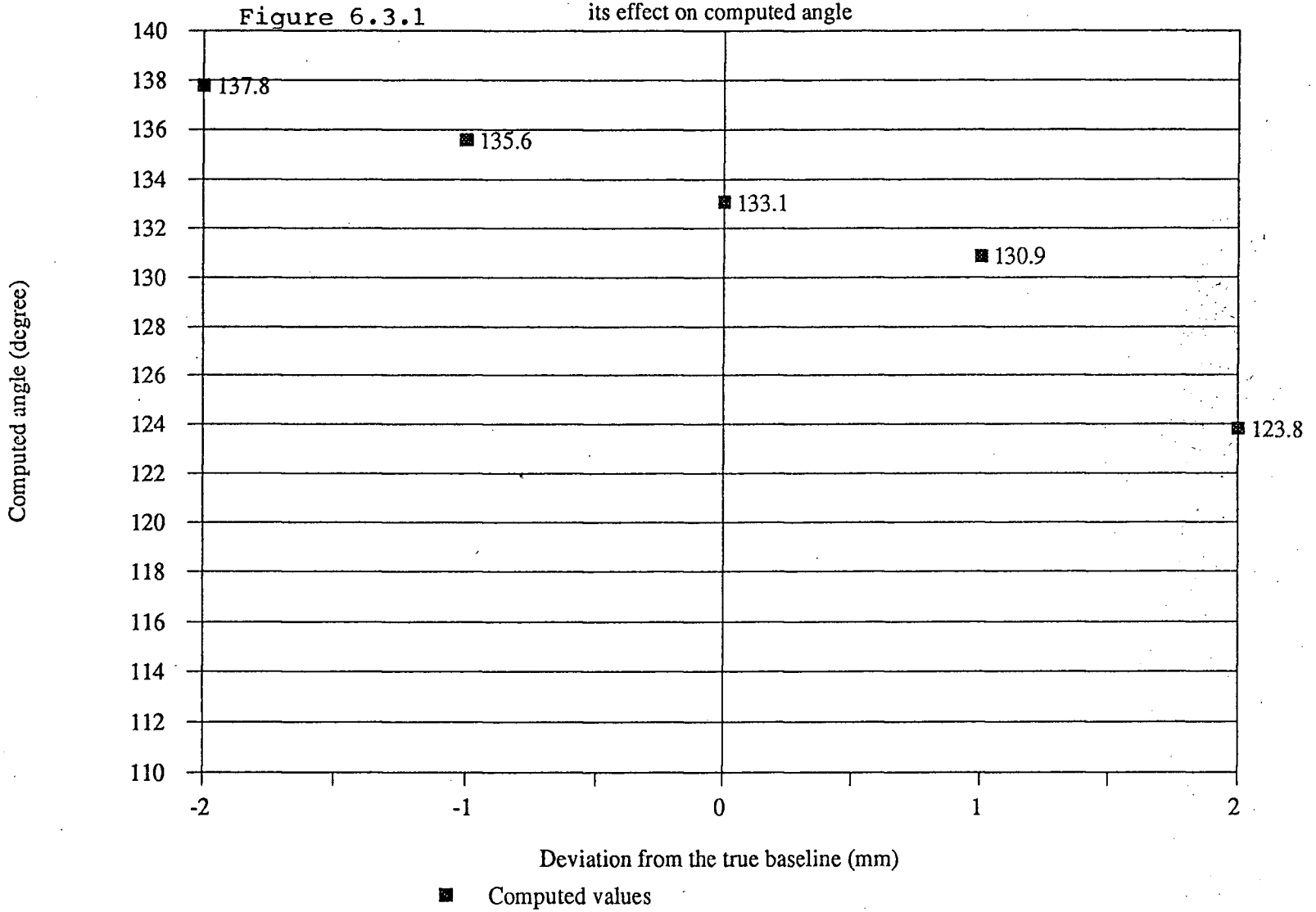

Positioning of the apex point of a drop

Figure 6.3.2 and its effect on computed angle value

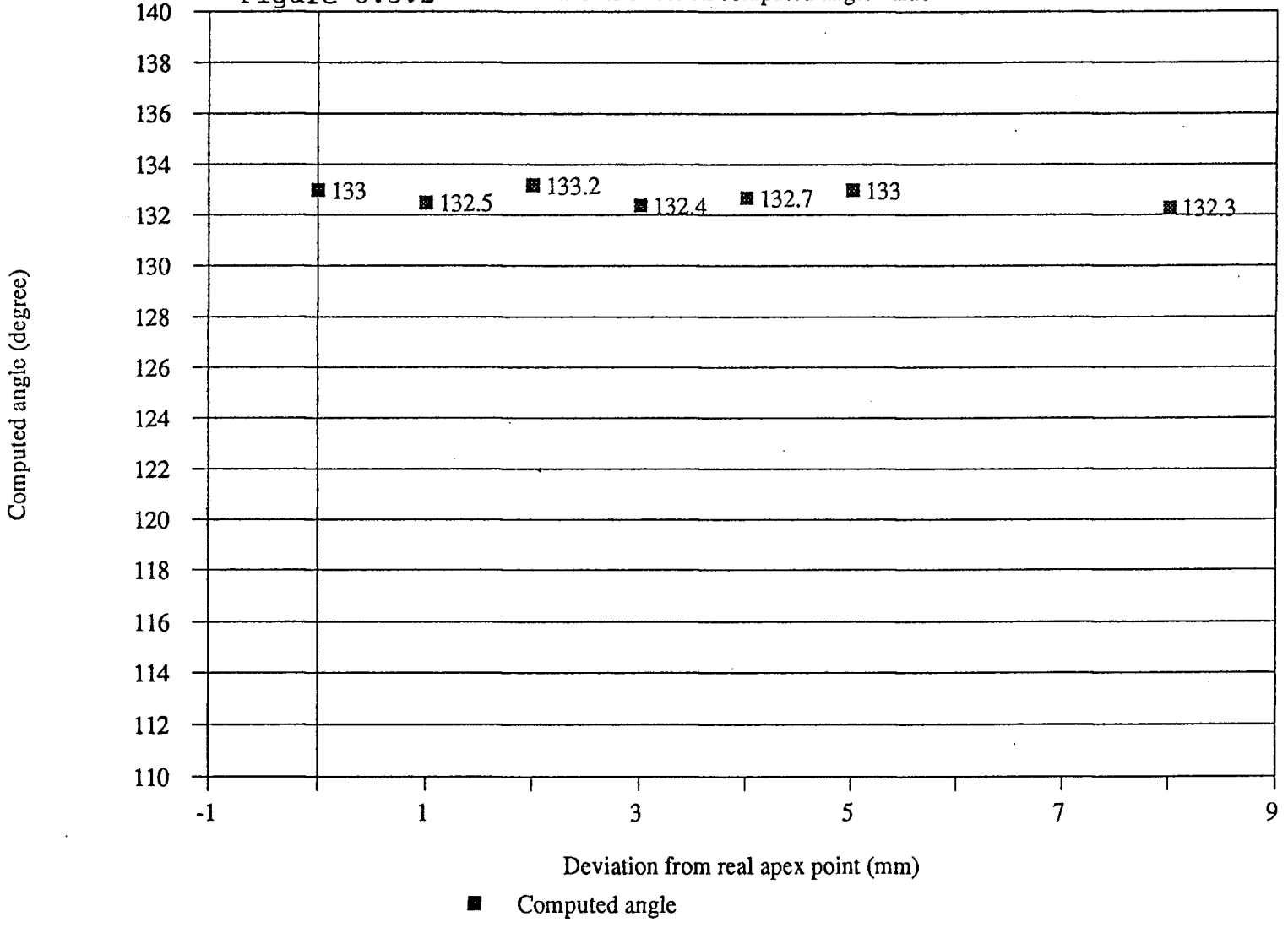

Measurement of scaling factor and its

Figure 6.3.3 effect on the computed angles

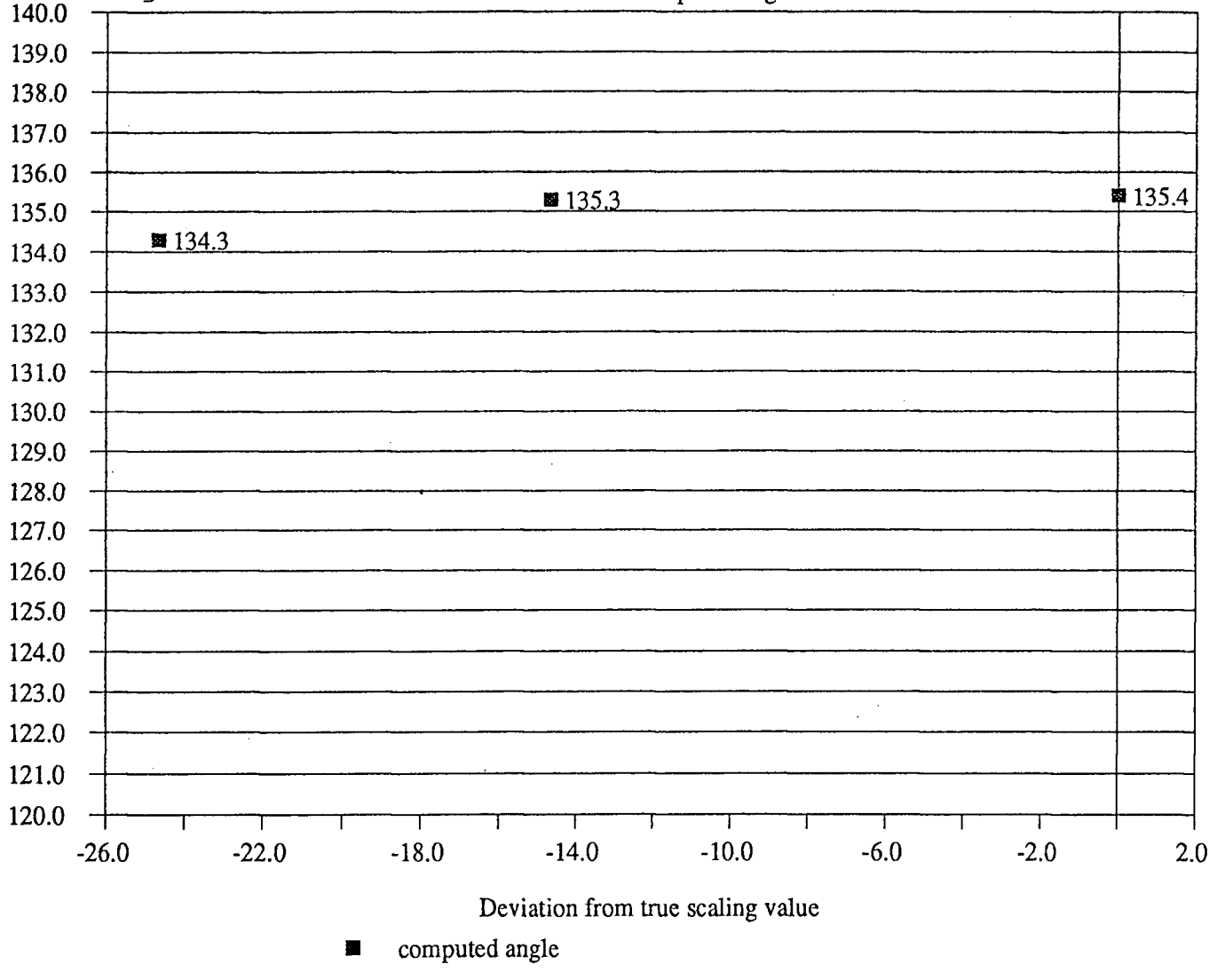

Accuracy of liquid density measurement

Figure 6.3.4 and its effect on computed angle

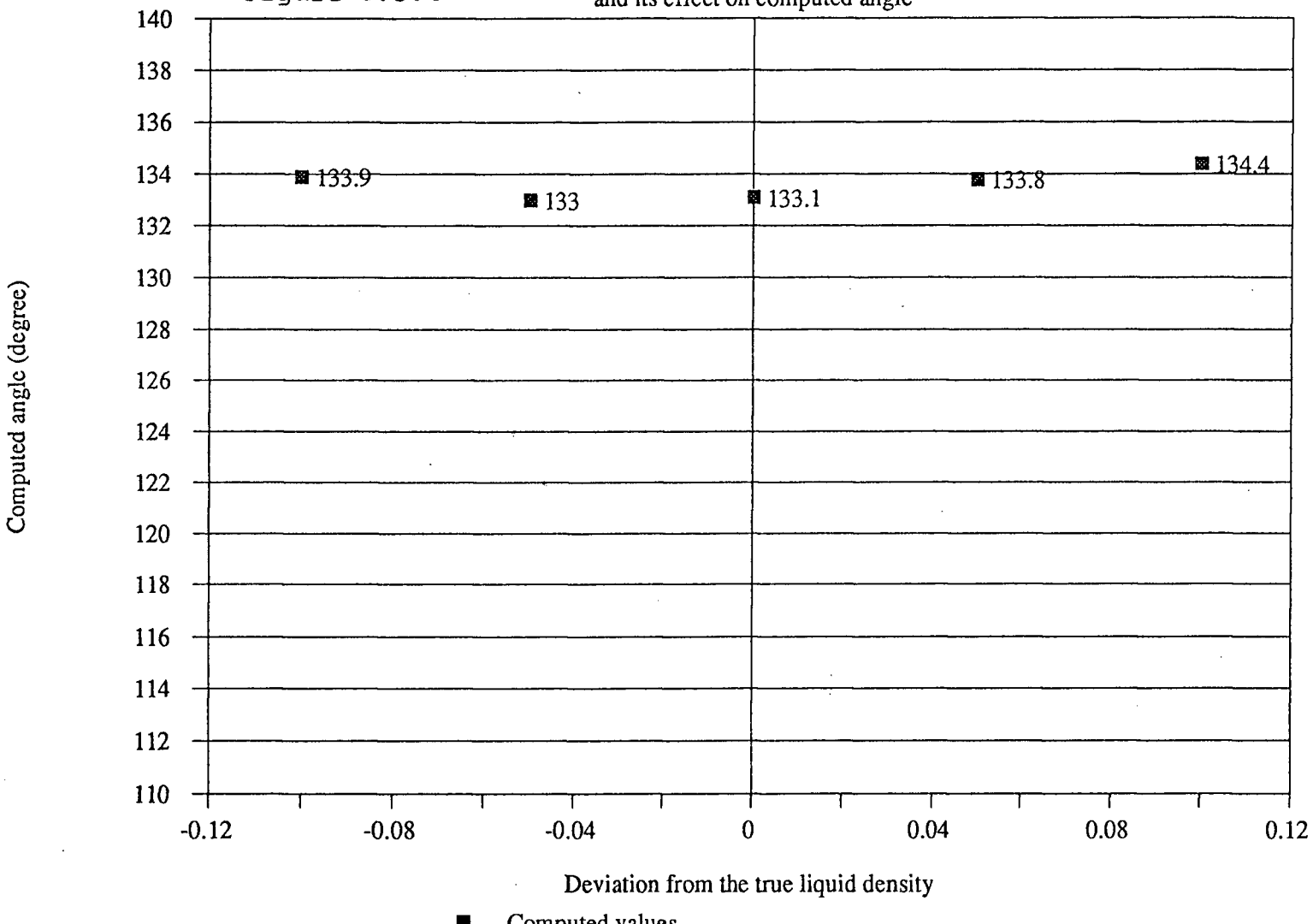

Figures 6.3.3 and 6.3.4 show that the two parameters have no significant influence on the computed angle value.

In conclusion, the series of the tests discussed above indicate that, between the two contact angle measurement methods, the computation method has much higher precision than the direct reading method. In later work, the computation method was employed unless noted.

6.4 CONTACT ANGLE AND DROP SIZE

Theoretically, the sessile drop size should not affect the contact angle on an ideal surface. There is one, and only one, equilibrium contact angle. However for the real contact angle system, this is rarely, if ever, the situation. It has been known empirically, for many years, that when the contact angle of a liquid is measured on a solid by the sessile drop or captive bubble method, the contact angle is a function of drop (or bubble) size <Shafrin and Zisman, 1952; Leja and Poling, 1960; Herzberg and Marian, 1970; Good, 1979>.

For the study of drop size effect, the advancing contact angle is usually measured versus the drop size. It was observed in a typical experiment that the contact angle of water on Teflon TFE <Herzberg and Marian, 1970> increases with the increase in drop size. For the captive air bubble method, a similar result was obtained by Leja and Poling <1960>. They found that the contact angle of water on polymethymeth-acrylate (Lucite) increased from 50° to about 70° when the diameter of air bubble decreases from 2 to 0.8 mm.

To explain this phenomenon, Leja and Poling assumed, that a drop or a bubble in contact with a solid could be

treated as a spherical cap and suggested that the size effect was due to the influence of gravity. While Good <1979> and Good and Koo <1979> attributed the size effect to heterogeneity which could lead to contortion of drop interface near the solid surface.

To observe the behaviour of contact angle versus drop size on a pellet, two procedures of forming different size drops were used in this work. In the first procedure, drops with various predetermined volumes (1.0 to 20.0 μlitre) were first formed at the calibrated micro-syringe tip and then the whole syringe set with the liquid drop on its tip was lowered slowly and smoothly until the drop met with pellet surface. The whole syringe set was again raised up slowly and left a free sessile drop on the pellet surface.

The second procedure employed was to increase the sessile drop size by incremental addition of the liquid (1 μlitre) to the previously formed one. The droplet was first formed on the syringe tip and then was lowered together with the syringe on to the apex of the previously formed sessile drop sitting on the pellet surface.

Figure 6.4.1 shows the results plotted on the contact angle versus drop size for -1.3 density fraction of Bullmoose coal. It can be seen that the advancing angle obtained by the first procedure increases with drop volume

Effect of drop volume on contact angle

Figure 6.4.1 Drop volume increased in two ways

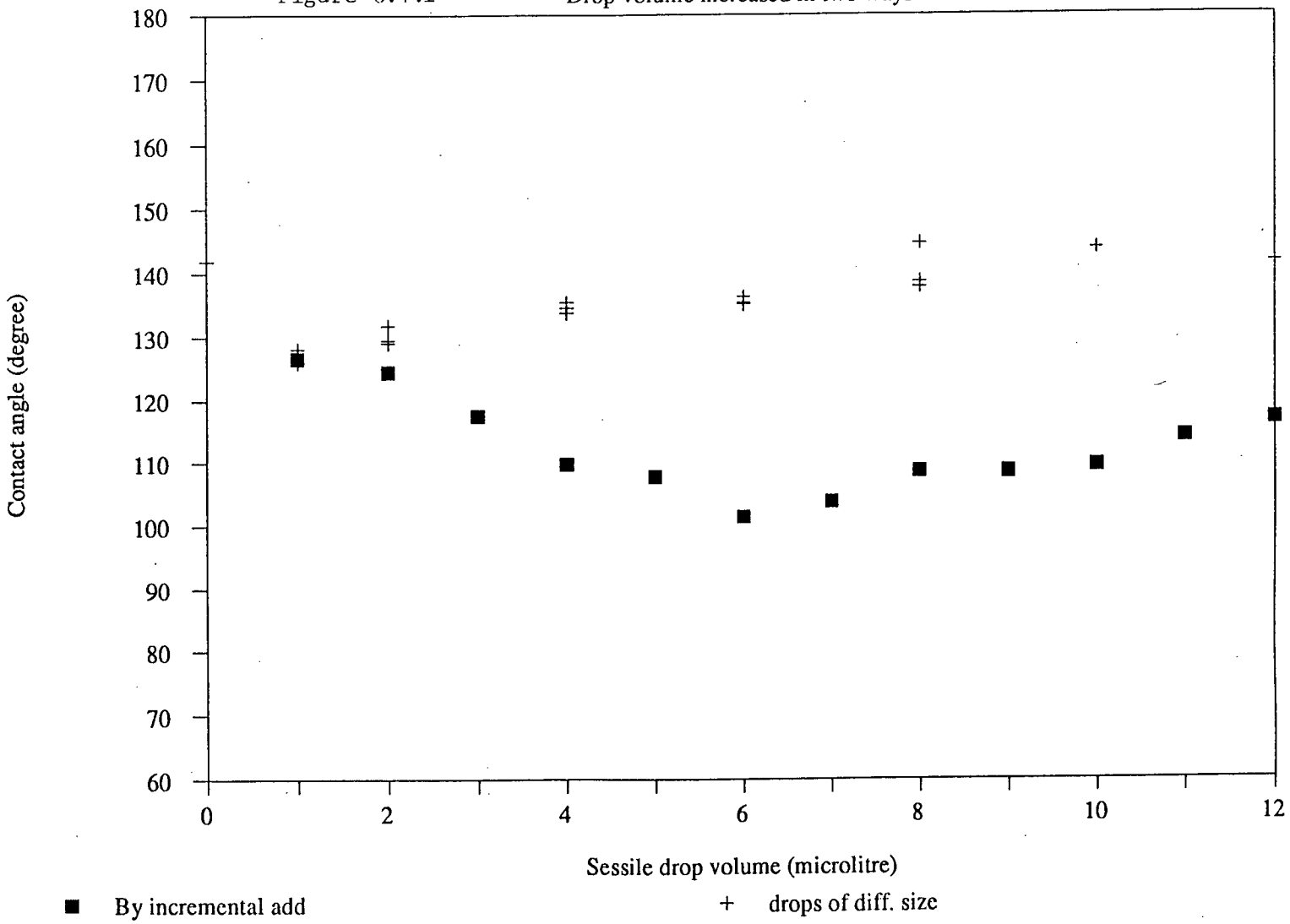

slowly until the drop volume reached about 8 μlitres. Beyond this, the contact angle value was essentially constant. These results are in a good accordance with those obtained previously by others <Herzberg and Marian, 1970; Good, 1979; Good and Koo, 1979>.

In contrast to the above result, the plot of the contact angle versus drop size as obtained from the second procedure is quite different. As shown in Figure 6.4.1, the contact angle first decreased with the increase of a drop volume, then started rising again forming a minimum value at around 6 μlitres. This result is very different from what has been reported before.

It is worthy of mention that the contact angle values in Figure 6.4.1 were obtained by axisymmetric drop method. The contact angle values for different drop sizes were not known until their photographs were digitized and angles calculated all in a batch. This excluded possible subjective influence in the measurement.

In order to confirm this phenomenon's reproducibility several sets of tests were conducted on the 1.3-1.4 density fraction (Figure 6.4.2) and on the oven-heated -1.3 density fraction (Figure 6.4.3 to 6.4.5). All the figures revealed two major features.

DROP SIZE EFFECT ON CONTACT ANGLE

Figure 6.4.2 1.3-1.4 density fraction P=31.0 MPa

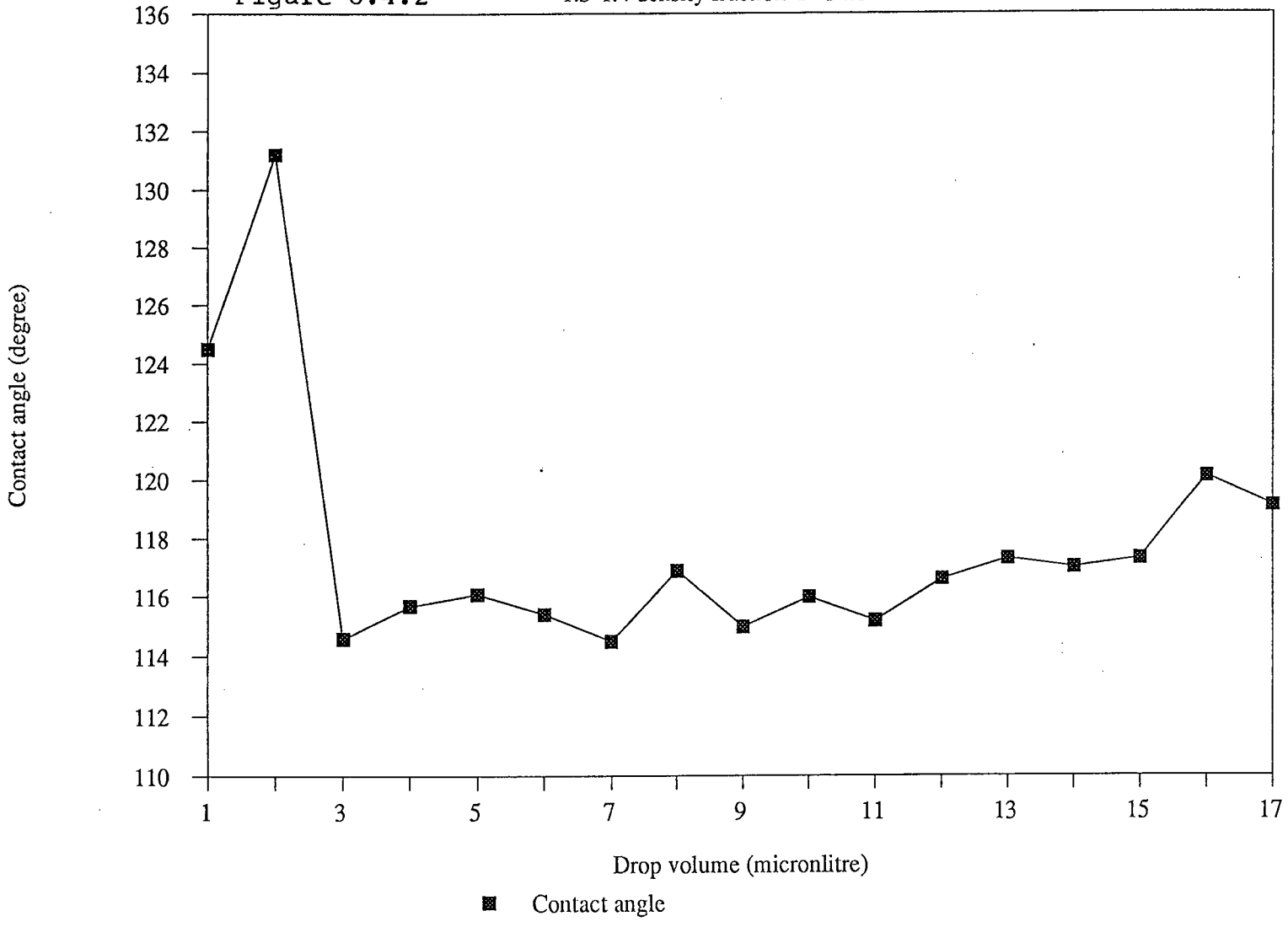

Drop size effect on contact angle

Figure 6.4.3

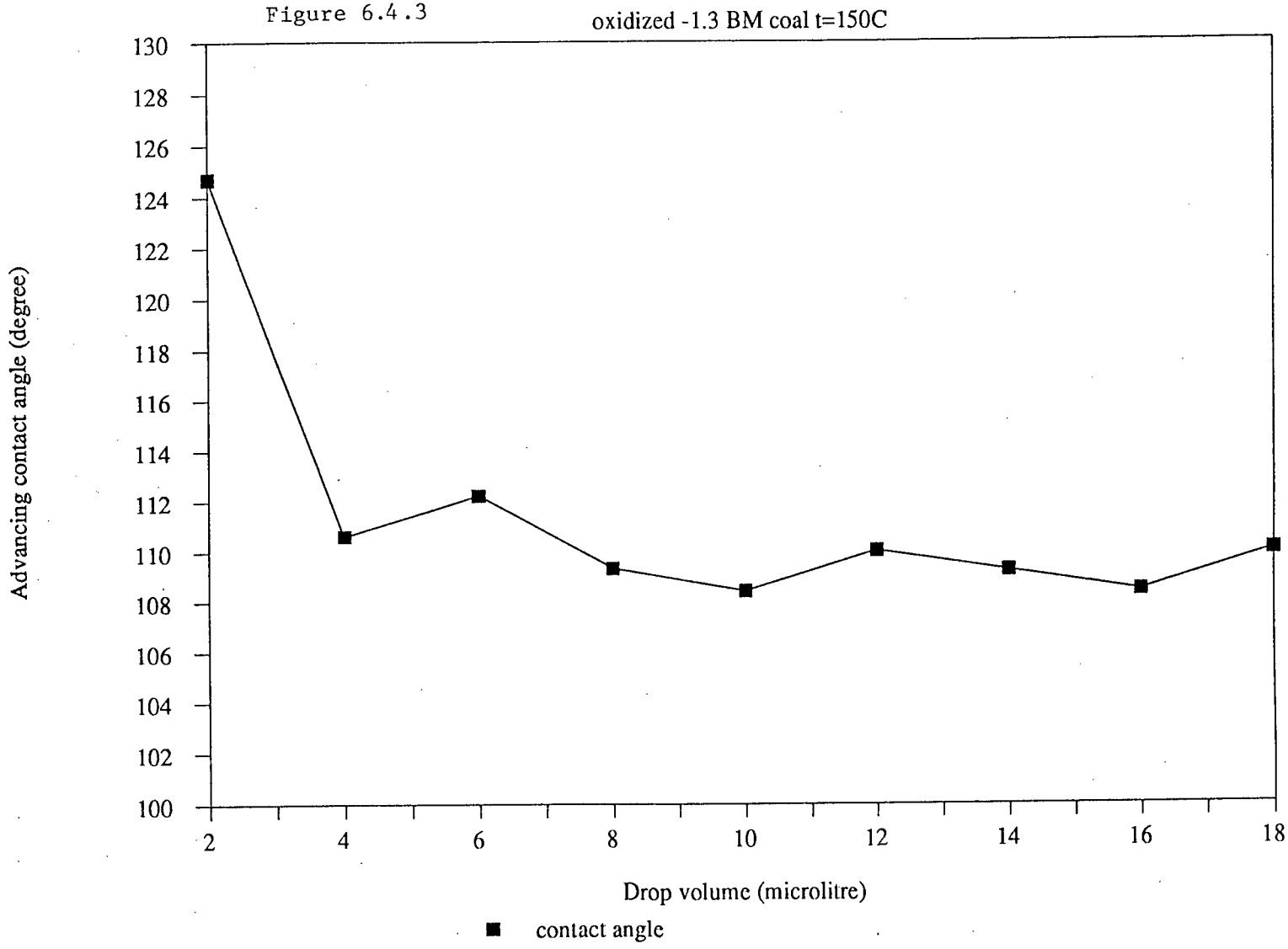

Drop size effect on contact angle

Figure 6.4.4

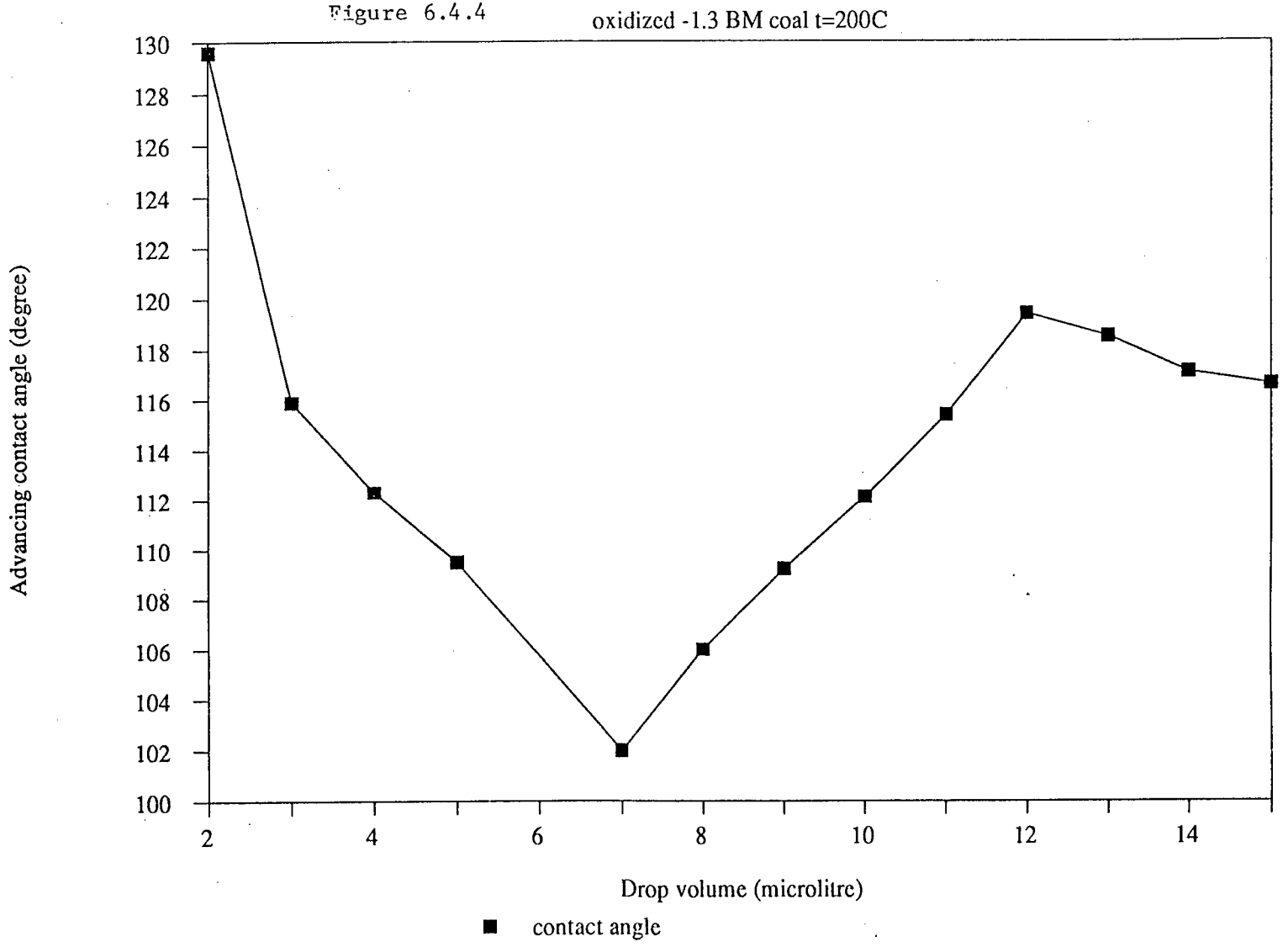

Drop size effect on contact angle

Figure 6.4.5 oxidized -1.3 BM coal t=250C

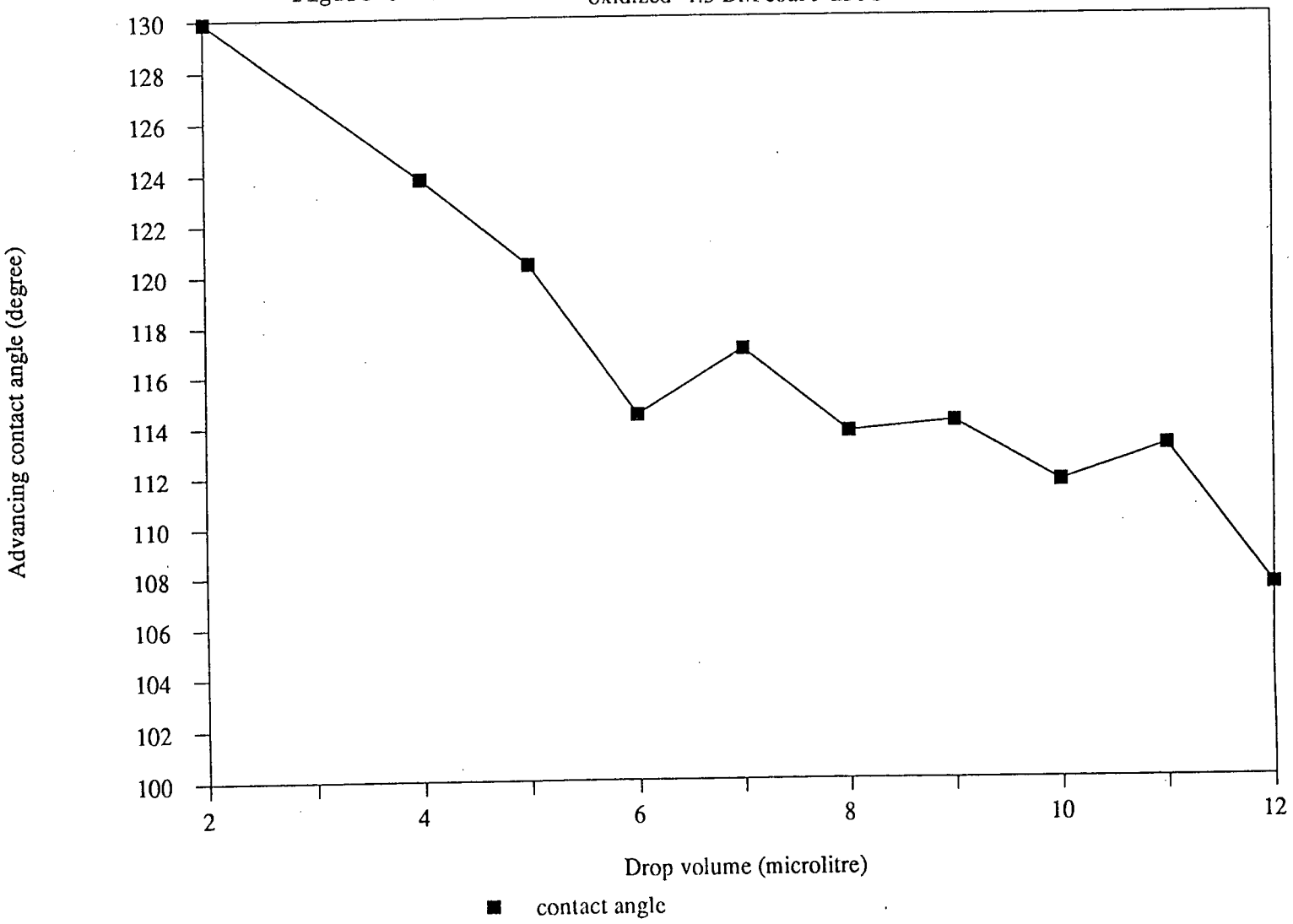

First, they are generally V-shaped. All contact angles exhibit a decrease versus drop volume at the beginning. Then, beyond a certain volume (8 to 17 μlitres) the contact angle starts to increase again. This phenomenon may be explained as a joint effect of two factors: gravitational force and contact angle hysteresis. At the beginning when sessile drop volume on the pellet surface is very small, each incremental addition substantially increases the sessile drop height, and the gravitation force moves the sessile drop profile downward to assume a smaller contact angle. A continuous decrease in contact angle versus volume is observed. Beyond a certain volume, further addition of the liquid to the sessile drop does not increase notably the sessile drop height any more. The sessile drop only continues to expand horizontally. As a result, the curve exhibits a clear minimum.

After the minimum is reached, the further increase in sessile drop volume can only lead to its horizontal expansion. The second factor, the contact angle hysteresis, becomes a major effect. It attempts to obstruct the advance of the three-phase contact line. As a result, the contact angle began to increase.

The second feature presented by these figures is that all curves are sawtooth-shaped. This can be attributed to the hysteresis energy barrier. An incremental increase in

the sessile drop size on the pellet surface is accompanied by an expansion of the three-phase contact line. The expansion of the three-phase contact line was opposed by the hysteresis energy barrier. This may lead to an increase of the contact angle value.

The energy accumulated within the sessile drop after subsequent additions of one or two incremental droplets may be sufficient to overcome the energy barrier. This process is accompanied by a decrease in the contact angle. The whole cycle, when more incremental liquid is added to the sessile drop, repeats continuously. A sawtooth-shaped contact angle versus drop volume curve results.

Apparently for such a phenomenon to appear, the energy introduced by each droplet should be lower than the hysteresis energy barrier. That is, the droplet should be very small (1 μlitre in this case). Otherwise the energy introduced by each droplet is so large relatively to the energy barrier, that the effect of energy barrier may be overshadowed.

The present methodology may be further developed to study the hysteresis energy barrier by correlating the saw-teeth height with energy.

6.5 CONTACT ANGLE VERSUS TIME

It was perceived that contact angles measured in the open air and in an enclosed thermostated chamber may vary. However, it was not known whether equilibrium, or, at least meta-equilibrium of the sessile drop on the pellet was established within certain period. If not, the question is how long it will take to reach such an equilibrium. In order to answer such a question, additional experiments were carried out.

The first observation was aimed at testing the relationship between the contact angle at a sessile drop and its life time on the pellet. The tests were performed in a thermostated chamber at ambient temperature. The reservoir within the chamber was filled with distilled water to keep the humidity constant. After lowering the tested pellet onto the stage within the chamber, the main lip was closed. 10 minutes later, a sessile drop was placed on the pellet surface through a small hole on top of the chamber. The chamber was equipped with viewing windows, so the contact angle could be taken without touching the chamber and disturbing the sessile drop.

The results obtained for different density fractions of Line Creek Coal are presented in Figure 6.5.1. For

CONTACT ANGLE vs. TIME

Figure 6.5.1 FOR DIFF. DENSITY FRACTIONS OF LC COAL

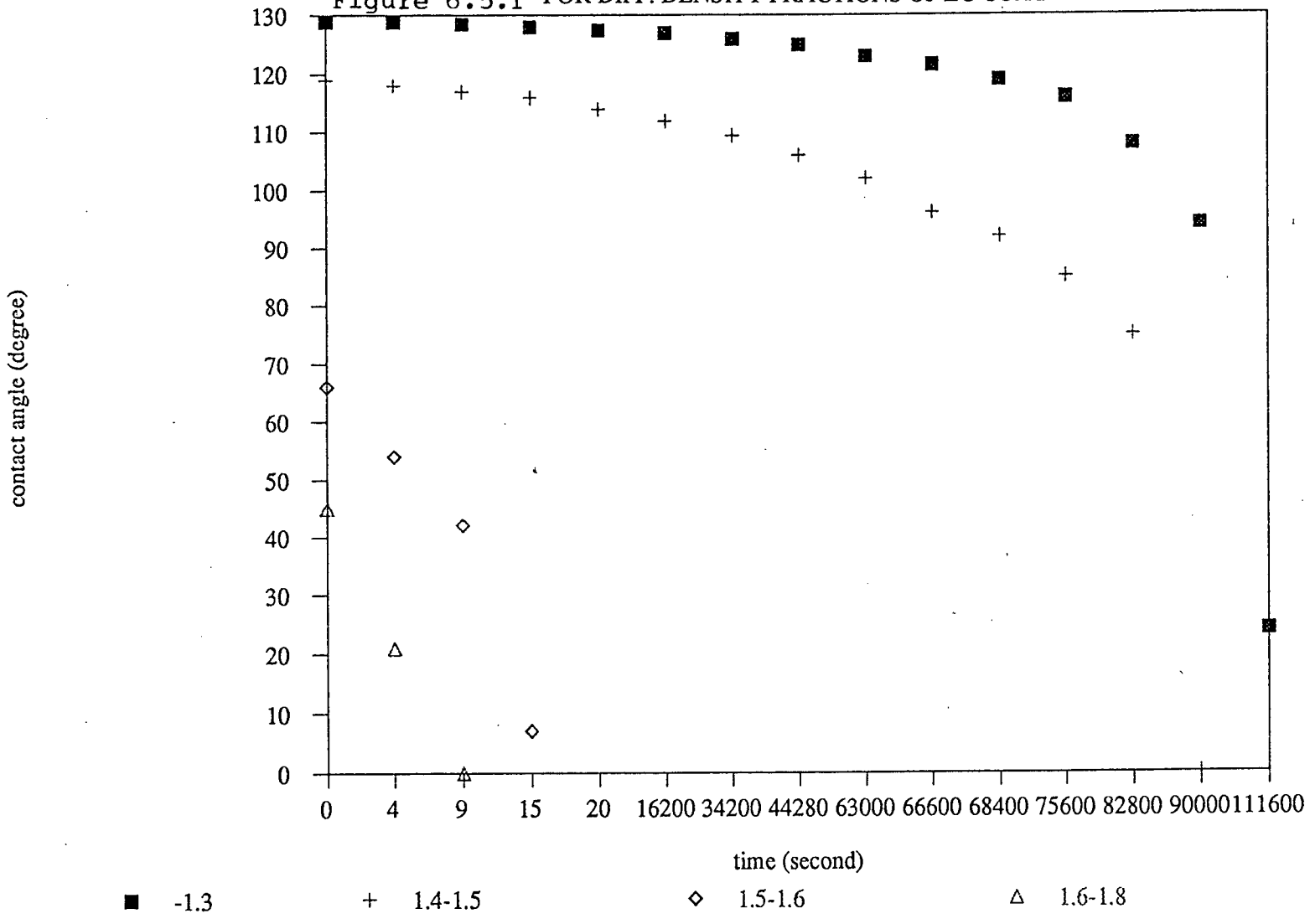

density fractions lower than 1.5, the contact angles were very stable and only varied very slightly even over a two day period, Then a quick decline followed.

Liquid evaporation, pellet surface oxidation, and the penetration of liquid into the pellet can be the factors responsible for such a behaviour. For low density fractions, the effect of liquid penetration was initially negligible. The slow decrease in contact angle was principally due to the sessile drop evaporation. The reason is that the sessile drop interface and the surface of bulk liquid in the reservoir possessed different curvatures (see Kelvin's equation).

Therefore, it can be expected that the sessile drop volume decreases with time. As time proceeds, the pellet surface oxidation becomes significant, and the liquid begins to penetrate into the pellet. Consequently, the contact angle starts decreasing quickly.

The horizontal parts of the curves (Fig. 6.5.1) reveal that the equilibrium state for the -1.5 fraction of coal sample can establish very quickly, i.e., within one minute. So in the actual measurement, it is not necessary to wait long for the establishment of equilibrium. The contact angle in open air was compared with the result in Figure 6.5.1. It was observed that the angle values in open air

were approximately equal to the values at the horizontal part of the curve. This was in agreement with other researchers' observationy <R. Crawford, L.K. Koopal and J. Ralston, 1987>. According to this observation, the thermostated chamber is not considered to be necessary in the practical contact angle measurements, and, therefore, all contact angles were measured in open air.

The contact angles of water on the pellets were much smaller than 90° for the +1.5 g/cm^3 density fractions. The contact angle on pellet surface decreases very quickly because of the significant liquid penetration into the pellet.

6.6 FACTORS AFFECTING CONTACT ANGLE

In this section, the factors that influence the contact angle on a pellet were tested. They are pellet oxidation and pellet-making pressure.

6.6.1 Oxidation

Oxidation was found to decrease the hydrophobicity of coal surface. Sun's early studies <1954> of the effect of oxidation on coal flotation indicated that as oxidation proceeds, coal becomes progressingly more hydrophilic. It was also noted <Iskra and Laskowski, 1967> that reduction in hydrophobicity of lower rank coals was more affected by oxidation than was that of higher rank bituminous coals.

To evaluate the change in hydrophobicity of coal powder due to oxidation, both the contact angle and the rate of penetration techniques were used. The rate of penetration technique will be discussed in detail in Chapters 7 and 8.

Various oxidation procedures have been considered. In one procedure recommended by Fuerstenau, Yang and Laskowski <1986>, the powdered Bullmoose coal was contained in a beaker and oxidized in a fan ventilated oven at 150°C,

200°C, and 250°C, respectively, for a period of 8 hours. After oxidation, the coal powder was compressed under pressure of 27.6 MPa into pellets and the contact angles were measured as already discussed.

The results are shown in Table 6.6.1. Although the change in contact angles was, according to the significance test, statistically insignificant, the trend still can be seen. An anomaly appeared at 250°C where a slight increase in contact angle was observed.

These oxidized and un-oxidized coal powders were again tested by the rate of penetration technique. The penetrating liquid was kerosene. The slope value of the penetration curve was directly related to the contact angle (see Chapter 7). For simplicity, only the slope values instead of the calculated angles were presented for comparison since this is only a qualitative comparison. They were tabulated together with the directly measured contact angles in Table 6.6.2.

Kerosene can penetrate into a column of hydrophobic material more quickly than into a hydrophilic one. So in the table, the slope value of penetration value for un-oxidized coal should be greater than that for oxidized coal. Following the same trend as the contact angle, the slope value became smaller for the coals oxidized at 150 and

Table 6.6.1 The contact angle on pellet of oxidized coal

the -1.3 density fraction Bullmoose coal

Pellet No.	Unoxidized		150°C	200°C	250°C
	130.5	131.5	129.8	130.5	125.0
	127.5	129.0	135.5	130.5	132.8
	128.5	132.0	129.8	133.5	131.0
	125.5	131.5	128.8	135.0	134.0
1st	127.0	127.0	126.0	127.0	132.3
	129.0	132.0	129.3	129.8	133.0
	130.5	136.0	128.5	132.8	127.3
	126.0	132.5	127.5	125.8	131.5
	132.5	129.5	129.3	121.0	128.8
	127.5	135.0	126.5	125.0	127.5
	128.5	133.0	127.3	125.5	132.3
	129.5	135.5	128.3	127.8	130.8
2nd	127.0	135.5	127.3	130.5	130.0
	131.0	130.0	123.8	126.5	129.0
	130.5	130.0	129.0	122.0	131.3
			127.0	124.5	
	131.0	132.5	125.5	123.8	128.0
	131.0	127.5	129.3	127.5	128.8
	132.5	126.6	125.8	129.8	129.5
	128.5	133.5	136.5	129.0	129.5
3rd	135.5	130.5	126.3	132.8	130.3
	129.5	131.0	126.0		132.3
	128.5	126.0	126.3		129.8
			125.8		129.0
			129.3		129.8
Average:		130.34	128.18	128.18	130.15
Std Deviatn:		2.75	2.79	3.71	2.06

* The period of oxidation time is 8 hours
* Pellet-making pressure is 27.6 MPa

Table 6.6.2
Comparison of the contact angles with the rate of penetration measured on different coals

method	unoxidized	150°C	200°C	250°C
measured angle degree	130.34	128.18	128.18	130.15
rate of penetratn slope	0.945	0.904	0.864	0.958

* The direct contact angle measurement values are quoted from chapter 5

* Bullmoose coal -1.3 density fraction

* Column making pressure is 13.8 MPa

200°C. The anomaly for the coal powder oxidized at 250°C was again observed. The slope value was 0.958 and apparently greater than others. This means that the coal powder oxidized at 250°C became more hydrophobic.

The similar results obtained from the two different techniques confirmed that an increase in hydrophobicity for the coal powder heated at 250°C did occur. The possible reason for this may be attributed to the decomposition or breakup of the hydrophilic functional groups (carboxyl groups) on coal surface in the heating process <Ye, et al., 1986>. Even though oxidation was still going on, the functional groups could be effectively split from the coal surface and evaporated at higher temperature. While at lower temperature, the functional groups could not be split so effectively as at high temperature. The coal surface became more and more hydrophilic.

A similar phenomenon was observed before by Ye, Jin, and Miller <1986> in their study on thermal treatment of low-rank coal and its relationship to flotation response. They found that properly controlled heating can actually improve coal flotation and its separation from mineral matter, especially for low-rank-coal.

It was alleged by Yordon and Yoon <1988> and many others that the oxidation mechanism of coal and the reaction

CONTACT ANGLE vs. OXIDATION TIME

Figure 6.6.1

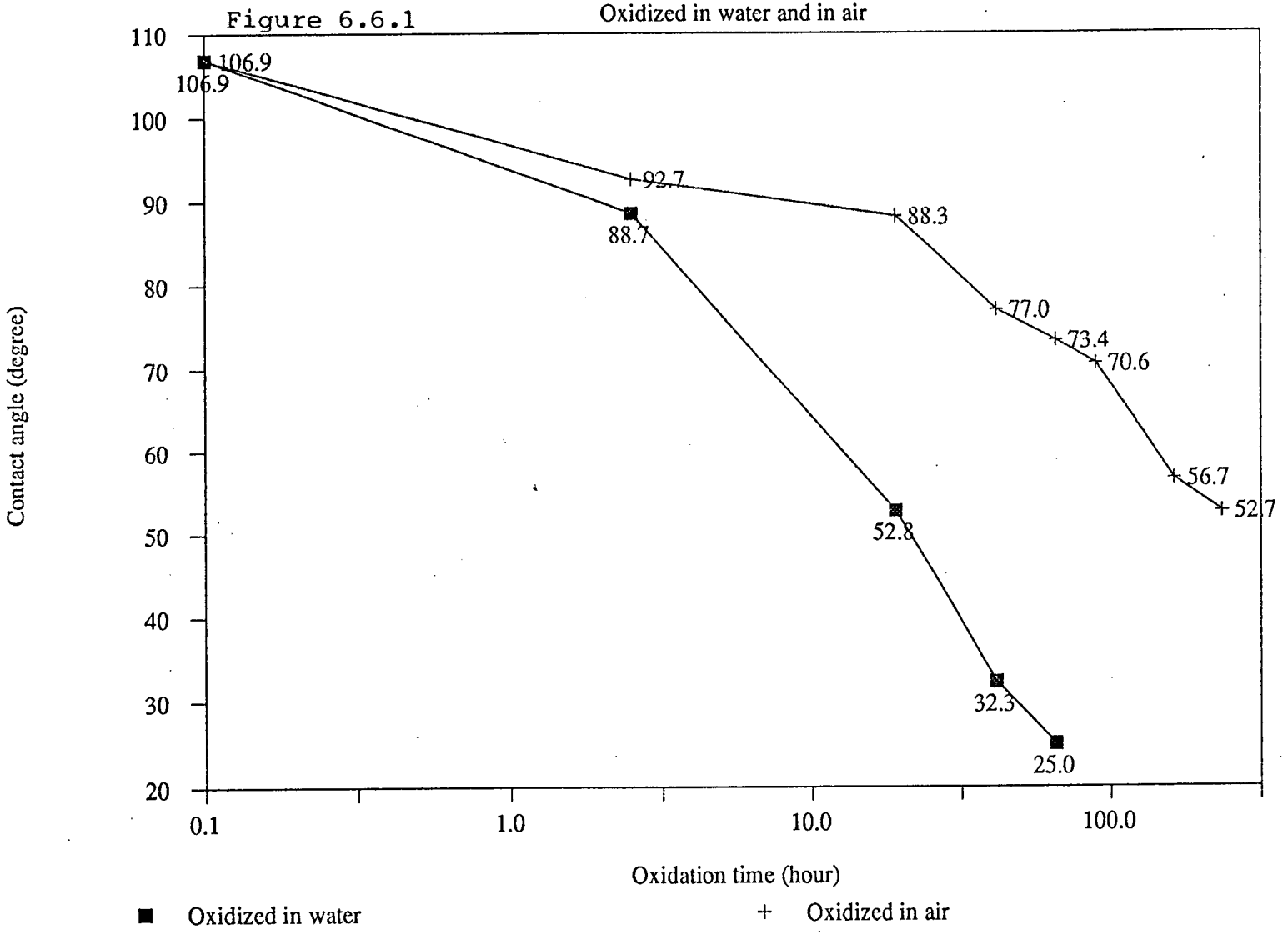

products under dry conditions can be significantly different from those of the low-temperature oxidation that take place in a moist or wet environment.

In this work, wet oxidation of coal was also tested. In the process, a pellet of the Line Creek coal was made following the same procedure as mentioned above and held on a small holder with its surface exposed to water. Then, the whole set was immersed in distilled water and the oven temperature was maintained at 100°C.

For comparison, another pellet was dry-heated together with the above pellet in the same oven in the air. After a period of time, the two pellets were taken out from oven to determine the contact angle. Then, they were put back into the oven to continue the oxidation process. The procedure was repeated. A curve of contact angle versus oxidation time could be obtained for each pellet.

The results are given in Figure 6.6.1. Apparently, the rate of wet oxidation is much larger than dry oxidation.

6.6.2 Contact Angle versus Pressure

Contact angles measured on the porous pellet

surfaces are not the true contact angles. The pellet-making pressure can influence the contact angle on a pellet surface through changing its fractional area of pores.

To test this hypothesis, the contact angles on a series of pellets made under different pressures were tested. Results for the -1.3 g/cm^3 density fraction of both Line Creek and Bullmoose coals are given in Figures 6.6.2 and 6.6.3, respectively. As shown in Figure 6.6.2, at low pressures, the contact angle decreases with an increase in pressure (3.4 - 17.2 MPa). Further increases in pressure above 17.2 MPa have only a very small impact on the contact angle value.

In addition, the pellet-making pressure also influences the reproducibility of the data. The data in Figure 6.6.3 were statistically analyzed. The standard deviations are shown in Figure 6.6.4. As the pellet-making pressure increases, the reproducibility of the contact angle data becomes better.

The influence of the pellet-making pressure on the value of the contact angle may result from the alterations of solid surface properties, surface roughness, and fractional area of pores on pellet surface.

The SEM photographs (Section 6.8) show that the

CONTACT ANGLE vs.PELLET-MAKING PRESSURE

Figure 6.6.2

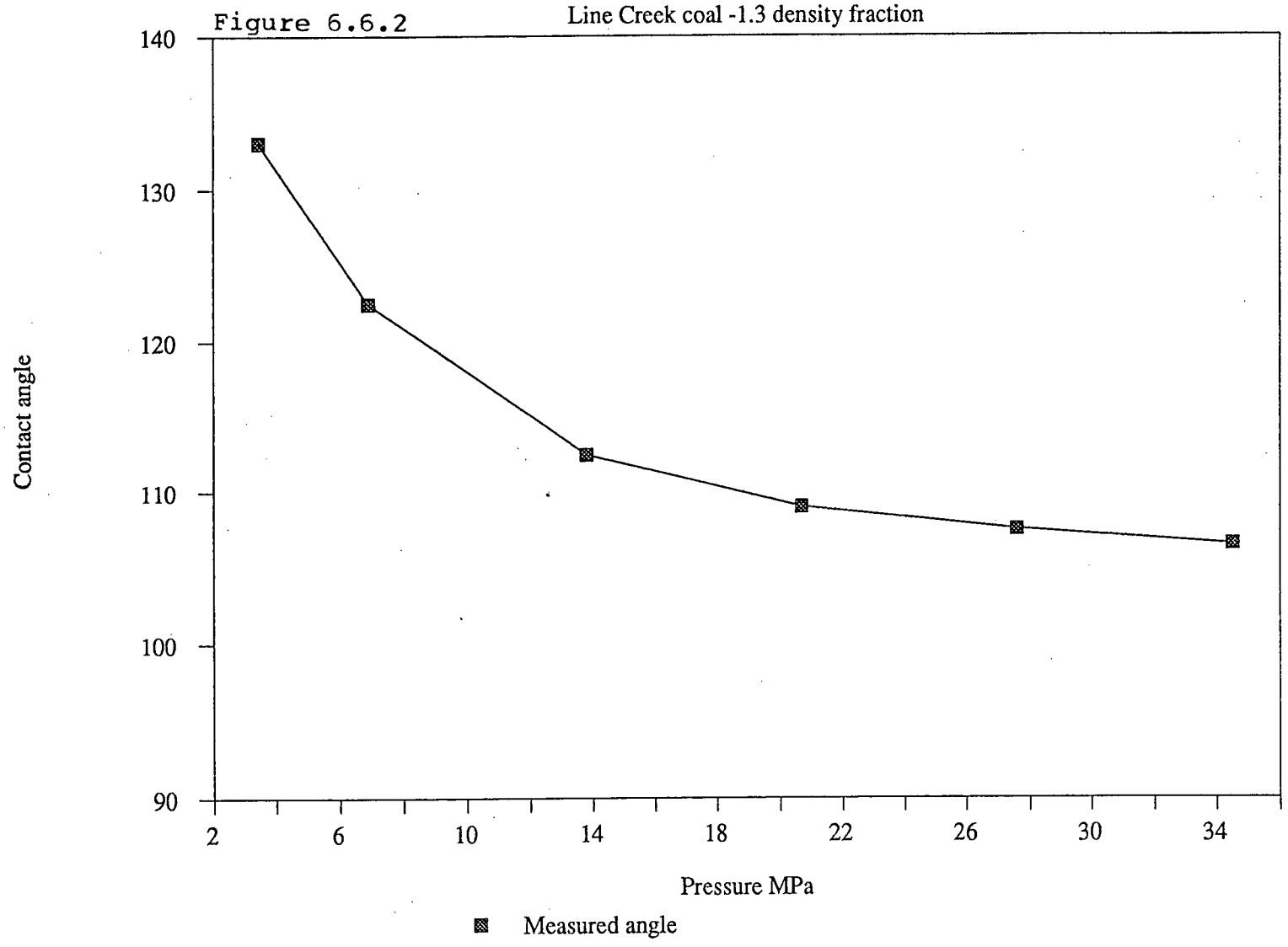

Effect of pellet-making pressure on

Figure 6.6.3 contact angle -1.3 fraction BM coal

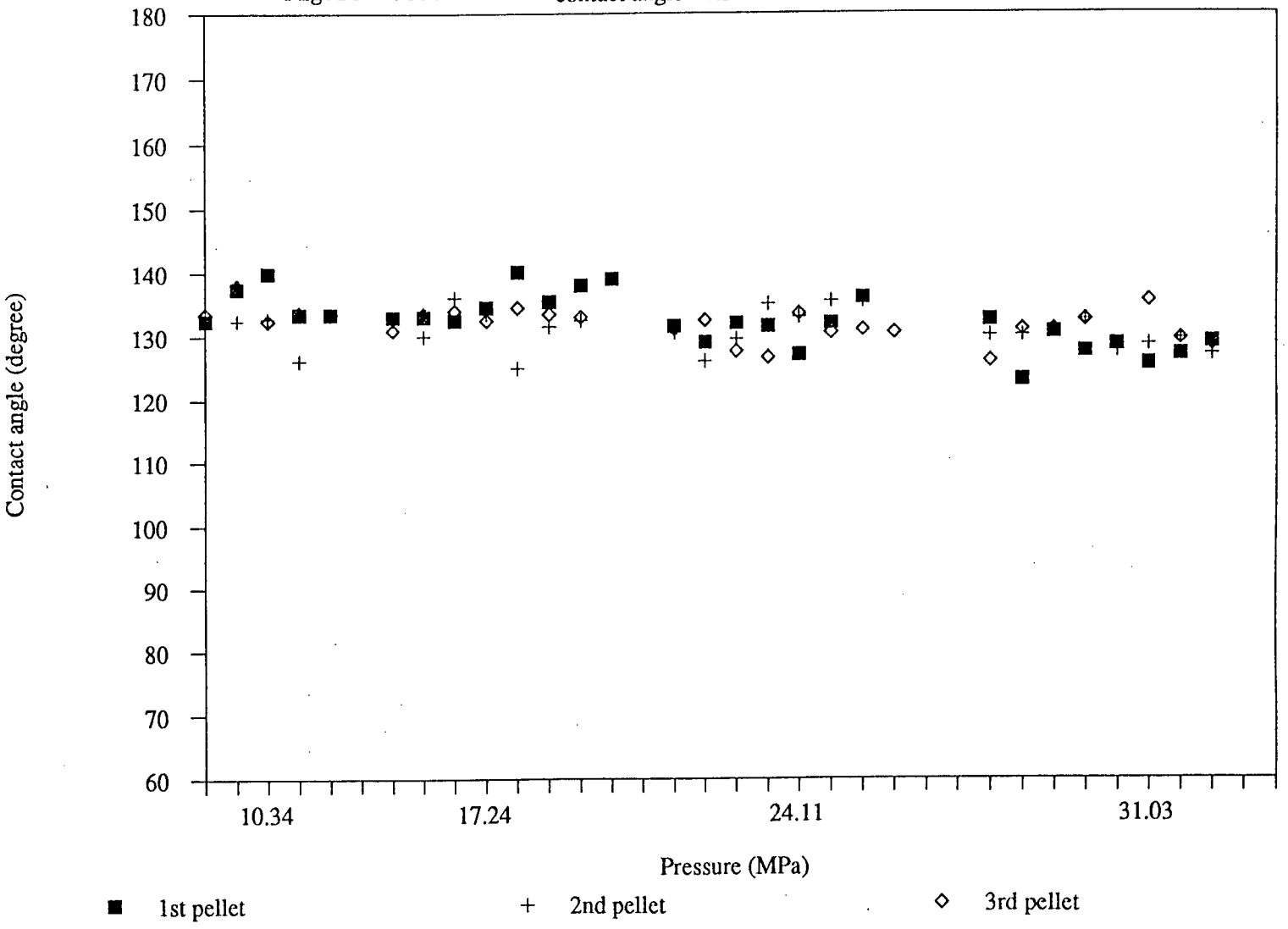

Figure 6.6.4 **Influence of pellet-making presssure**

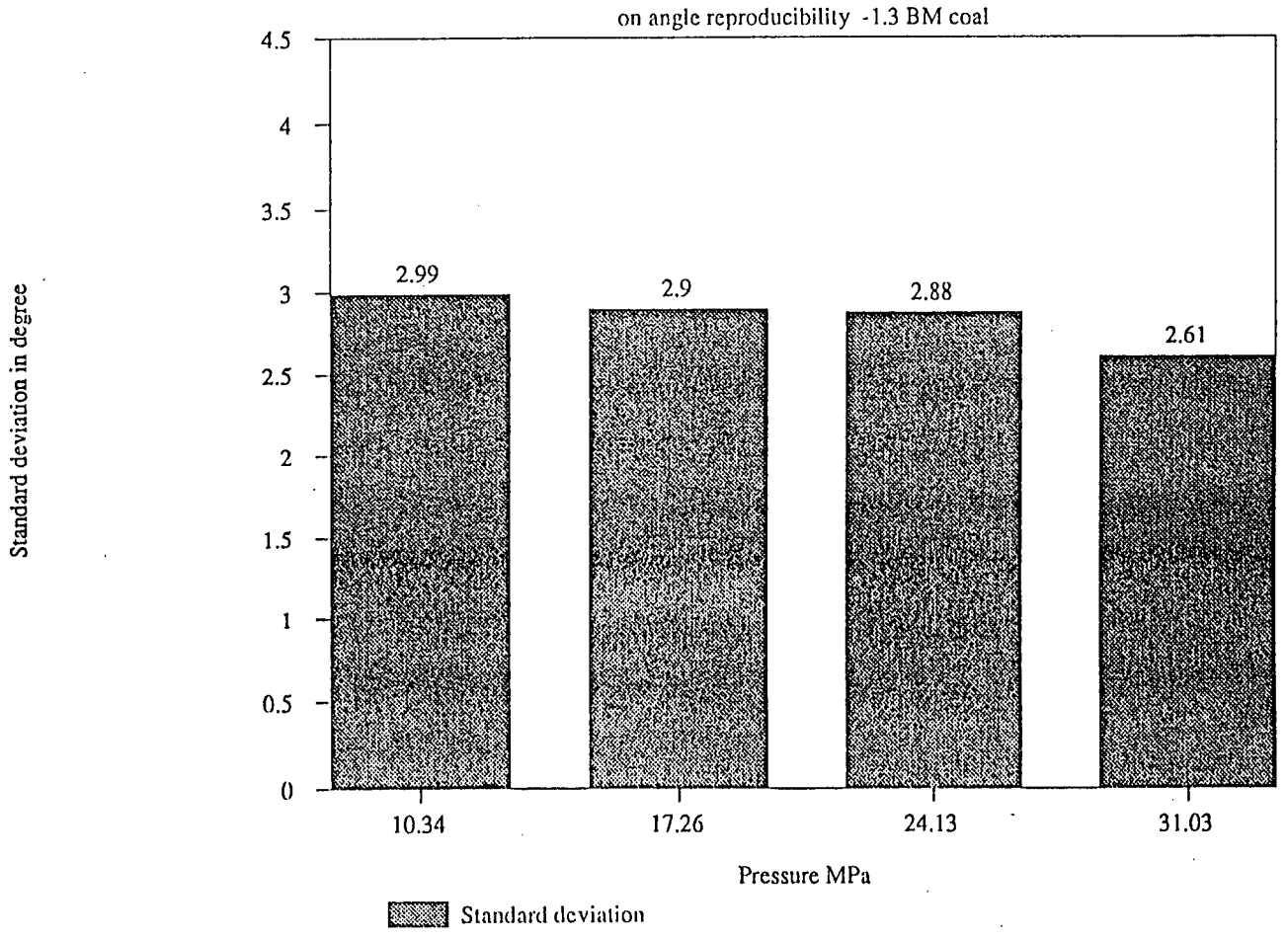

pellet-making pressure of 27.6 MPa caused only negligible particle crushing on the pellet surface. It is unlikely that this static pressing force would alter the coal surface properties noticeably.

In fact, the pellet-making pressure influenced the contact angle mainly through changing the fractional area of pores on a pellet surface. The increase in pressure can reduce both fractional area of pores and surface roughness of a pellet. The results in section 6.9 show that the surface roughness has a minor effect on contact angle hysteresis, whereas the fraction area of pores is the major factor. Detailed discussion of this effect will be given in the following sections.

6.7 POROSITY

The compressed pellet surfaces looked glossy and were macroscopically flat. Although tiny air voids and pores on the pellet surface are not detectable to the naked eyes, these pores exert a significant effect on the contact angles on pellet surfaces.

Cassie and Baxter <1944> considered the contact angle on a composite surface as an overall contributions from all the components in contact with the liquid drop, including the air pores as one of the components. The contact angle of water on these air pores is 180°. The effect of pores can be quantitatively corrected from the measured contact angle (the apparent contact angle) by utilizing the Cassie-Baxter equation (see Chapter 2).

$$\cos\theta = \sigma_1 \cdot \cos\theta_0 - \sigma_2 \qquad 2.1.10$$

However, such correction requires the fractional area of pores on pellet surface, σ_2, be quantitatively known.

There has been no direct technique, in practice, to measure the fractional area of pores on a pellet surface, while the pellet bulk porosity can be directly measured through some simple techniques. It was considered that there

must exist certain correlation between the fractional area of pores on pellet surface and the pellet bulk porosity. In the present study, the fractional area of pores on the pellet surface was estimated from the measurement of the pellet bulk porosity (see section 6.8).

For compressed pellets of coal powder, there are two types of porosities: the inter-particle porosity caused by the air trapped in between particles, and intra-particle porosity within individual particles. Unlike other inorganic minerals, coal is extremely porous. There are tremendous amount of tiny pores and capillaries with only several microns in diameter within coal particles. However, the total volume of these pores and voids within coal particles is much smaller than that trapped in-between particles. The pellet porosity is, therefore, controlled by inter-particle porosity.

In the present work, kerosene was used as a replacing liquid. The volume of kerosene needed to displace the air trapped in the pores within a pellet can be directly converted into porosity.

In the process, the pellet was brought into contact with kerosene. Because of the capillary effect, kerosene penetrates into, and saturates the pellet by displacing the air from it. The pellet weights before and after the

penetration were determined. The difference was the weight of kerosene penetrated into the pellet; which volume is equal to the volume of pores within a pellet.

Kerosene was used instead of water because it wets the coal surface and can penetrate into pellets of any density fraction of coal very quickly. The time required by kerosene to penetrate a pellet from bottom to top was less than 10 minutes. In order to ensure complete saturation, the pellet was left overnight in contact with kerosene until no further increase in the pellet weight was observed.

The porosity tests were conducted on all the density fractions of Line Creek coals. Results are shown in Figures 6.7.1 to 6.7.2. At low pellet-making pressure (below 13.8 MPa), the porosity decreases with the increase in pressure more quickly than that at high pressures. When pressure reached a certain value (above 24.1 MPa), further increases in the pressure had a negligible influence on porosity. It was believed that the pellet had reached the closest packing condition at this pressure. Further increases in the pressure could not change such a packing structure. Unless the pressure was extremely high and particle crushing took place, no further decrease in porosity was possible.

It can be observed from Figures 6.7.1 and 6.7.2 that the porosity versus pressure curve shifts downward to a

THE PELLET POROCITY vs. PRESSURE

Figure 6.7.1 For diff. density fractions of LC coal

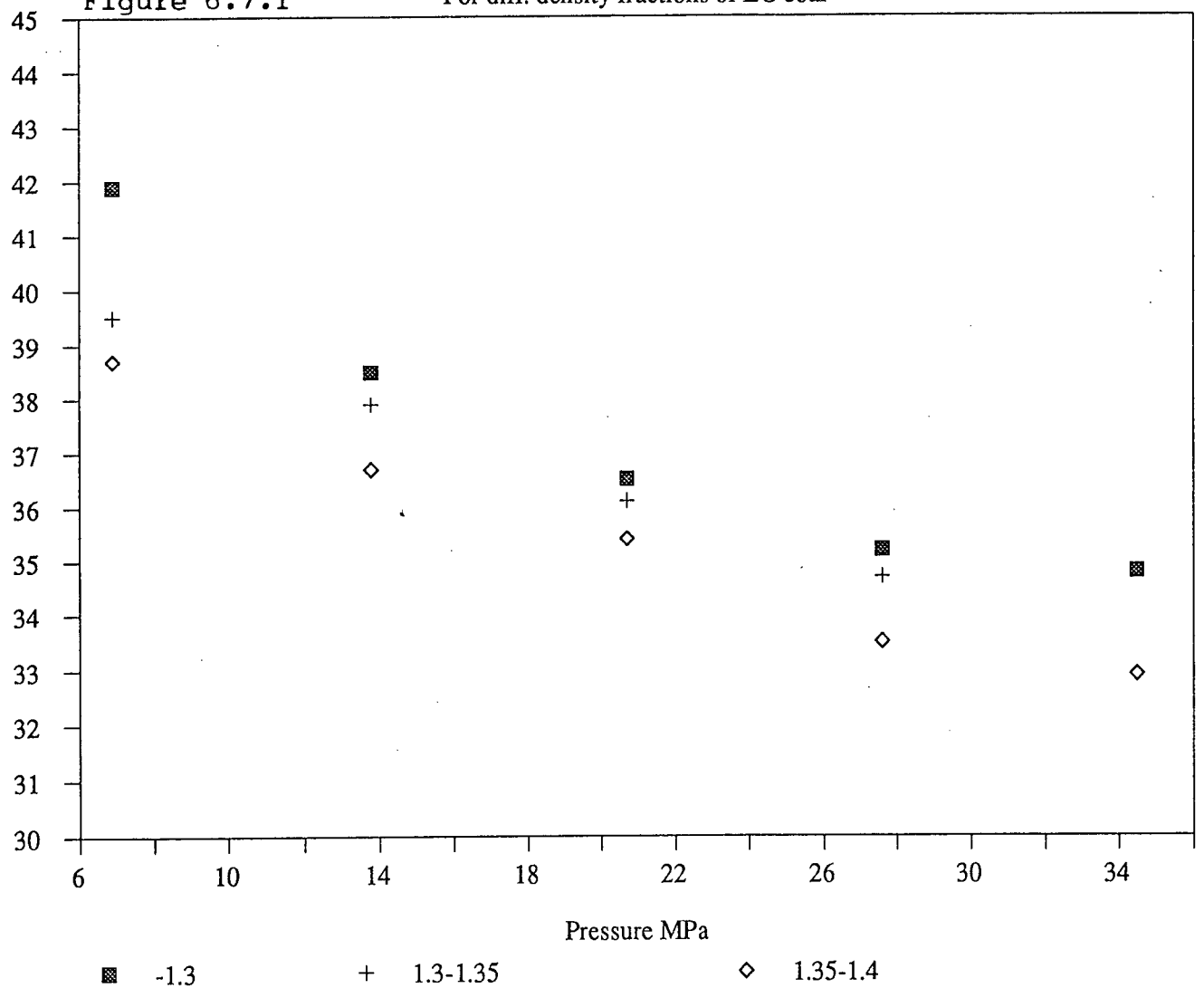

THE PELLET POROCITY vs. PRESSURE

Figure 6.7.2 For diff. density fractions of LC coal

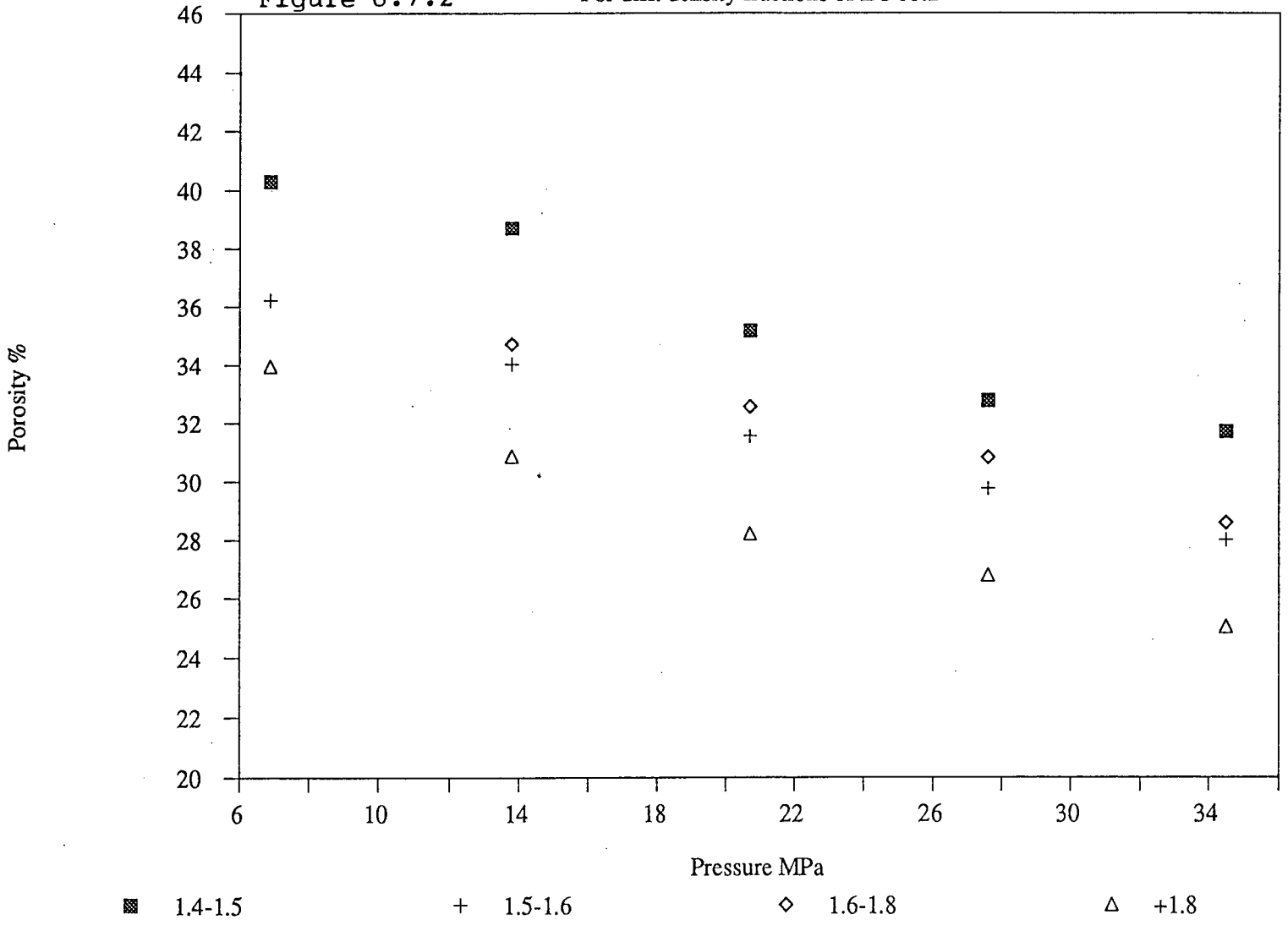

lower position as the coal density increases and they are parallel.

In the grinding process, the particle sizes of coal powders for all the density fractions were closely controlled to ensure that they had as narrow particle size distributions as possible. The particle size analysis results for different density fractions of the Line Creek coal are presented in Figure 6.7.3. For each density fraction, two different characteristic sizes (log mean and median) of the powder were determined.

As described in Chapter 8.5, the pellets made under the same pressure and from the materials with the same or similar size distributions, should be characterized by the same porosity. The porosity indicated above is the inter-particle porosity and it can be changed by pressure. The fact that all the curves are parallel (Figures 6.7.1 and 6.7.2) strongly supported such a conclusion.

While the pellet-making pressure cannot change the coal porosity (intra-particle), it only affects inter-particle porosity. The particles of the lower density fraction exhibited higher intra-particle porosities.

If the curves are extrapolated to the Y-axis, the intercepts are the porosities when powders are loosely piled

CHARACTERISTIC PARTICLE SIZES

Figure 6.7.3 For diff. density fractions of LC coal

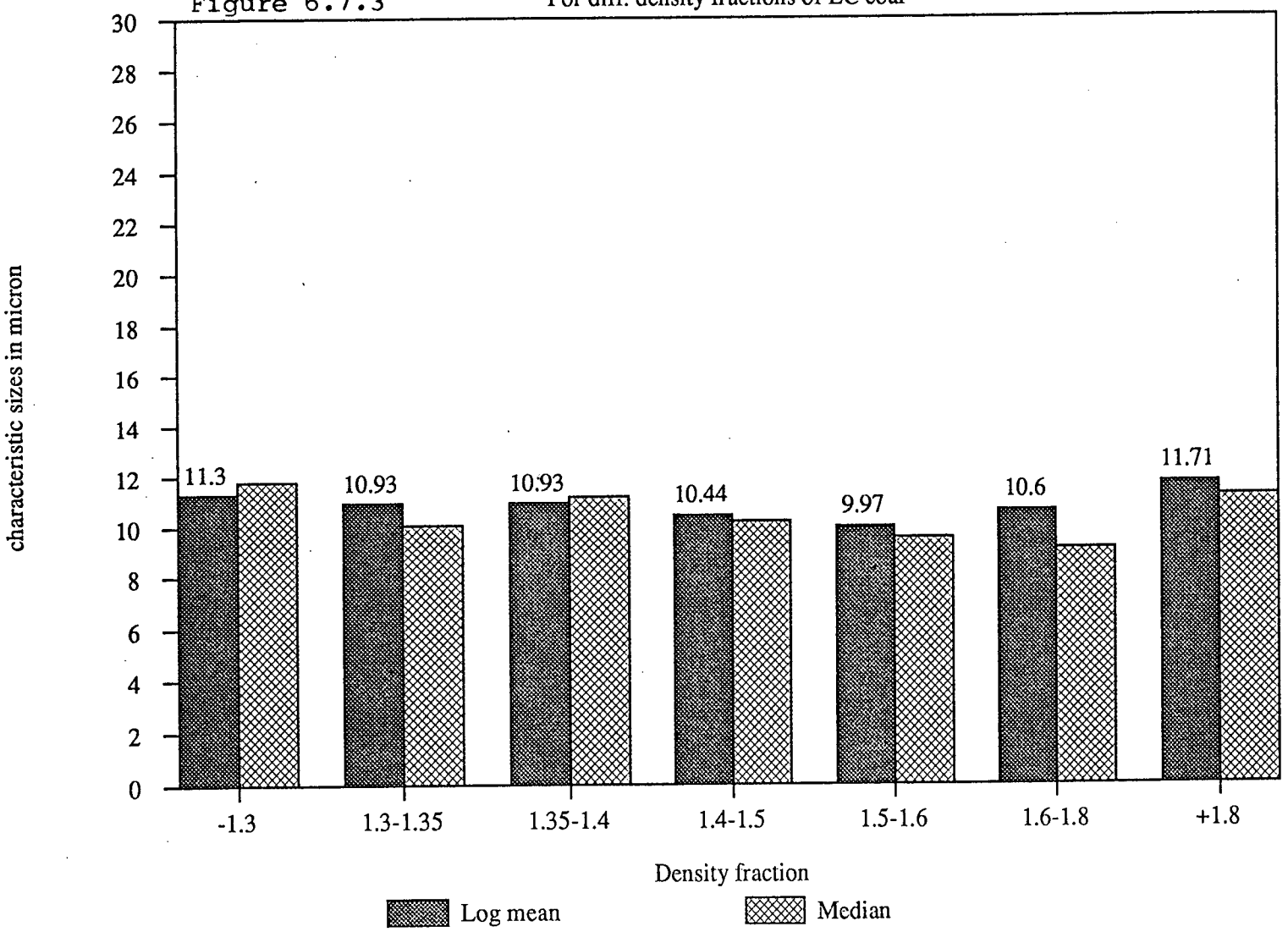

without any compression. It was observed that when pellet-making pressures above 20.7 MPa were employed, very good reproducibility for pellet properties could be obtained. When pellet-making pressure is decreased down to 6.9 MPa, the pellet properties such as porosity were severely scattered. Reproducibility is, therefore, better at higher pellet-making pressures. In chapter 8, a detailed discussion on the effect of pressure on column properties will be given. The conclusions obtained from those experiments are still applicable to pellets.

6.8 SURFACE EXAMINATION AND ASSUMPTION FOR FRACTIONAL AREA OF PORES

As has already been mentioned, it was assumed that there is a correlation between the fractional area of pores on a pellet surface and the pellet bulk porosity. The method was proposed to obtain the fractional area of pores through such a correlation.

The penetration behaviour of a liquid into a pellet through capillary effect gives the hint. Pellets compressed from powders are porous. In order to explain the penetration phenomenon, the pores inside the pellet are statistically equalized as a bundle of capillary tubes which are tortuous along the column's axis direction. This methodology was utilized in solving the present problem.

If under an idealized condition, a bundle of straight and thin capillary tubes are parallel perforating through a solid pellet along its axis direction, the correlation between the fractional area of pores and the bulk porosity inside the pellet can be easily obtained from a simple geometry derivation. By definition, the fractional area of pores is the ratio of the total cross section area of capillary tubes (pores) to the whole area of pellet bottom surface. That is

$$\phi = n \cdot \pi \cdot r^2 / \pi \cdot R^2$$

$$\phi = n \cdot r^2 / R^2 \qquad 6.8.1$$

where ϕ is the fractional area of pores, n the number of capillary tubes perforating through the pellet, r radius of the capillary tubes, and R the radius of the pellet. The porosity of the pellet is given by

$$\wp = n \cdot \pi \cdot r^2 \cdot h / \pi \cdot R^2 \cdot h$$

$$= n \cdot r^2 / R^2 \qquad 6.8.2$$

where $\wp$ is the pellet porosity, and h the height of the pellet. Combining Equations 6.8.1 and 6.8.2, one can get

$$\phi = \wp \qquad 6.8.3$$

That is, the fractional area of pores on pellet bottom surface is equal to the bulk porosity inside a pellet in an idealized condition.

For a pellet made of compressed powder, the capillary tubes inside it are tortuous and vary in radius. Under such a case, the question to be answered is whether the above conclusion still holds. One can consider that the

pellet is composed of a large number of thin layers piled one over another. They are so thin and the capillary tubes inside it are so short that the capillary tubes are considered straight and their radii uniform. Therefore, for these individual thin layers the above conclusion still holds. Additionally, the fractional areas of pores on those thin layers' surfaces should be statistically equal to one another. And so are the bulk porosities inside those layers. When all those thin layers are piled together to form a pellet, that is, for a compressed pellet of powder the Eq.6.8.3 still applies.

One possible problem which renders above assumption invalid is the crushing action that may occur on the outmost surface of pellet during compressing process. The breakage of particles on the top surface of the pellet can not only reveal new interfaces but also smear soft material on the top surface and lead to the blockage of capillary cross sections. If this occurs, the above assumption will be invalid.

To examine the possible breakage, the rate of penetration experiment was designed (for detail see Chapters 7 and 8), in which two groups of columns were made under exactly the same conditions. The basic idea for this was that if the breaking and smearing actions did occur, the fractional area of pores on the top and bottom surfaces of

the pellet should be smaller than that on any cross sectional surface inside the column. The penetration rate of a liquid into the column will be slower because of the existence of the thin layer inhibiting the process. Based on this idea, one group of the columns was specially processed to remove the thin layer on the outmost surface of the pellet using abrasive. The penetration rate should become higher for these columns if the breaking action occur.

The experimental results for the +1.8 fraction of Bullmoose coal are shown in Figure 6.8.1. The data points for the two groups of columns have fallen on the same line. This indicates that the postulated breaking action did not happen.

To confirm this conclusion, the Scanning Electron Microscopic (SEM) inspection was carried out to examine the surface state of the pellet surface under different magnifications.

The SEM photographs are given in Figure 6.8.2. As the magnification goes up, the glossy pellet surface becomes more and more visibly porous. When the magnification reached above 3000, the packing state of particles become clearly visible.

It can be seen from the photographs that the crushing

Test for fractional area of pores

Figure 6.8.1 on different cross sectional surfaces

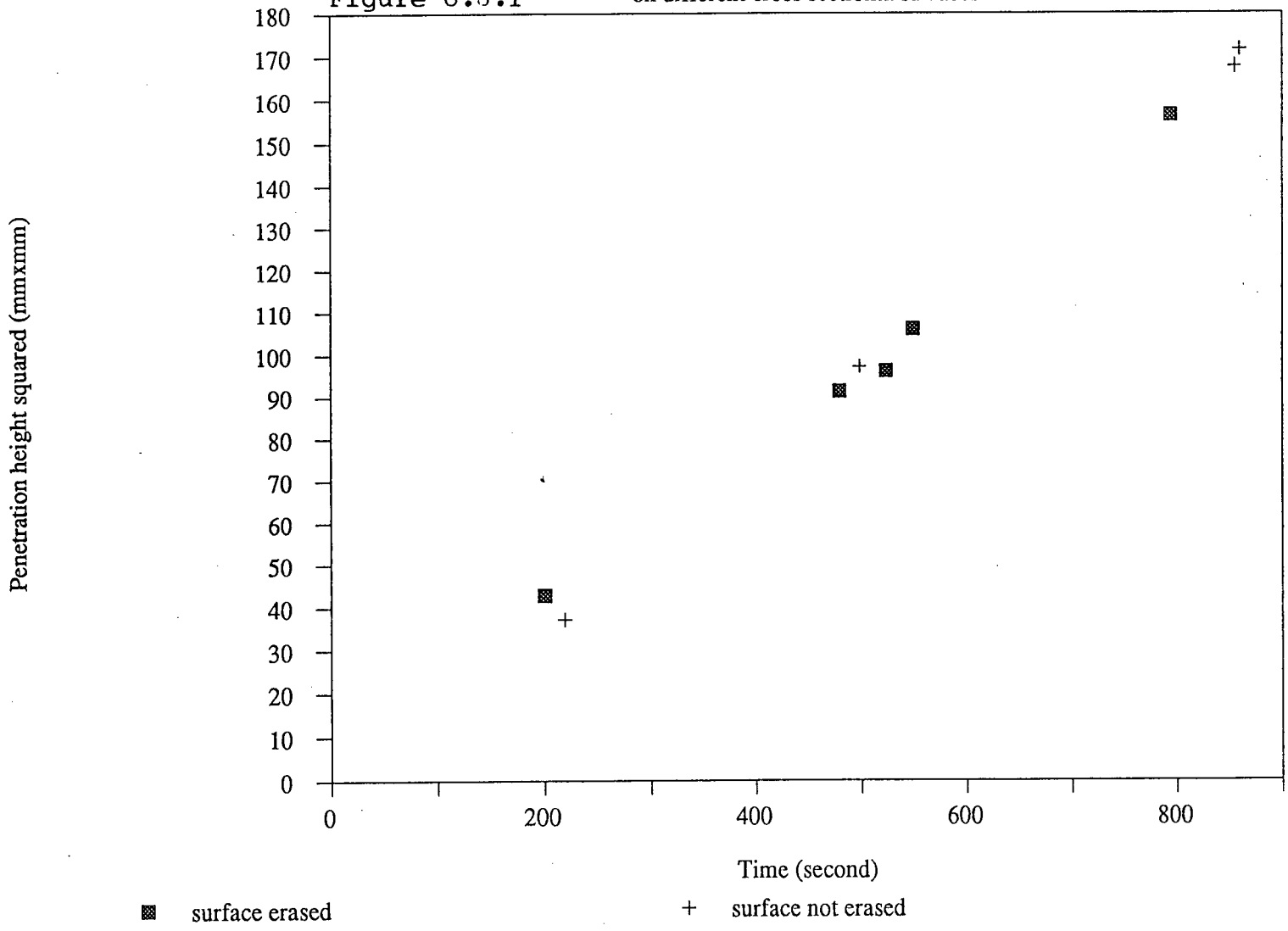

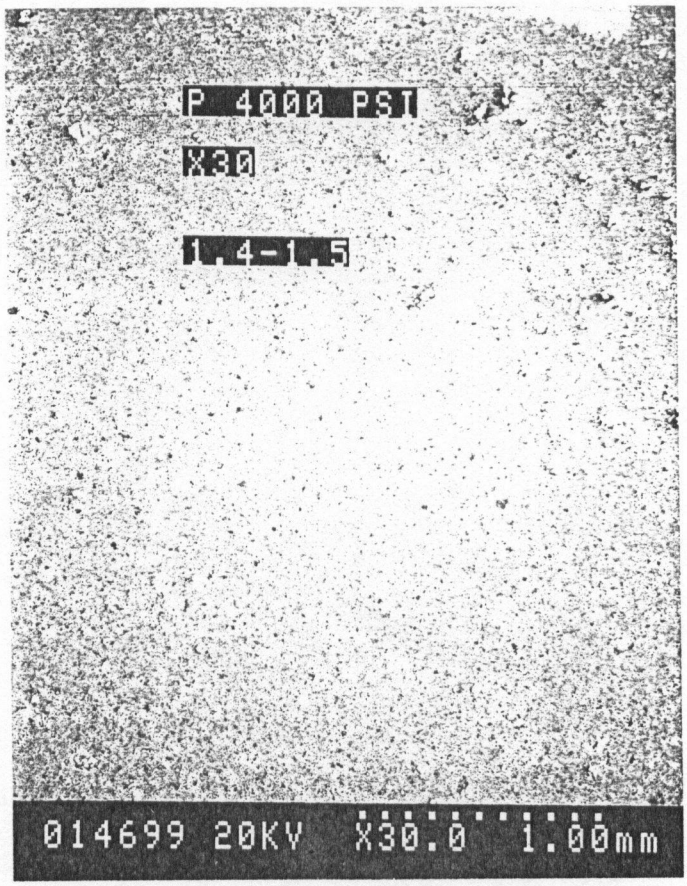

Figure 6.8.2(a) SEM photograph of a pellet surface magnified by 30 times.

The 1.4-1.5 density fraction of Bullmoose coal, pellet-making pressure is 27.6 mPa (4000 psi)

Figure 6.8.2 (b) SEM photograph of the same pellet surface Magnified by 2500 times

action has rarely happened. Only some plastic deformations occurred at some spots; and the asperity has been flattened. If any crushing action had happened, a cluster of small particles piled together would be found in the photographs.

6.9 A MODEL

6.9.1 A Compressed Pellet Surface Model

The SEM photographs shown in Figure 6.8.2 and the capillary properties of a pellet led to a model of compressed pellet surface shown in Figure 6.9.1. There are two domains on the model surface: solid and air pores. Under the pellet-making pressure as high as 27.6 MPa, all particles are closely squeezed together and the crevices between large particles will be filled with smaller ones. The particles on the outermost surface of the pellet are oriented with one side or edge touched at a plane; and some protruding edges are plasticly deformed or crushed locally to match this plane. Thus the compressed surface is very flat if the air craters and pores distributed on the pellet surface are not taken into account.

The pellet surface can thus be considered as a composite surface consisting of two domains i.e. solid and air pores. Such domains are very small (see Figure 6.8.2), they are less than 5 microns. Although under highly magnified SEM photograph the pellet surface looks very uneven, the pellet surface is still macro-scopically very flat.

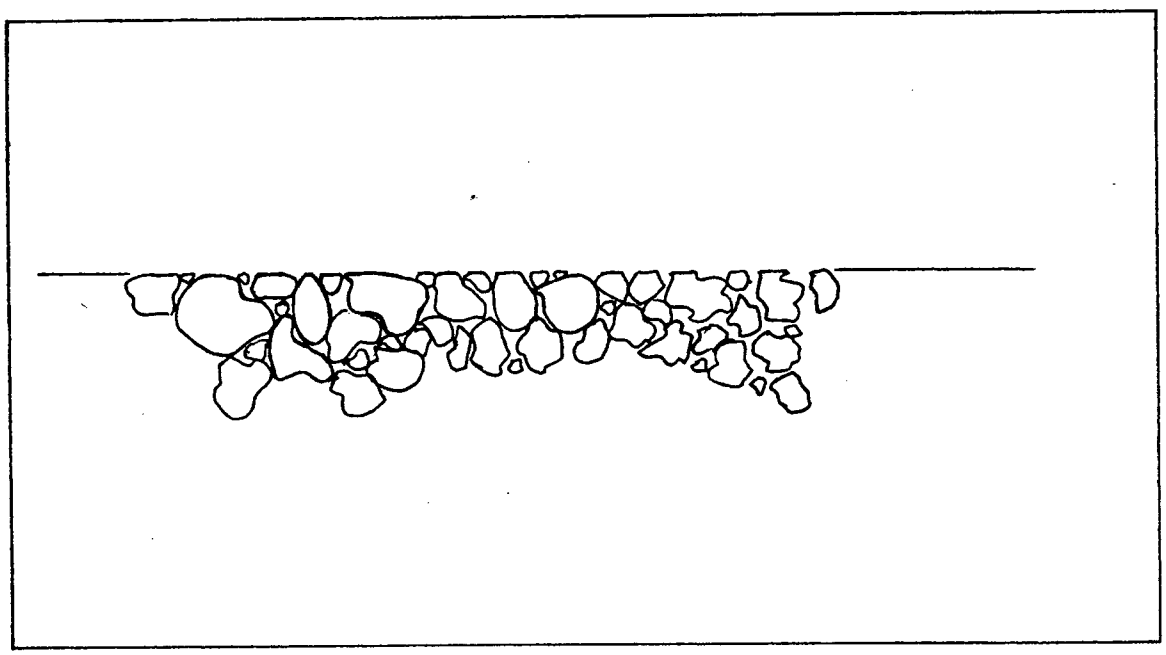

Figure 6.9.1 A model of compressed pellet surface

The distinction between macroscopic and microscopic states is arbitrary. Good <1979> set the limit of macro in a range of resolution of lines separated by about 0.02 - 0.1 mm. The scanning electron microscopic examinations (Figure 8.2.12) showed that the sizes of particles and air pores on pellet surface are normally smaller than 0.05 mm. Therefore, the compressed pellet surface is macroscopically homogeneous and flat.

As it is known (Chapter 2), the hysteresis is caused by two major factors: surface heterogeneity, and surface roughness. Therefore, both roughness and heterogeneity of the pellet surface can be investigated by the examining the contact angle hysteresis. It was observed that the heterogeneity could more significantly influence the hysteresis; while the surface roughness exhibited only a minor effect.

To test the effect of the surface roughness, it was first isolated from heterogeneity by coating the pellet surface with a very thin layer of kerosene. Because the wettability of monolayer coated surfaces is determined by the nature and packing of the outmost surface atoms or organic radicals, and not by the nature and arrangements of atoms in the solid substrate 10 to 20 Angstroms below the surface layer <Zisman, 1964>, the pellet surface thus coated

became homogeneous and its surface roughness remained unchanged. The surface roughness became the only factor affecting the contact angle hysteresis and could be easily detected.

The coating was prepared by placing the pellet on a cotton bed saturated with kerosene. Upon the contact, the kerosene spontaneously penetrates upward into the pellet through capillary effects and eventually reaches the top surface. The pores within the pellet become filled with kerosene and the particles on the pellet top surface are coated with a very thin layer of kerosene. The pellet surface, then, becomes homogeneous in respect to contact angle measurement. Such a pellet was used to test the contact angle hysteresis.

The observation showed that the contact angle hysteresis on all the kerosene-coated pellet surfaces was very small. It ranged from 3 to 8 degrees. In comparison, the hysteresis on the un-coated pellet surfaces all exceeded 90 degrees. The significant difference between the two hysteresis values confirmed that the pellet surface roughness played an insignificant role in contact angle hysteresis with heterogeneity being the predominant factor.

6.9.2 Contact Angle Correction And Comparison

As mentioned above, the surface heterogeneity has a significant influence on the contact angle measurement. The contact angle on a heterogeneous surface results from contributions of all the components (especially the air pores) on the pellet surface (see literature review 5.1.2). Therefore, the contact angle measured on a pellet surface (the apparent contact angle) needs to be corrected.

According to the pellet surface model proposed in Figure 6.9.1, if a liquid drop comes in contact with this proposed model surface, a composite configuration will undoutedly be established. Therefore, the Cassie-Baxter equation (2.1.10) can be readily applied

$$\cos\theta' = \sigma_1 \cdot \cos\theta_1 - \sigma_2$$

where $$\sigma_1 = A_{s1}/A'$$

and $$\sigma_2 = A_{1g}/A'$$

where A_{s1} is the total area of the solid in contact with the liquid; A_{1g} is the free liquid-air interface area under the liquid drop; and θ' and θ_1 are the measured contact angle and the contact angle on the solid without any pores, respectively.

Since the dimension of air pores on a pellet surface is extremely small (less than 10 microns), the curvature of the free liquid-air interface under the liquid drop can be neglected and considered to be flat. Therefore, σ_2 is equal to the fractional area of pores of the pellet surface. Under the assumption made in Section 6.8, it (and therefore σ_1) can be directly obtained from the pellet bulk porosity measurement.

In Figure 6.9.2, both the measured and corrected contact angles of water on the Line Creek coal were plotted versus ash content. The contact angle versus pressure data in Figure 6.6.2 were also corrected and re-plotted in Figure 6.9.3.

In Figure 6.9.2, the pellets for different density fractions of the Line Creek coal were made at the same pressure of 27.6 MPa (4000 psi). The pellet porosity value correponding to each density fraction can be read in Figures 6.7.1 and 6.7.2.

In Figure 6.9.3, the pellets of the -1.3 Line Creek coal were made at different pressures; and the corresponding pellet porosity values are obtained from Figure 6.7.1. It can be observed, from Figure 6.9.2, that the contact angle directly measured decreases noticeably with increase of the

pellet-making pressure. Apparently, this is due to the effects of both air pores and surface roughness.

The corrected value of contact angle, however, changes only at low pressures (less than 14 MPa). At higher pressures, the corrected contact angle values do not change when the pressure is further increased. This indicates that, at low pressure, the surface roughness of a pellet decreases very rapidly with increase in the pellet-making pressure. Once the pressure reaches 20.7 MPa, further increase of pressure does not change the pellet surface roughness notably.

For comparison, the contact angle was also measured on the polished surface of Line Creek coal. Some large chunks of Line Creek coal were selected, and flat surfaces were polished on these large particles. The contact angle values measured on these surfaces are shown below

Contact angles measured on polished
Line Creek coal surface (degree)

77.4	76.5	78.0	74.8	77.5	78.4	73.2	75.9
78.3	76.3	79.5					
Average: 76.9							

CONTACT ANGLE vs ASH CONTENT OF LC COAL

Figure 6.9.2 both the measured and the corrected

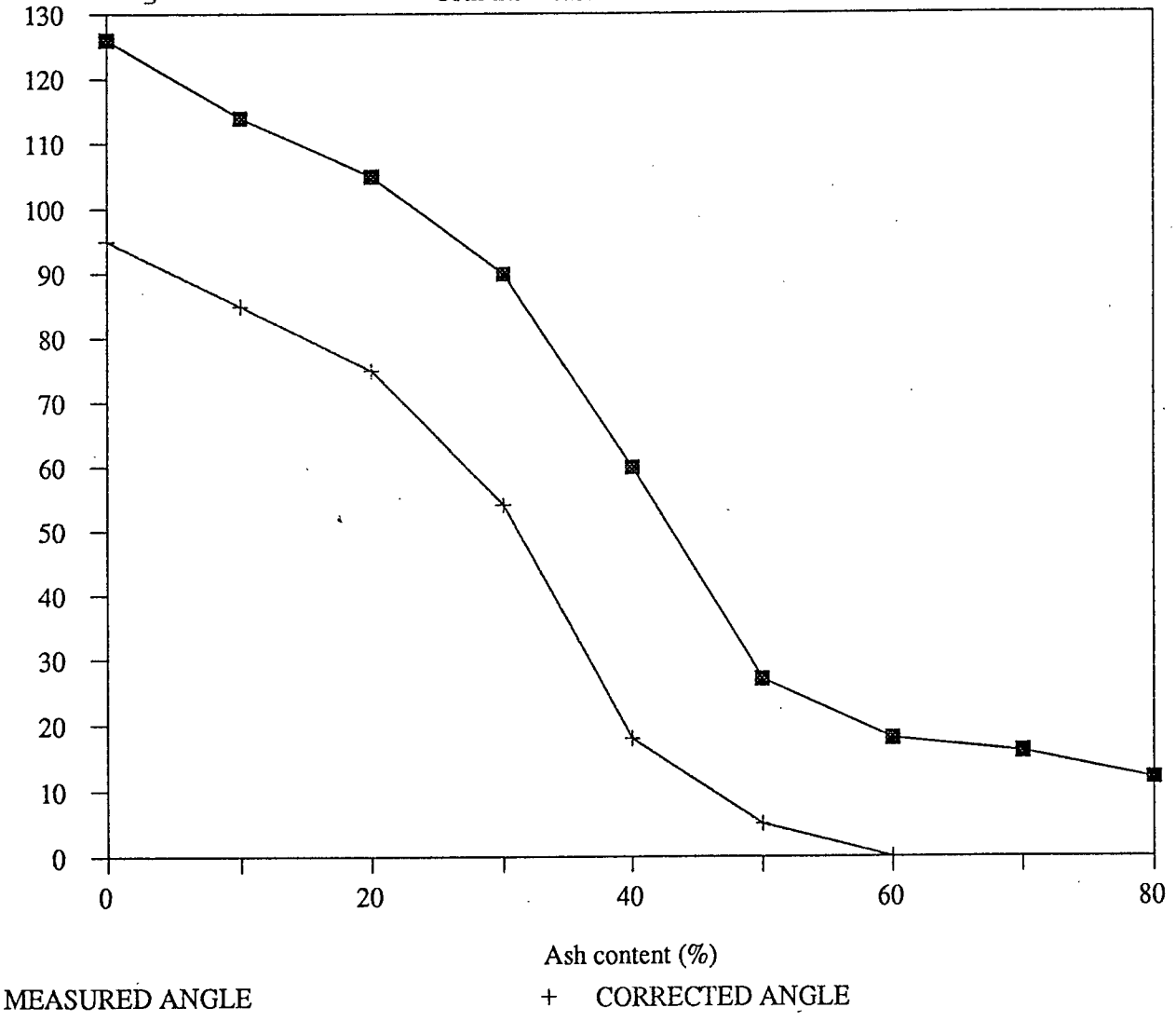

CONTACT ANGLE vs.PELLET-MAKING PRESSURE

Figure 6.9.3 Line Creek coal -1.3 density fraction

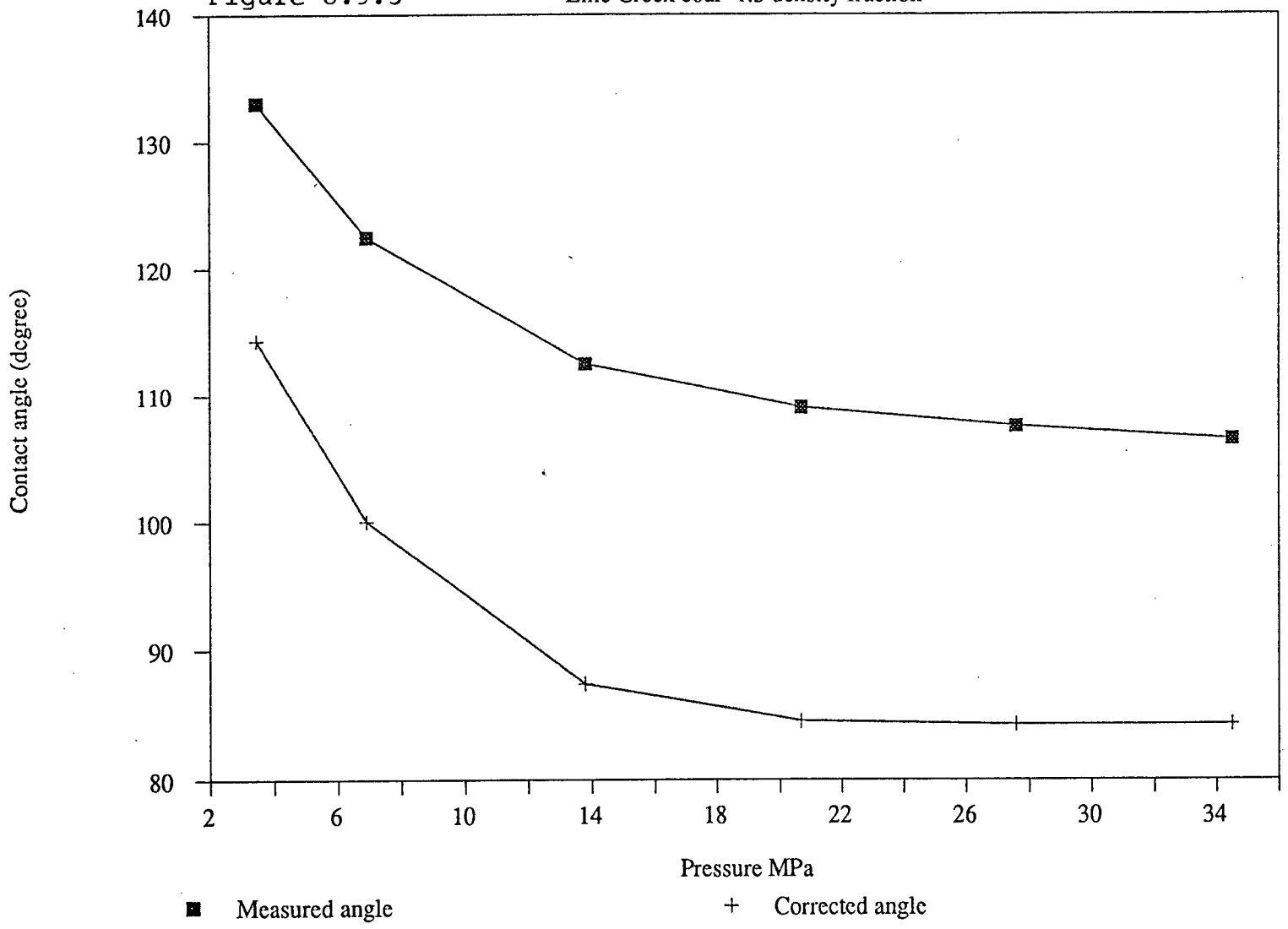

The average angle value on polished coal surface 76.9 degrees.

According to the results shown in Figure 6.9.3, the apparent contact angle on the pellet surface of -1.3 density fraction of Line Creek coal is as large as 107 degree. While the corresponding corrected contact angle is 84.2 which is still greater than the angle value measured on polished surface. It should be remembered that the polished coal chunk was randomly selected from the sample. It may be a mixture of the different density fractions. On average, its density is greater than 1.3 g/cm^3. Therefore the contact angle on the polished coal chuck is lower than the corrected angle on the pellet surface of -1.3 density fraction.

6.10 SUMMARY AND DISCUSSIONS

The contact angle on fine coal particles was measured in this project by making pellets 2.54 cm in diameter and 0.3 to 0.5 cm in height under high pressure (6.9 to 28 MPa) An artificial surface formed on the pellet was utilized to accommodate liquid sessile drop and measure the contact angle. The pellet surface was macroscopically flat and glossy.

The contact angles were measured in two different ways. either directly through the goniometer by constructing a tangent to the sessile drop profile at the three phase contact point, or with the use of camera attached to the goniometer telescope to take a photograph of the sessile drop profile. The standard deviation of the angle values measured on the pellets ranged from 2.06 to 3.71 degrees.

The profile data on the photograph were taken by digitizer. According to these data, the contact angle was calculated by using a computer program developed by Rotenberg, et al.<Rotenberg, Boruvka, and Neumann, 1983>. The reproducibility of this method was high with the standard deviation of the measured angle values being ±0.32 degrees.

Because of the effect of heterogeneity and surface roughness, the angles measured by the two methods were different. While the value obtained by the first method reflects the contact angle of water on the higher energy surface area, the value obtained by the second method is the weighed average of the angle values on all the components of the heterogeneous surface.

The effect of the sessile drop size on the advancing contact angle was also tested in the present work. The drop size was increased in two different procedures. In the first, a drop of preset volume was formed on the micro-syringe tip. Then it was lowered with the whole set of syringe and rested on the pellet surface as a free sessile drop. To increase the drop size, the same procedure was followed to form another independent sessile drop with larger size. In the second procedure, the drop size was enlarged by incremental addition of the liquid to the previous sessile drop.

The results show that the contact angle measured following the first procedure increases continuously with the size of the drop.. After the drop size is increased to a certain value, the drop size effect diminishes and contact angle changes only randomly around a certain value. This phenomenon is attributed to the contact angle hysteresis arising from the surface roughness.

In the second procedure, the contact angle initially decreases with the drop size, but then starts to increase resulting in a V-shaped curve. The gravitational force, the surface roughness, and kinetic energy introduced when increasing the drop size by incremental addition play the major roles in the process.

At the beginning when sessile drop size is small, each addition of the incremental drop increases the sessile drop height substantially. The gravitational force tends to push the sessile drop downwards. The kinetic energy which is large relatively to the energy barrier helps the three phase contact line to overcome the energy barrier and expand. Thus the sessile drop assumes a lower value of the contact angle. Further increase in the drop size only makes the drop expand horizontally. The effect of gravitational force and kinetic energy diminishes, and the surface roughness becomes predominant. In this range, the contact angle increases with the drop size.

The contact angle of water on the coal pellet surface was tested versus time. For lower density fractions (-1.3 to 1.4-1.5), the sessile drop and the contact angle are very stable even after several hours (see Figure 6.5.1). However, they are not stable on higher density fractions of coal (1.5-1.6 to +1.8). Because the contact angle on higher coal

density fractions is small, the water drop starts to penetrate into the pellet during the experiment.

Although the pellet surface was glossy and flat visually, the pellet is actually very porous both inside and on its surface. The porosity of the pellet is represented by the value of the pellet bulk porosity. The pellet porosity is composed of two parts: intra-particle porosity and inter-particle porosity. The intra-particle porosity is the porosity inside an individual coal particle. Its value is higher for lower coal density fractions and becomes smaller for higher density fractions. The inter-particle porosity is the space between particles. The pellet-making pressure has a major effect on the inter-particle porosity; the inter-particle porosity decreases when the pressure is increased.

With the use of the data obtained from a Scanning Electron Microscope a pellet surface model was proposed. In the model, the coal particles on the outmost surface of the pellet orient themselves or experience some local plastic deformation to match a plane. Thus the compressed pellet surface is very flat, provided that the air pores distributed on the pellet surface are neglected.

Under the Scanning Electron Microscope, the pellet surface was found to consist of two major components: solid and air. The directly measured contact angle (the apparent

contact angle) results from the contributions from the wettability of both components. According to the proposed pellet surface model, a correction procedure applying Cassie-Baxter equation was employed to correct the effect of air component on the contact angle value and transform the apparent contact angle into the real contact angle on the solid alone.

The corrected angle value (real angle value) was 84.2 degree on a -1.3 g/cm^{-3} density fraction of the Bullmoose coal. The contact angle measured on a polished surface of the coal chunk was about 76 degrees. These two values are more comparable and the difference seems to be quite acceptable.

CHAPTER 7

THE RATE OF PENETRATION TECHNIQUE

7.1 INTRODUCTION

From a more practical point of view, assessment of hydrophobicity/hydrophilicity through the study of the wetting characteristics of a mass of particles may provide a more realistic correlation with the performance of various technological processes. Coal is a heterogeneous material, only its overall composition can reflect its behaviour and, therefore, must be taken into account. The rate of penetration is one of such measurement. Many authors have derived theoretical and semi-empirical relationships <Bruil and Good, 1979> to interrelate the velocity of the rising liquid with interfacial parameters such as contact angles. The measurements of contact angles by such capillary rise methods have the advantage over the optical method (direct contact angle measurement) in that it gives a "mean" value obtained for a large number of particles which are not polished and are not contaminated from the abrasive agent used in the polishing.

Compression of powder into a pellet, on the other

hand, can raise the porosity problem. When the contact angle on the compressed pellet surface is much smaller than 90°, penetration of the liquid into the pellet is significant and sessile drop equilibrium can not be consequently established. Under such conditions, the dynamic contact angle technique is likely to be more reliable <Crawford et al. 1987>.

As one of the dynamic contact angle techniques, the rate of penetration method shows considerable promise. However, in spite of the simplicity of this method, it has not been employed extensively. The publications on this method are relatively few compared with direct contact angle measurements over the past decade.

Conventionally, the rate of penetration technique is based on the unopposed penetration of a liquid through a compressed column of powder, and is regarded as a relative technique for that a liquid with a known contact angle with the solid is needed to calibrate the column tortuosity constant; the influence of many factors such as column packing density and particle size has not been carefully studied. In addition, major problems associated with this method are incomparability of results obtained at different times by different persons originating from the fact that the columns were packed by manual tapping. The effect of the difference in wettability between the powder material and

the wall of holding column which can affect the column penetration front and make the accurate penetration front measurement difficult has not been evaluated either.

In the present work, a new approach for the rate of penetration method is studied to overcome these problems. High pressures (up to 27.6 MPa) were applied and precisely controlled to produce closely compacted column sufficiently strong to withstand handling and facilitate the experiment.

In addition, a new approach to calibrate the column tortuosity constant was introduced in the present work. This new approach may make the rate of penetration method from a relative technique to a absolute one, since the liquids with a zero contact angle on all the tested solid may not be required any more.

7.2 THEORY AND TECHNIQUES

7.2.1 Basic Theory

The capillary driving force for a liquid in a cylindrical tube of radius r is

$$\Delta P = 2\gamma_{lv} \cdot \cos\theta / r \qquad 7.2.1$$

where ΔP is the LaPlace pressure across the curved interface, γ_{lv} is the liquid surface tension, and θ are the liquid contact angle on the capillary .

One application of this theory is to measure the pressure, P', necessary to balance the LaPlace pressure, ΔP, which drives the liquid into a capillary bed <White, 1982>; the contact angle can then be calculated using Eq.5.2.1.

Washburn <1921> combined the capillary driving force for a cylindrical tube of radius r (Eq. 5.2.1) with the Poisseulle equation for viscous drag under conditions of steady flow

$$8\mu \cdot h/r^2 \cdot dh/dt = \Delta P \qquad 7.2.2$$

where μ is viscosity of the fluid, h the length of penetration in time t, r capillary radius, ΔP the pressure drop and obtained

$$d(h^2)/dt = \frac{r^2}{4\mu} \cdot \left(\frac{2\gamma_{lv} \cdot \cos\theta}{r} - \Delta\rho gh\right) \qquad 7.2.3$$

where $\Delta\rho$ is the difference in density between the liquid and the surrounding medium, g the gravitational acceleration, θ contact angle.

If the capillary is horizontal or the penetration length is small, the term $\Delta\rho gh$ in equation above can be neglected, and one can obtain:

$$d(h^2)/dt = \frac{r \cdot \gamma_{lv} \cdot \cos\theta}{2\mu} \qquad 7.2.4$$

The applicability of this equation to a powder column has been theoretically justified by Crowl and Wooldridge <1967> and Szekely et al. <1971>. In the case of a powder column, the capillaries inside the column are tortuous and their radii are not constant and vary from point to point within the column. The overall column penetration process is an average on all these individual process. The observed rate $d(h^2)/dt$ must correspond to an average value of r" in the place of r in Eq.5.2.4. Therefore a tortuosity constant

K was introduced in place of r <Ely and Pepper, 1944>, and Eq.5.2.4 becomes

$$d(h^2)/dt = \frac{K \cdot \gamma_{lv} \cdot \cos\theta}{2\mu} \qquad 7.2.5$$

The tortuosity constant K is a hypothetical mean radius.

Theoretically, the adsorption of some fluid molecules can take place onto the column particle surfaces. It was shown that <Good, 1973, Good and Lin, 1976 and White, 1982> if a porous body is initially devoid of any adsorbed film of the liquid that penetrate it, and if the molecules of the fluid are not transported ahead of the liquid at a rapid rate by diffusion, then the rate of penetration will be faster than that predicted by Washburn equation because of the spreading pressure. That is

$$r\gamma_{lv} \cdot \cos\theta/2\mu \leq d(h^2)/dt \leq r \cdot (\gamma_{lv} \cdot \cos\theta + \pi_e - \pi_0)/2\mu \qquad 7.2.6$$

where π_e is the equilibrium spreading pressure, and π_0 the spreading pressure at zero time

$$\pi_e = \gamma_s - \gamma_{sv} \qquad 7.2.7$$

$$\pi_0 = \gamma_s - \gamma_s(t=0) \qquad 7.2.8$$

The major drawback of applying the Washburn equation

to the powder column is that there has been no direct means to obtain the value of tortuosity constant K. Using Laplace equation, White<1982> obtained a quantitative equation defining the effective radius of the compressed powder column by thermodynamic derivation

$$r_e = 2\wp/(1-\wp)\rho\Psi \qquad 7.2.9$$

where $\wp$ is the column porosity, ρ is the mass density of the powder in the column, and Ψ is the specific area of powder per gram. If the porous column consists of identical vertical capillaries of radius r_e through a solid substrate of density ρ, one can derive the same relationship geometrically.

However, for the Poiseulle drag on the permeating liquid in compressed powder column, the hydrodynamic validity of Eq.7.2.9 for r_e in Eq.7.2.2 has never been tested. Once the application of Eq.7.2.9 to Eq.7.2.2 for compressed column could be justified, the tortuosity constant K in Eq.7.2.5 could conveniently be calculated from Eq.7.2.9.

In the common application of the Washburn equation, the tortuosity constant K was obtained by calibration in which the same measurement with a liquid that is known to have zero contact angle is taken, assuming the pore

structure and the penetration process to be the same as in the runs with different liquids. The measured rate of penetration value and cos0=1 inserted into Eq.7.2.4 allow the K to be calculated.

7.2.2 Techniques

In actual application of the Washburn equation to a porous column, a known weight of the dried powder was placed in a 0.8 cm diameter glass tube with an attached scale, and consolidated by manual tapping. The lower end of the column was supported on a small plug of cotton wool covered with a disc of filter paper. The packed tube containing the powder was dipped into a dish of the liquid and the time and corresponding penetrating height are recorded. This technique has been used with glass powder <Ely and Pepper, 1946>, carbon blacks <Studerbaker and Snow, 1955>, and pigments <Crowl and Wooldridge, 1967>.

It was observed<Good and Lin, 1976> that the rate data in studies of this kind generally exhibit a serious statistical scatter. A major reasons for this scatter are the non-uniformity of the column packing density and the change in structure of the packed bed with wetting<Neumann and Good, 1979>. Another drawback of this technique is the difficulties associated with obtaining the tortuosity

constant K in the Washburn equation. In the traditional calibration method, it is difficult to find a particular liquid which should have zero contact angle on the solid to be tested. This requirement has made the method only applicable to a limited number of specific materials like quartz etc. Since for majority of solids, it is an impossible task to find such a liquid.

To overcome above mentioned problems, in the modification discussed in this work, the hydraulic mounting press to make more closely packed column under accurately controlled higher pressures was employed. The columns thus made were much more uniform in its interior structure. The reproducibility and accuracy of the rate of penetration technique was substantially improved.

In addition, the tortuosity constant K in the Washburn equation has been brought under control in the modified technique, and has been calculated simultaneously with the contact angle. The old calibration method was not used any more and the problems associated with it ceased to exist. The detailed discussion will be presented in the following sections.

7.3 EXPERIMENTAL

7.3.1 Materials

The materials tested and the initial sample preparation procedure for the rate of penetration method are the same as that in the direct contact angle measurements. The same pulverized coal samples as used in the direct contact angle measurements were again utilized in this section.

The penetration liquids used include kerosene and water. The deodorized kerosene used was the product of J.T.Baker Chemical Co., Phillipsburg, NJ. The implication to use kerosene as the major penetration liquid is that, in addition to its lower hazardous degree compared to other chemicals, it is extensively used in the contemporary coal flotation as an effective and cheap collector. More importantly, rate of penetration is a quantitative measure of the capability of different fractions of coal to be wetted by kerosene. The coal fractions having higher lyophicity towards kerosene could be floated better in the real flotation processes when kerosene is utilized as a collector.

7.3.2 Column-Making

A MET-A-TEST mounting press was employed to make the column under high pressures ranging from 3.4 to 20.7 MPa. The column made in such a way is strong enough to withstand experimental handling without the holding glass tube; and the packing density can be accurately controlled and easily varied.

A series of coal powder samples ranging from 3 to 15 grams were weighed. They were individually put into the MET-A-TEST mounting press mould which was carefully cleaned with degreased cotton. Following the close of the upper cylindrical cover, the timer was set for five minutes, and pumping the hydraulic pressing to pre-set pressure was started. The pressing pressure drops slowly during the pressing period due to the squeezing of particles to a more closely packed configurations. This may need frequent adjustment.

7.3.3 Rate of Penetration Measurement

For each coal sample, a group of four to eight columns with different weights ranging from 3 to 12 grams were made under exactly the same conditions so that the columns with different heights but the same properties

(packing density) were obtained as shown in Figure 7.3.1.

The column diameter was 25.4 mm. Their heights, ranging from 5 to 25 mm, were accurately measured using vernier gauge with precision of ±0.025 mm.

A porous bed made of degreased cotton was prepared and fitted into a small container of 10 mm in height and 40 mm in diameter; then the bed was saturated with penetration liquid. The column, after its height was accurately measured with vernier gauge, was vertically rested gently on the bed; and at the same time, timing was started. A clearly visible horizontal penetration line along the cylindrical wall heading upward can be observed. No additional strong illumination was required. The liquid would flow slowly through the column and eventually reach the top.

The end of timing was selected when half of the top surface area was wetted. For each column, one data point, that is, the column height versus the time required for liquid to flow through the whole column was recorded. The same procedure was repeated for other columns. Finally a number of data points equal to the number of columns were acquired. It should be emphasized that these columns, though having different heights, must be made under exactly the same conditions (i.e. same pressure). For each data point, a straight line connecting this point and original of H_2

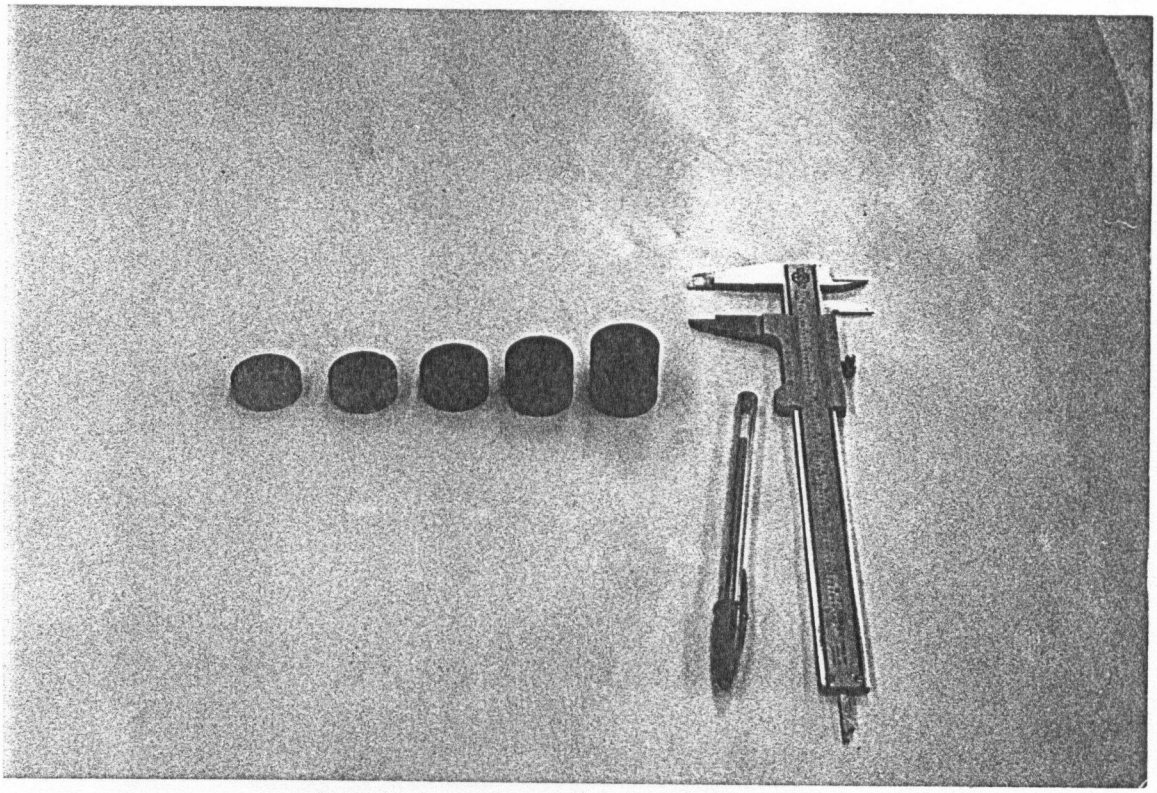

Figure 7.3.1 The columns made for the rate of penetration test

versus T coordinate could be drawn. Therefore each measurement in comparison to the conventional method could be considered as an individually repeated run because the lines thus obtained were for different columns. After these points were regressed, the linearity of the regressed line could be considered a representation of the reproducibility for the experiment.

Columns must be made at a minimum of two different pressures because the rate of penetration from the columns made under different pressures were essential parts of this technique in the calculation of contact angles.

7.3.4 Viscosity and Surface Tension

The Ostwald viscometer was used to measure the viscosity of liquid. According to the time of flow of a given volume V of the liquid through a vertical capillary tube under the influence of gravity, the viscosity was calculated by Poiseulle's law in the form

$$\frac{dV}{dt} = \frac{\pi r^4 (p_1 - p_2)}{8\mu L} \qquad 7.3.1$$

where dV/dt is the rate of liquid flow through a cylindrical tube of radius r and length L and (p_1-p_2) is the difference

in pressure between the two ends of the tube. In practice, above equation, at constant temperature, is simplified for a given total volume of liquid and a given cylindrical tube

$$\mu/\rho = Bt \qquad 7.3.2$$

where t is the time required for the upper meniscus to fall from the upper to the lower fiducial mark and B is an apparatus constant which is determined through calibration with a liquid of known viscosity (e.g. water).

The liquid surface tension was measured using a Cenco-du Nouy Tensiometer.

CHAPTER 8

RESULTS AND DISCUSSIONS <II>

8.1 APPLICABILITY TEST

The conventional method of making a penetration column is by manually tapping the tested powder held in a glass tube into a column<Crowl and Wooldridge, 1967, Szekely et al., 1971, Bruil and van Aartsen, 1973, Good and Lin, 1976>. Very low pressures (below 3.5 MPa) were exerted on the powdered material within the holding glass tube during tapping. Whether the Washburn equation is still applicable to the columns made under very high pressures up to 27.6 MPa has not been tested. In this section, the applicability of the Washburn equation has been first verified.

8.1.1 Some Features

Some preliminary observations were made to examine the features and behaviour of the liquid penetrating into columns compacted under high pressure. Because the columns in the penetration process were unwrapped, the penetrating lines were clearly observable. The periphery of the

penetrating front surface was apparently within a well defined horizontal plane.

The penetration in the interior of the columns was also examined. Since the column diameter is 25.4 mm and is much greater than diameter of a conventional one (8 mm), the crosswise penetration difference could be more perceptibly manifested. Observing from the top surface of the column, one could find that the wetting front surface, after certain time of penetration, would not reach the top surface of the column all over at the same time; instead, it emerges in a local area first and quickly spreads. This implies a non-flat penetration front surface. Sometimes the wetting front surface emerges from the central area and spreads outward concentrically which indicates a dome shaped wetting front within the column; on the other hand the wetting front was also observed to emerge peripherally and spread inward. Occasionally, the wetting front may start from one side of the top surface of the column and finished at another, which means a tilted wetting front.

The magnitude of the latitude differences between the highest point and the lowest one on the penetration front surface is not only a matter of probing the uniformity of the column interior penetration behaviour, but also a numerical index indicating the precision of the method. These details will be discussed in the next section.

Other features concerning the method are: the possible swelling of the columns after soaking with penetrating liquid; the lowest applicable pressure; and possible breakage of particles in the pressing process. All these variables were tested and will be discussed in the following sections.

One of the advantages of this technique is that the total surface area penetrated by liquid within a unit height of column is much greater than that in a conventional method. Therefore it is more statistically representative. In addition, the total height can be lowered to a range of 0.5 to 2 cm compared with the conventional range of 4 to 10 cm. Thus the penetration process could be subject, to a much less extent, to the effect of gravitational force.

8.1.2 Precision and Linearity

Since it is more difficult to measure accurately penetration distances on short columns, a different approach as described in section 7.3 was employed. The use of a vernier could reach absolute accuracy of ±0.0025 cm which is undoubtedly quite sufficient.

However, another aspect which affects the accuracy is the estimation of ending time point which was taken when

half of the top surface area of the column was wetted. If the liquid wetting front zigzagged up and seriously, not only the judgement of the ending time of penetration but also the method itself is questionable.

In order to answer these questions, the time when the wetting front starts to emerge from the top surface, and the time when the whole top surface was wetted, were measured. From the time span, the ruggedness (i.e. the maximum altitude difference between the lowest and the highest point) of the imaginary penetration front surface could be calculated.

The experiment was conducted on the 1.4-1.5 density fraction of the Bullmoose coal. Five columns with different heights were made in series and kerosene was used in the experiment. T_0 is the time after which the penetrating front emerges; and T_1 is the time for the whole top surface of the column to be wetted. The penetration distance from time T_0 to T_1 would be the altitude difference between the highest point and lowest point on the penetration front surface. The magnitude of this distance is a numerical representation of the ruggedness of the penetration front surface.

The middle point between T_0 and T_1, in the actual measurement, was taken as the ending point of penetration, T. The T values and corresponding column heights were

tabulated (Table 8.1.1). The H^2 versus T regression result was shown in the lower part of the table. According to this regression equation, the penetration distance between time T_0 to T_1 could be calculated. Here

$$H^2 = 0.625 \cdot T$$

so

$$\text{Ruggedness} = H(T_1) - H(T_0) \qquad 8.1.1$$

$$= \sqrt{(0.625 \cdot T_1)} - \sqrt{(0.625 \cdot T_0)}$$

The ruggedness is defined as the maximum altitude difference on the penetration front surfaces. The ruggedness results shown in Table 8.1.1, are in the range from 0.18 to 0.6 mm. This indicates that the penetration front surfaces are quite flat considering the very large penetration front area with diameter of 25.4 mm.

Since in the real observation, the reading was taken when one half of the total penetration front surface emerged, the observation error of the penetration front was limited to a half of the ruggedness, that is, 0.09 to 0.3 mm. This is a quite high accuracy which may hardly be attained by the conventional graduation method. In addition the graduation method only the peripheral penetration line can be observed while the interior penetration behaviour is ignored.

The applicability of the Washburn equation to this

Test for the ruggedness of penetration front
on 1.4 - 1.5 density fraction

Table 8.1.1 P = 13.8 MPa

Measured data					Calculated reesults		
H mm	HxH	T0 sec	T1 sec	T1-T0	H0 mm	H1 mm	H1-H0
0.00	0	0	0	0	0.00	0.00	0.00
6.63	43.96	73	77	4	6.76	6.94	0.18
7.30	53.29	93	100	7	7.63	7.91	0.28
16.70	278.89	454	464	10	16.85	17.03	0.18
23.66	559.79	871	901	30	23.34	23.73	0.40
34.61	1197.85	1882	1955	73	34.30	34.96	0.66

* H in mm is the liquid penetration height

** T0 in second is the time when penetration front emerge from the top surface of the column

*** T1 is the time when the whole penetration front emerges out

Regression Output

Constant	0
Std dvtn of HxH Est	4.171126
R Squared	0.999918
No of Observation	6
Degrees of Freedom	5
T Coefficient	0.625173
Std dvtn of Coef.	0.001927

HxH = 0.625 T

method can be simply tested by observing linearity and reproducibility of H versus T curves and by observing whether different wettability materials have different penetration lines.

A series of experiments has been conducted on different density fractions of the Bullmoose coal to test the linearity of the rate of penetration curves, under constant column-making pressure of 6.9 to 20.7 MPa. The penetration data for all six density fractions were plotted in Figures 8.2.1 to 8.2.3. Essentially all the lines pass through the origin. The linearity of the penetration curves, which is numerically represented by the R squared value ($0 \leq R \leq 1$), and other regression results are presented in Tables 8.2.1 to 8.2.4. As can be seen, all six R squared values for the regression lines are close to unit value illustrating very good linearity.

In terms of reproducibility, it should be emphasized that the data acquisition procedure in the present method is quite different from that of the conventional one. In the conventional method, all the experimental points on a penetration curve were obtained from one column by taking the reading of penetration length at different times. Accordingly, the experimental reproducibility was tested by examining deviation of the penetration curves obtained from different columns.

In the present method, only one point was obtained on a column. To draw a penetration line including 5 data points on it, an equal number of columns with different heights are needed to carry out five separate penetration tests. Each data point could be considered independently as a repeated run. Therefore, the linearity denoted by R squared and standard deviation, at the same time, were also the measures of the experimental reproducibility.

Judging from both the R squared value and the standard deviation of the coefficients, it can be confirmed that the Washburn equation is well applicable to the columns made under very high pressures.

8.1.3 Height Limit

As the column reaches certain height, the H^2 plotted versus T begins to deviate from linearity; this is especially true for columns made under lower pressures (see Figure 8.1.1). Several factors may attribute to this phenomenon. The gravitational force could be one of them. By recalling the general rate of capillary penetration equation 7.2.3

$$d(h^2)/dt = \frac{r^2}{4\mu}\left(\frac{2\gamma_{lv}\cdot\cos\theta}{r} - \Delta\rho gh\right) \qquad 7.2.3$$

APPLICABILITY TEST OF WASHBURN EQUATION

Figure 8.1.1 PRESSURE 17.2 MPa, +1.8 FRACT'N BM COAL

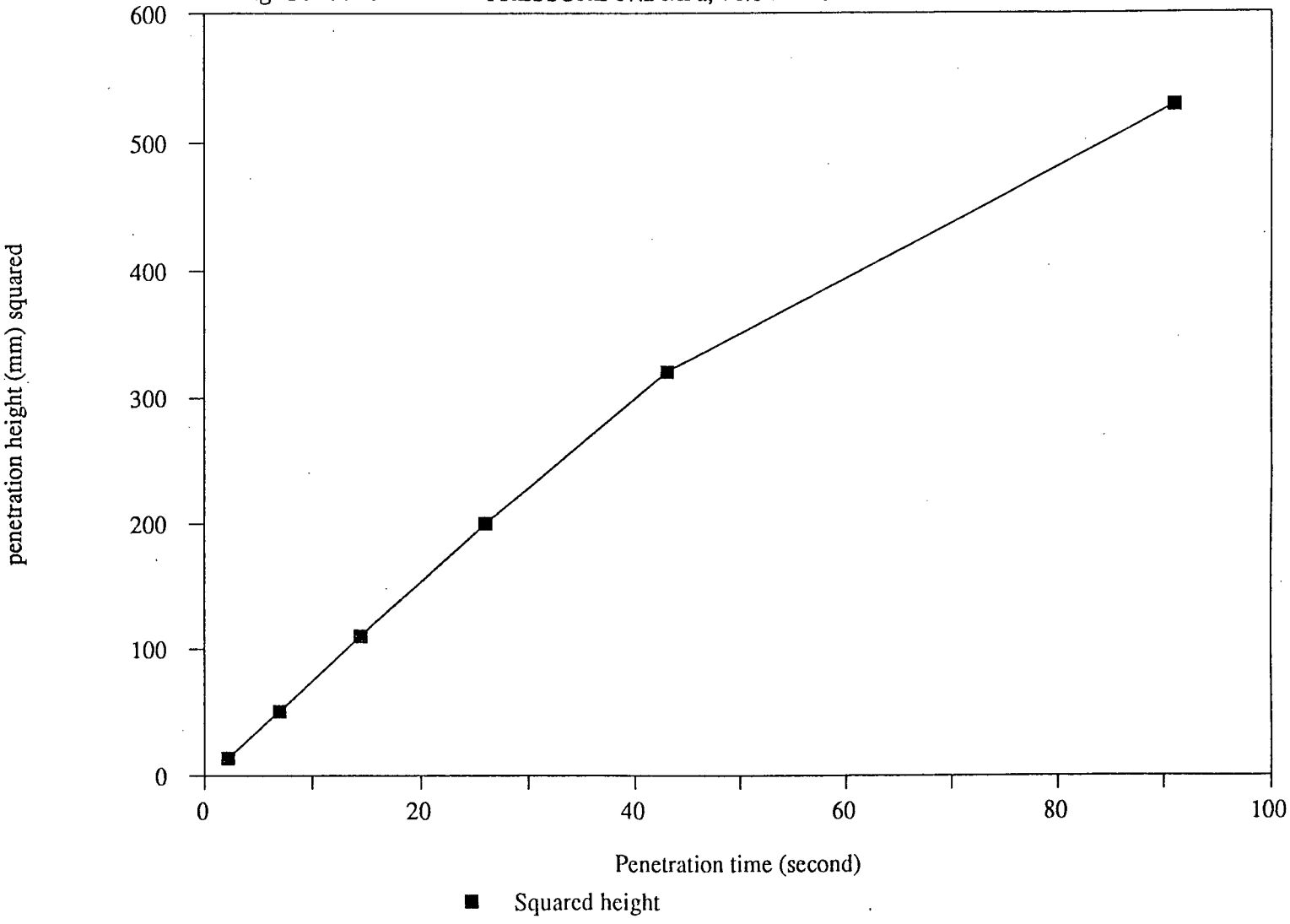

one can notice that, in the actual application of the Washburn equation to the packed column, the term $\Delta\rho gh$ was neglected under the condition that penetration height, h, was small. Once h is large, the term $\Delta\rho gh$ is comparable in magnitude with the first term in the parenthesis in the above equation and H^2 versus T curve can lose linearity and level off. It was observed that the columns packed under lower pressures had lower height limits than the columns packed under higher pressures. This could be due to the influence of the column packing pressure on capillary diameters distribution inside the column. As the pressure increases, the capillary radii, r's, in column become smaller, while the first term $2\gamma_{lv}\cdot\cos\theta/r$ in the parenthesis of Eq.7.2.3 becomes greater relative to the second term $\Delta\rho gh$. Therefore the column height limit raises up when pressure is increased.

The friction between the mould of a MET-A-TEST press and the column within it in the column-making process could be another affecting factor of column height limit. The friction, when the column is high enough, could considerably alter the packing densities at different parts of the column and, as a consequence, change the penetration behaviour and make the rate of penetration line to be non-linear. The influence of the friction will be further discussed in section 8.5.

8.2 COLUMN-MAKING PRESSURE

It was claimed<Good and Lin, 1976, Neumann and Good, 1979> that the column-making pressure had no perceptible effect on the penetration rate. This conclusion was obtained from the columns which were packed by manual tapping. However, it may not be true in the case of a machine-compressed column. The column-making pressure should have a pronounced effect on both the rate of penetration of liquid into the columns and the measurement accuracy, and reproducibility. The rationality behind this is that a change in column-making pressure could change the porosity (or the equivalent capillary diameter) within the column, and consequently, as shown in Eqs.7.2.4 and 7.2.5, alter the rate of penetration. Under higher pressure, the column could be more uniformly packed and measurement accuracy and reproducibility should be higher.

8.2.1 The Effect of Pressure on Reproducibility and Linearity

In order to study the effect of column-making pressures on the experiment reproducibility and linearity, several series of columns from different coal density fractions were compressed under various pressures and were

Rate of penetra. curves for columns of

Figure 8.2.1 -1.3 fraction made under dif. pressures

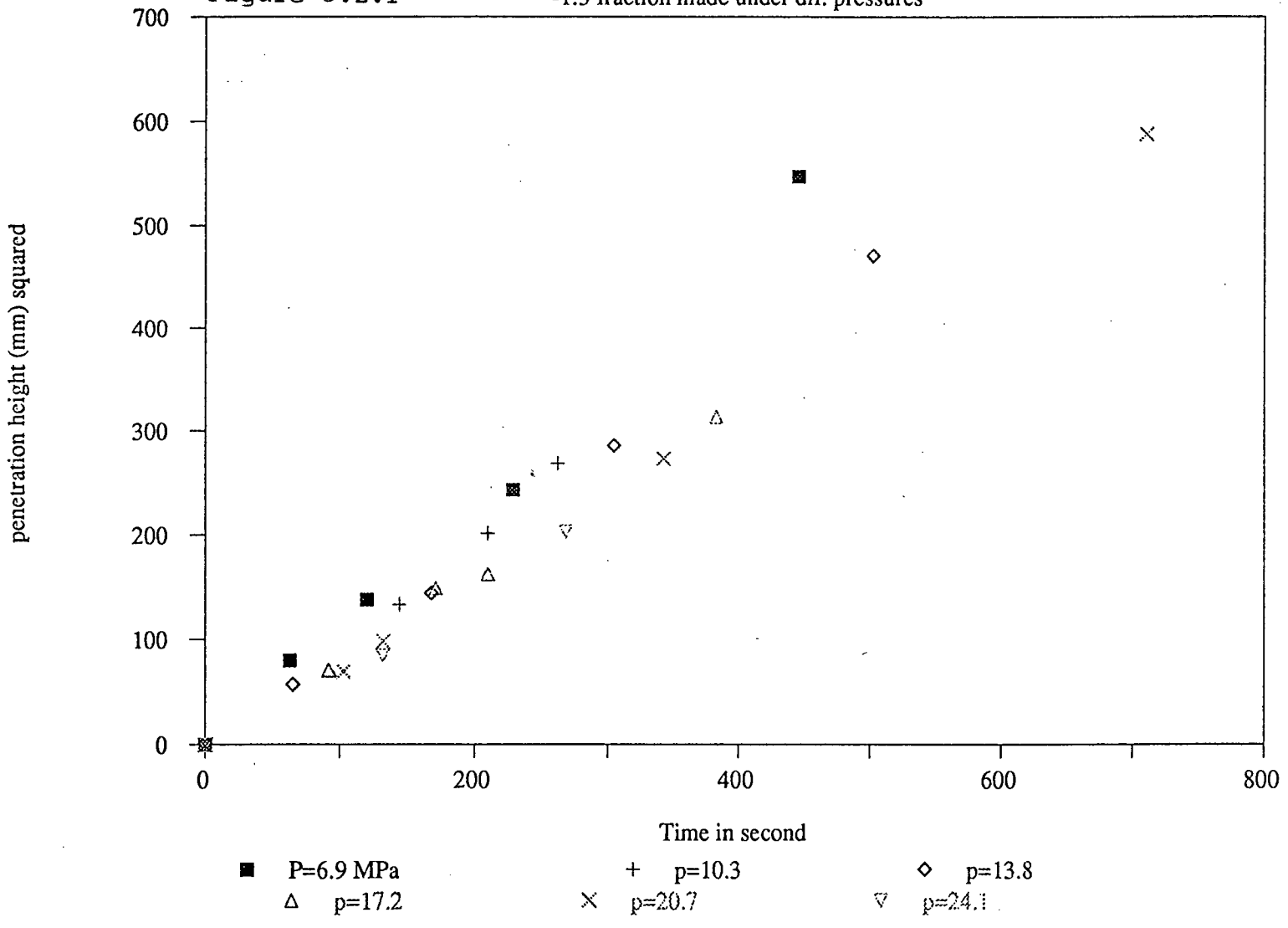

Rate of penetra. curves for columns of

Figure 8.2.2 1.3-1.4 made under dif. pressures

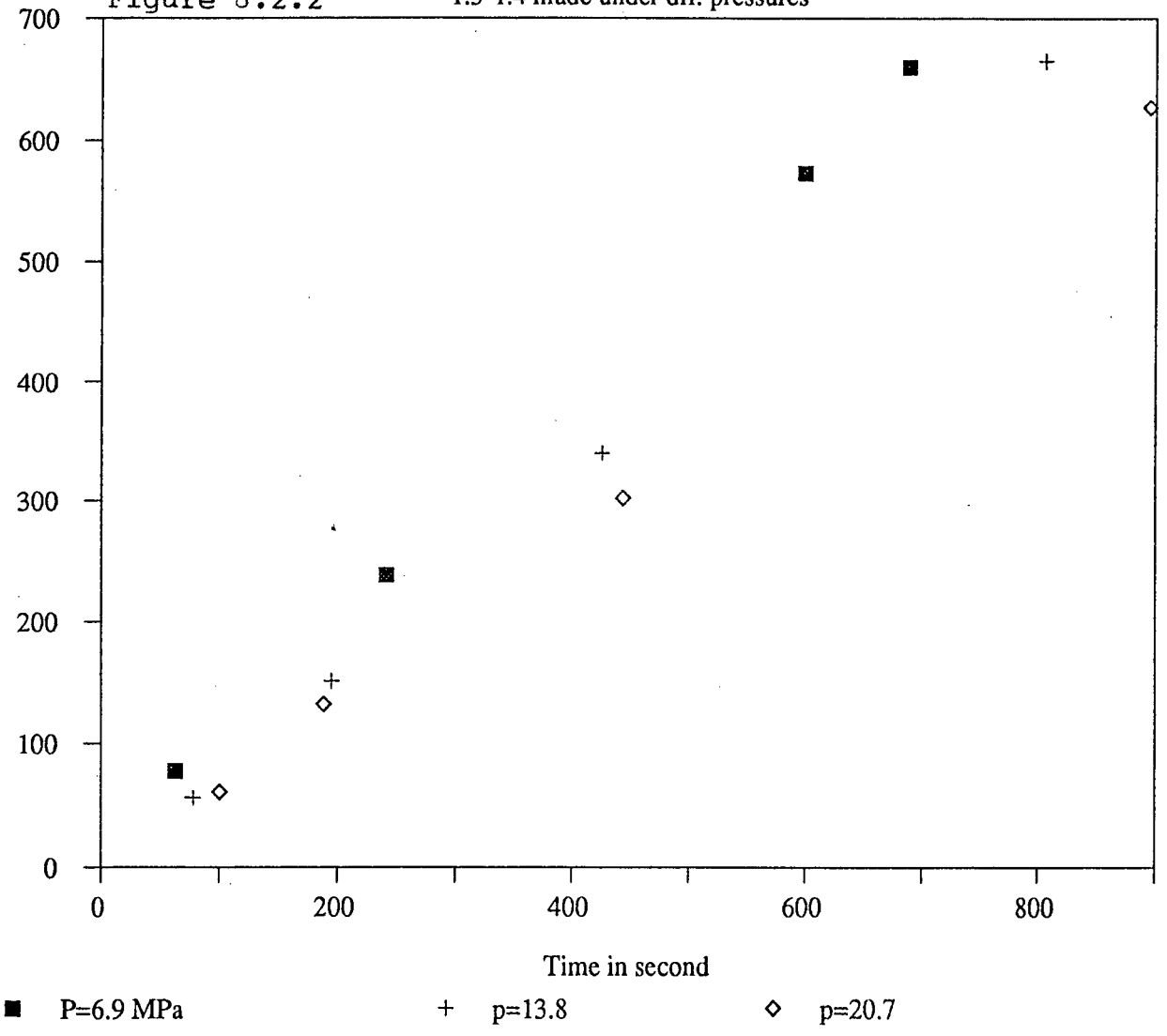

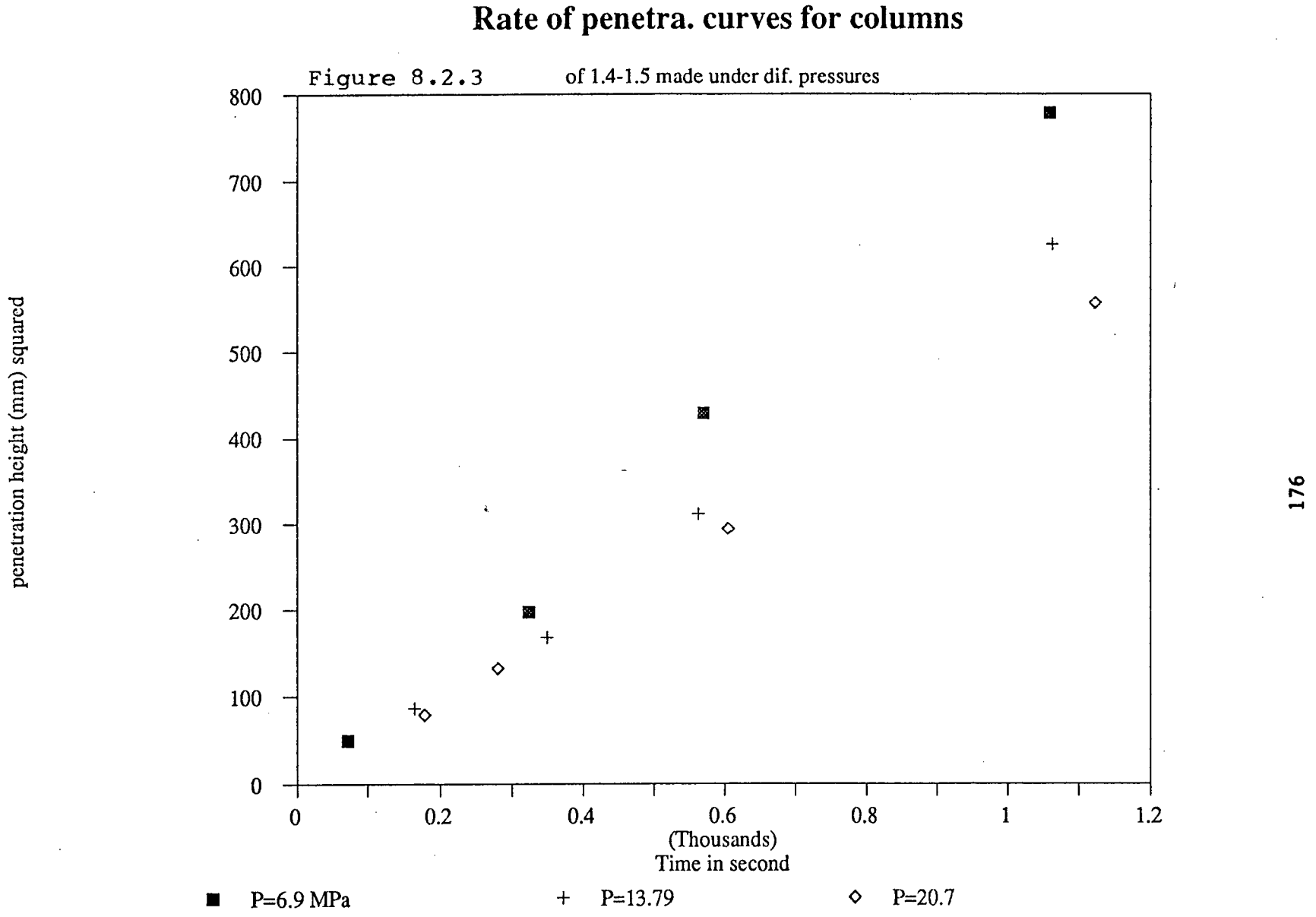
Rate of penetra. curves for columns
Figure 8.2.3 of 1.4-1.5 made under dif. pressures
penetration height (mm) squared
800
700
600
500
400
300
200
100
0
0
0.2
0.4
0.6
0.8
1
1.2
(Thousands)
Time in second
P=6.9 MPa
P=13.79
P=20.7

Rate of penetra. curves for columns of

Figure 8.2.4 1.5-1.6 made under different pressures

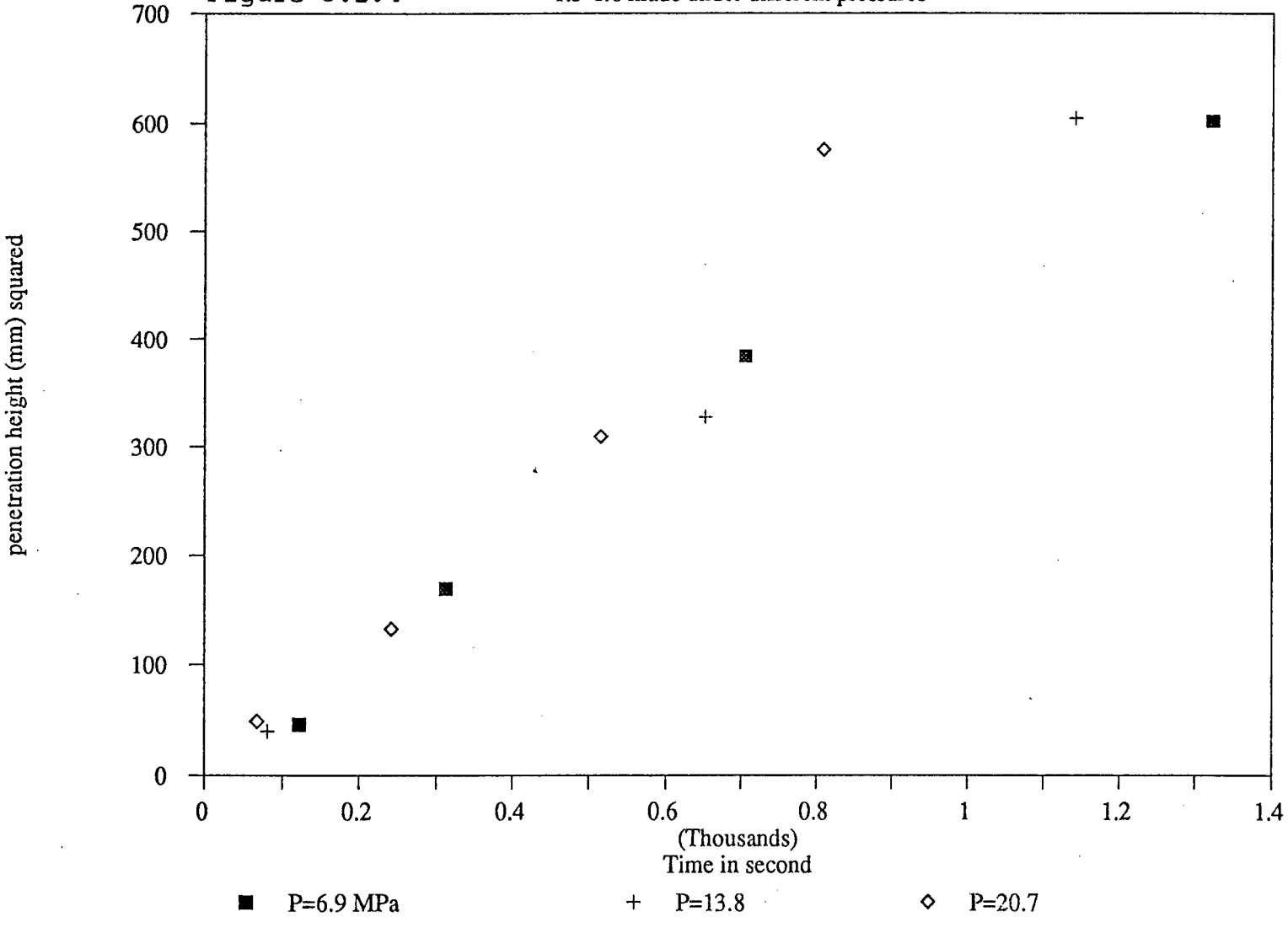

Rate of penetra. curves for columns of

Figure 8.2.5 1.6-1.8 made under different pressures

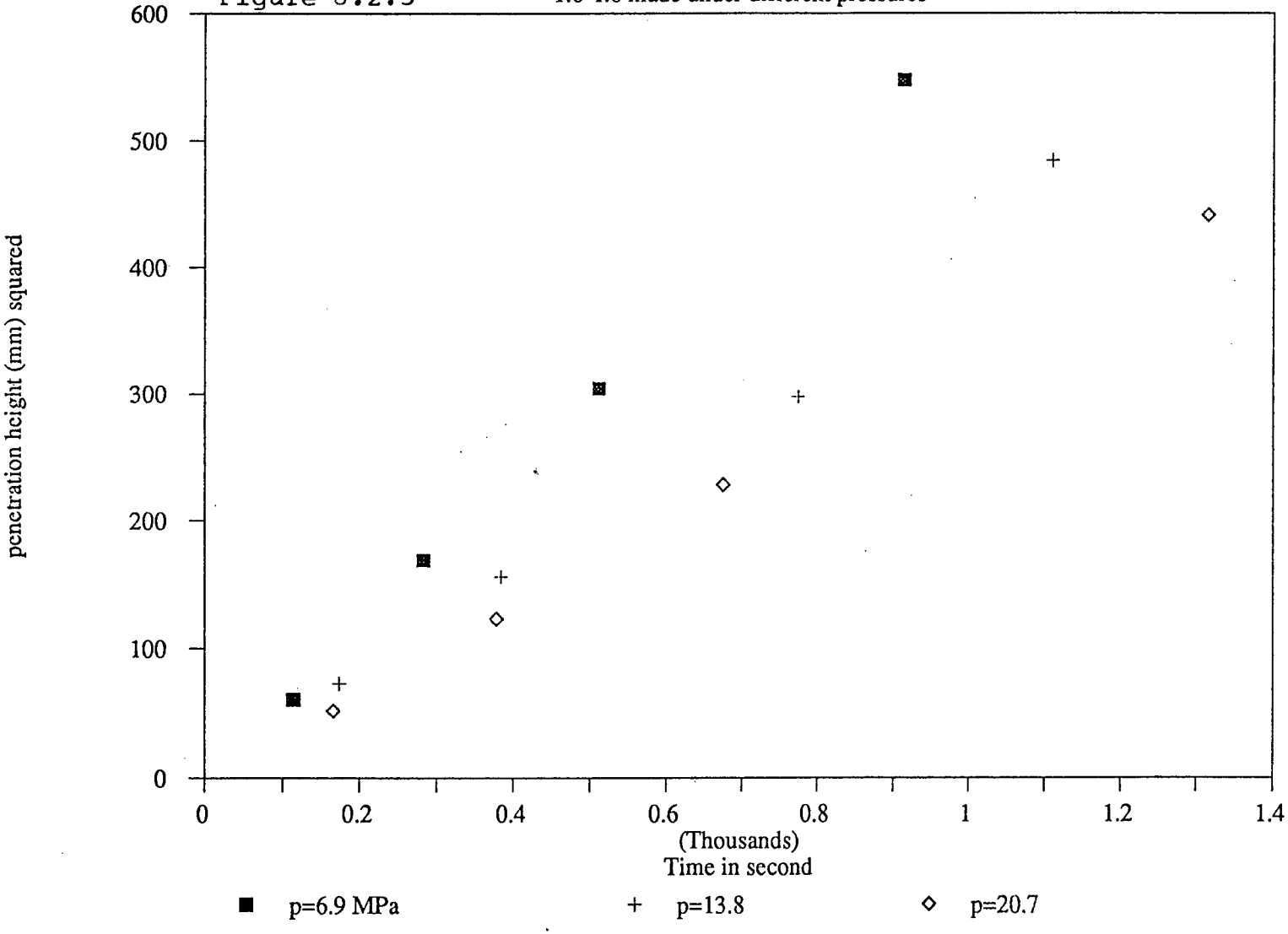

Rate of penetra. curves for columns of

Figure 8.2.6 +1.8 made under different pressures

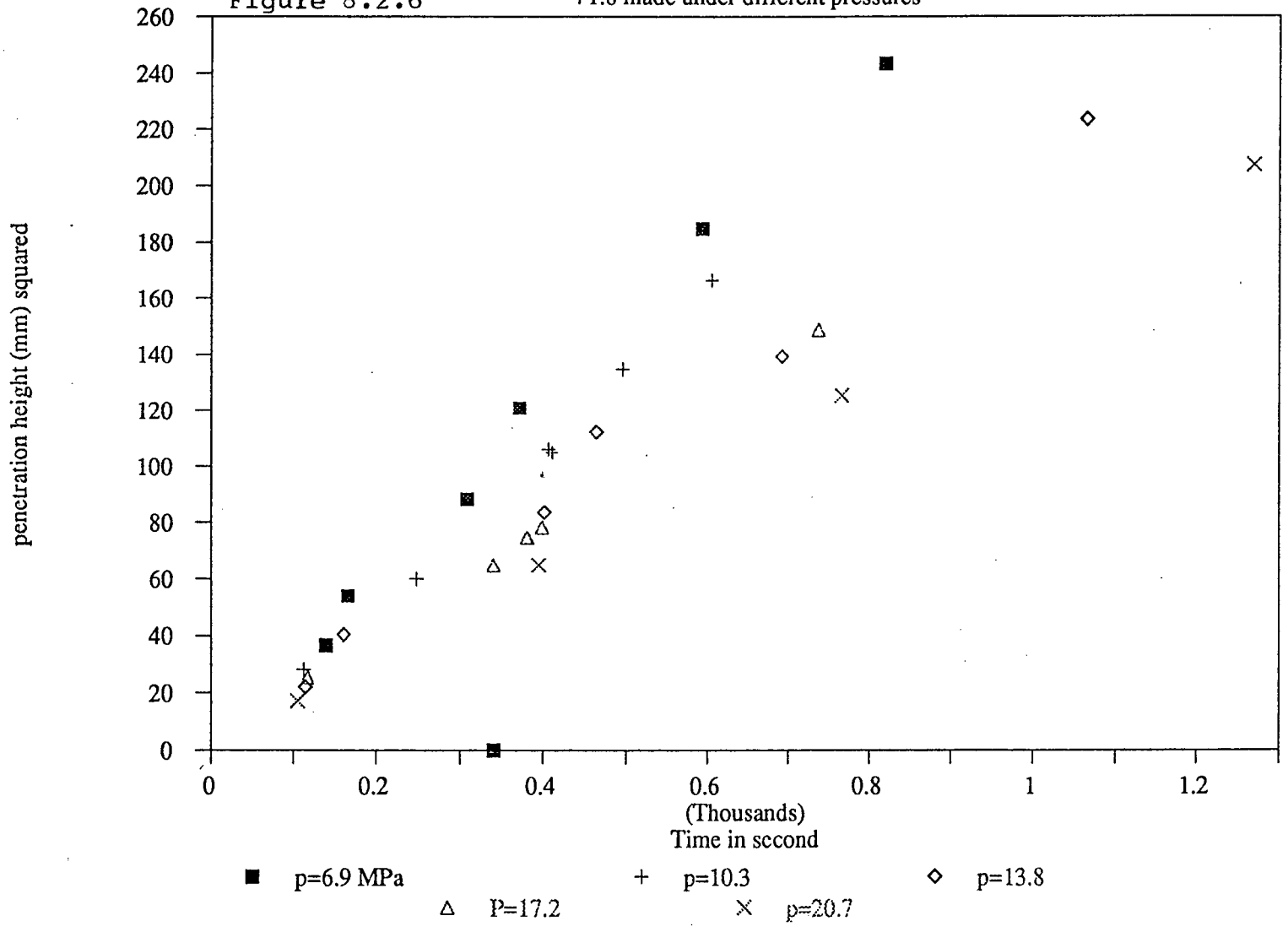

tested separately. Figures 8.2.1 to 8.2.6 are the results in a graphical form. Clearly, for each density fraction and under a constant pressure, a corresponding straight line was obtained. However, if the column making-pressure was changed for the same sample, the rate of penetration line would have different slopes. A group of penetration lines with different slopes can be obtained if one increases the column-making pressure gradually. The higher is the column-making pressure, the slower is the rate of penetration (smaller slope value of H^2 versus T line). Figures 8.2.7 to 8.2.9 were re-plotted from Figures 8.2.1 to 8.2.6 placing all the rate of penetration lines for six density fractions together in one graph.

Tables 8.2.1 to 8.2.3 give the regression results for these data.

The experimental reproducibility and accuracy are evaluated from R squared and standard deviation of these coefficients. They are given in Table 8.2.4. By examining the table, one can find a general tendency that both the standard error of H^2 (or Y) and the standard deviation decrease as the pressure increases for all the six density fractions. The R squared values for all six density fractions increase toward unit value with the increase in pressure. All this suggests the positive effect of higher column-making pressures.

Rate of Penetra. for Diff. SG Fractions

Figure 8.2.7 columns made under 6.9 MPa

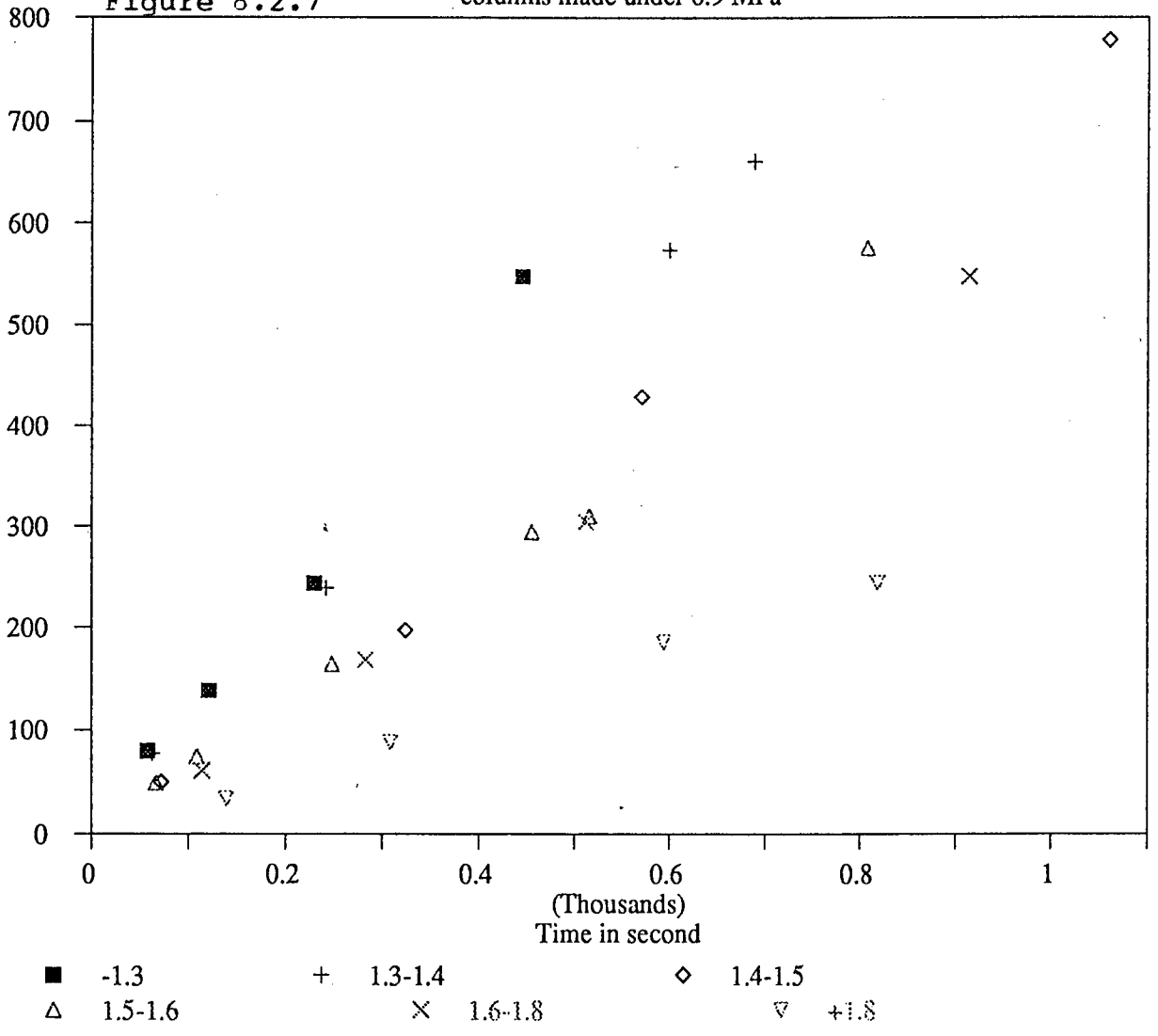

Rate of Penetra. for Diff. SG Fractions

Figure 8.2.8 columns made under 13.8 MPa

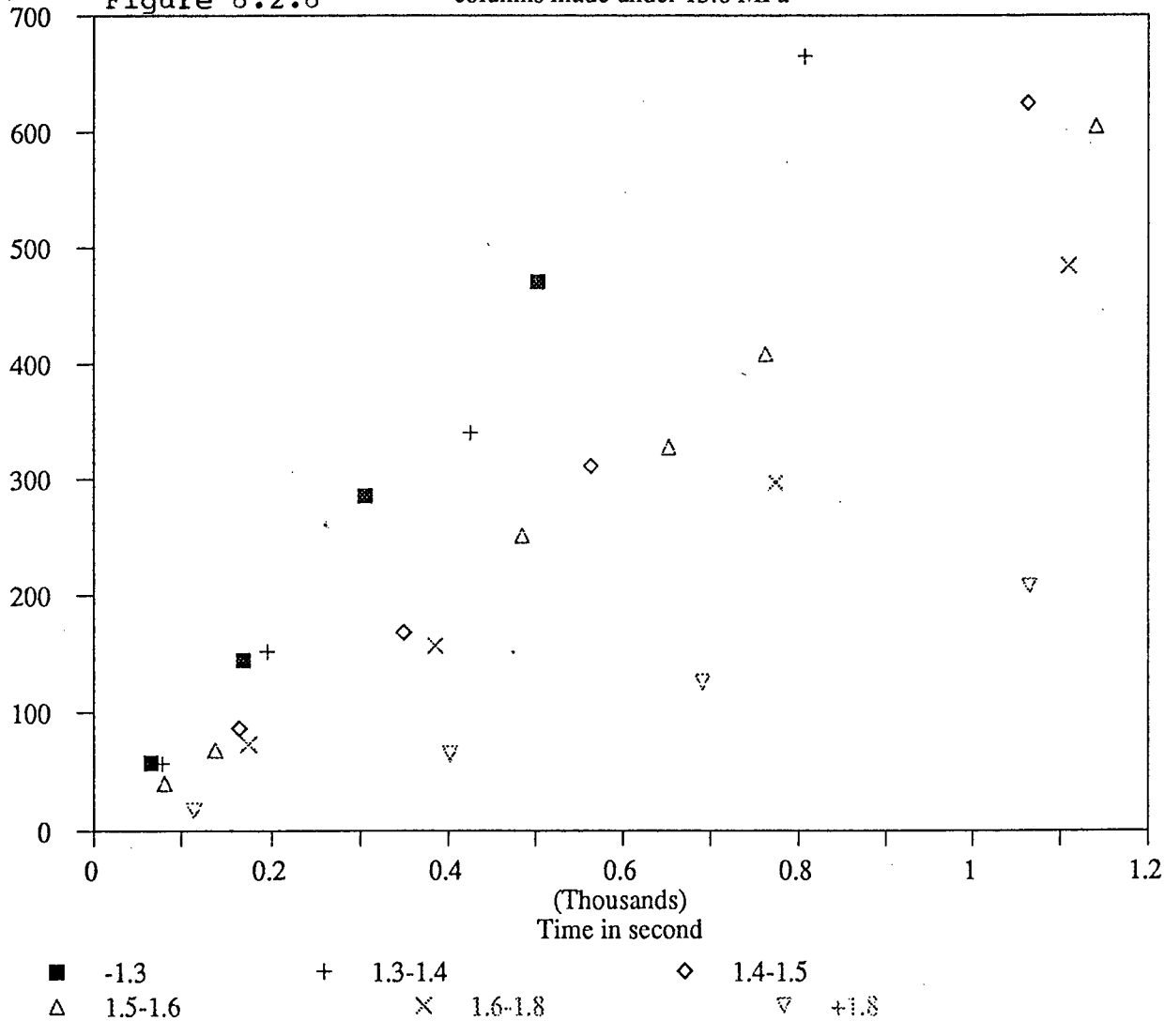

Rate of Penetra. for Diff. SG Fractions

Figure 8.2.9 columns made under 20.7 MPa

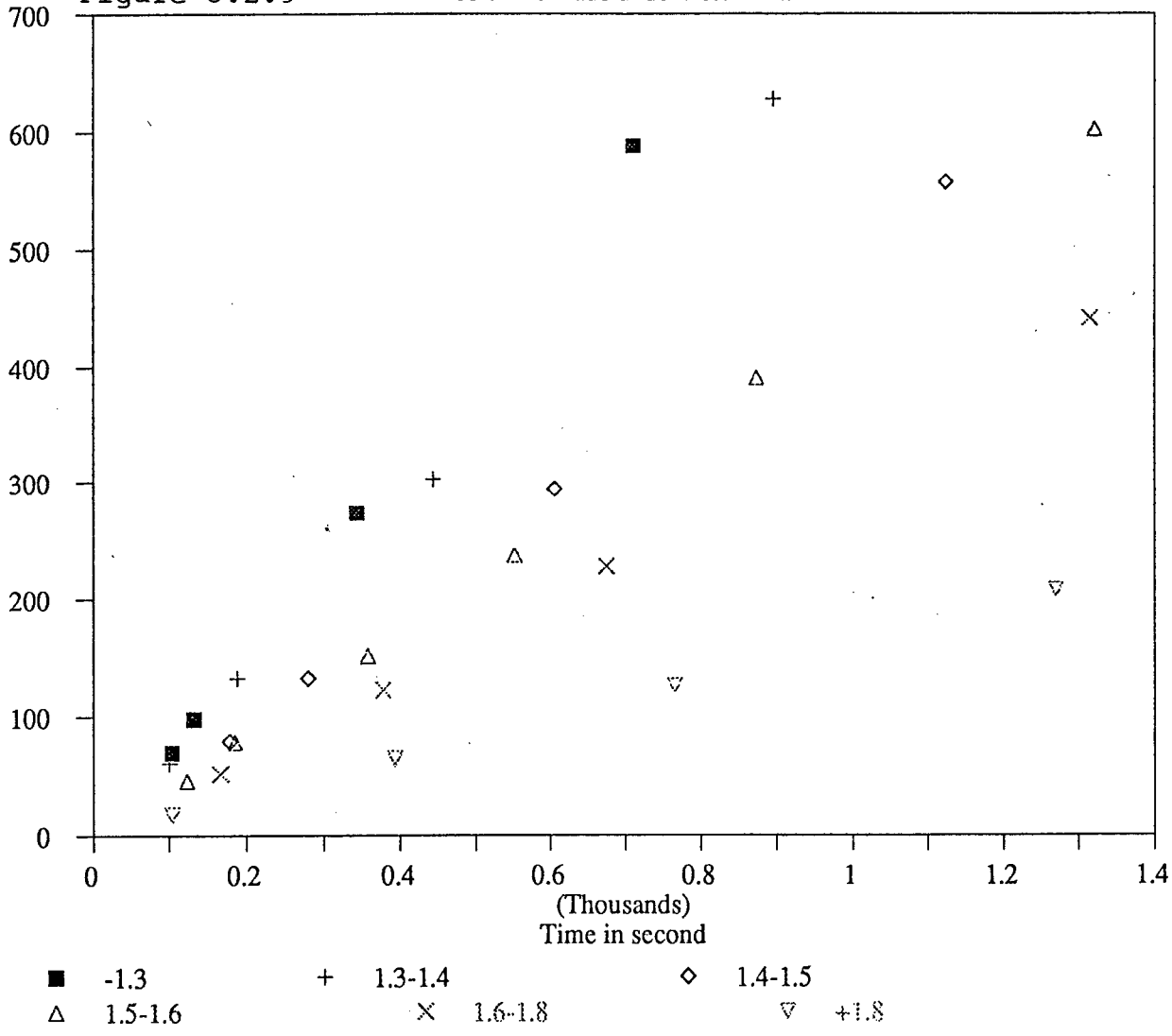

Table 8.2.1
STATISTIC ANALYSIS OF PENETRATION DATA
For BM coal, Pressure is 6.9 MPa

Density Fraction	Regression Equation	Std dvtn of Y estimate	Std dvtn of slope values	R Squared
-1.3	Y = -4.05 + 1.21 X	20.61	0.059	0.993
1.3-1.4	Y = 8.92 + 0.946 X	7.45	0.012	0.9995
1.4-1.5	Y = -10.0 + 0.743 X	21.81	0.025	0.997
1.5-1.6	Y = -5.38 + 0.684 X	22.45	0.031	0.9896
1.6-1.8	Y = -0.30 + 0.603 X	3.52	0.0049	0.9998
+1.8	Y = -3.64 + 0.306 X	5.92	0.009	0.997

* Std dvtn - Standard deviation
** The unit of density in this table and following tables is gram per cubic centimeter

Table 8.2.2

STATISTIC ANALYSIS OF PENETRATION DATA
for BM coal, pressure is 13.8 MPa

density fraction	Regression Equation	Std dvtn of Y estimate	Std dvtn of slope values
-1.3	Y = -4.98 + 0.945 X	6.54	0.016
1.3-1.4	Y = -6.75 + 0.829 X	5.88	0.009
1.4-1.5	Y = -15.1 + 0.592 X	17.78	0.02
1.5-1.6	Y = -4.21 + 0.53 X	7.75	0.0076
1.6-1.8	Y = -5.17 + 0.195 X	18.61	0.02
+1.8	Y = 5.62 + 0.195 X	6.69	0.008

Table 8.2.3
STATISTIC ANALYSIS OF PENETRATION DATA
For BM coal, Pressure is 20.7 MPa

density fraction	Regresion Equation	Std dvtn of Y estimate	Std dvtn of slope values	R Squared
-1.3	Y = -9.82 + 0.836 X	7.58	0.013	0.9992
1.3-1.4	Y = -4.03 + 0.703 X	5.47	0.0076	0.9996
1.4-1.5	Y = -5.66 + 0.499 X	4.49	0.0051	0.9997
1.5-1.6	Y = -8.52 + 0.458 X	6.15	0.0053	0.9993
1.6-1.8	Y = -2.11 + 0.337 X	2.55	0.0025	0.9998
+1.8	Y = 0.250 + 0.163 X	0.29	0.0003	1.0000

Table 8.2.4 The effect of column-making pressure on accuracy and linearity of the rate of penetration line

density fraction	Std dvtn of Y estimate			Std dvtn of slope values			R squared		
	P-6.9 MPa	13.8	20.7	P-6.9 MPa	13.8	20.7	P-6.9 MPa	13.8	20.7
-1.3	20.61	6.54	7.58	0.0590	0.0160	0.0130	0.9930		0.9992
1.3-1.4	7.45	5.88	5.47	0.0120	0.0090	0.0076	0.9995		0.9996
1.4-1.5	21.81	17.78	4.49	0.0250	0.0200	0.0015	0.9970		0.9997
1.5-1.6	22.45	7.75	6.15	0.0310	0.0076	0.0053	0.9896		0.9993
1.6-1.8	3.52	18.61	2.55	0.0049	0.0200	0.0025	0.9998		0.9998
+1.8	5.92	6.69	0.29	0.0090	0.0080	0.0003	0.9970		1.0000

The low pressure of 3.5 MPa, which is comparable with manual packing, was also tested. Under this low pressure, the experimental data are significantly scattered. This might be the reason why Good and Lin <1976> and Neumann and Good<1979> concluded that the rate of penetration data in the studies generally exhibit a serious statistical scatter. They have attributed this scatter to the change in structure of the packed column with wetting. This could be part of the reason. Another reason, as implied by this study, might be the inconsistency in structure of packed column itself. Especially under lower pressure the particles do not orient themselves properly for the best packing density and their irregular configuration would trap large amount of irregular air pockets within the column. These configurations can significantly vary from one to another. Therefore the rate of penetration can be different in various parts of the column. When high pressure was applied, these air-trapped configurations collapse and particles re-orient themselves to form better packed configurations which tend to be more uniform.

By checking the published literature, one may find that the penetration lines for the same material from the repeated runs did not observe the same slope even though an individual line, which was measured from a single column, had a very good linearity <Crowl and Wooldridge, 1967>. The

poor reproducibility, according to the above analysis, is likely to be due to the inability of manual tapping to produce the columns with reproducible interior configurations. The column-packing pressure is, therefore, an exceptionally important factor. It should be high enough and kept constant to attain high reproducibility of the experiments.

8.2.2 Effect on Rate of Penetration

The column-making pressure can not only change the experimental accuracy and reproducibility, as delineated above, but also alter the rate of penetration. As shown in Figures 8.2.1 to 8.2.6, the increase in pressure can rotate H^2 versus T line around the origin of coordinate to the position with smaller slope value. The question which will be answered is what is the general relationship between the slope, S, and pressure, P, and what it stands for.

The influence of pressure on the rate of penetration was studied by testing the columns made under various pressures. The slope value, S, for each penetration line was calculated by statistical regression of the penetration line and was plotted versus pressure in Figure 8.2.10. Obviously the effect of pressure on the rate of penetration is substantial. According to the Washburn equation 7.2.5

The effect of column-making pressure on

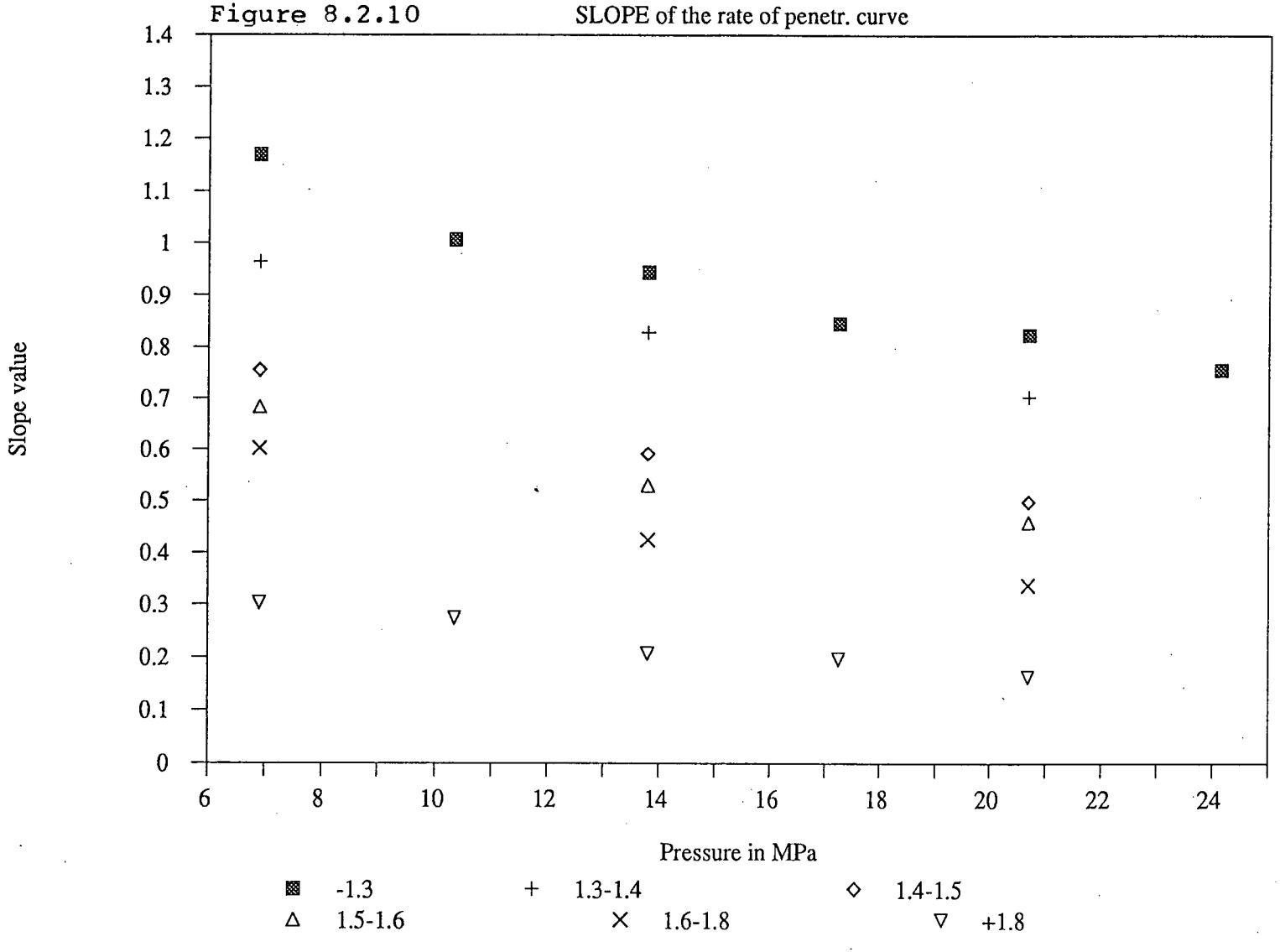

$$d(H^2)/dt = K \cdot \gamma \cdot \cos\theta / 2\mu \qquad 7.2.5$$

The slope of penetration line should be

$$S = K \cdot \gamma \cdot \cos\theta / 2\mu \qquad 8.2.1$$

A general tendency in Figure 8.2.10 is that the slope values, S's, for all the six density fractions are decreasing with increasing pressure. The band of the lines at lower pressure is wider and becomes narrower as the pressure increases.

In Eq.8.2.1, θ is what we intend to determine; γ and μ are the penetration liquid properties and are known from accurate measurements; S could be obtained through the regression of measured data. If tortuosity constant K were known, θ value could be readily calculated. Unfortunately K is unknown.

In the experimental process for testing the effect of pressure on rate of penetration, γ and μ were considered unchanged for the same liquid. And θ was also presumably regarded unchanged for the same liquid-solid system to be tested if the pressure is not high enough to change the solid surface properties (this will be discussed in section 8.2.3). Therefore according to Eq.8.2.1, the change in the

slope value, S, versus pressure, P, was only associated with the change in tortuosity constant, K. That is, the pressure was only influencing the liquid penetration through changing the column tortuosity constant, K.

The tortuosity constant K, which is an equivalent of capillary radius r, is only a physical property of the columns. It is, like capillary radius r, independent of surface wettabilities and is only determined by material particle size distribution, packing density, etc.. That is to say, if two columns are of the same particle size distribution and same packing density, they should have the same tortuosity constant K, even though these two material have quite different surface properties. Based on this useful conclusion, it is possible to procure the tortuosity constant value without the reference to the calibration liquid.

There is still no way to find out directly the value of the tortuosity constant, K from Fig.8.2.10. But Fig. 8.2.10, Eq.7.4.1, and above considerations do provide some clue how to calculate the K value. A new approach using above idea will be presented in section 8.5.2 which is entirely devoted entirely to the calculation of K values under various column-making pressures and the contact angle values for different density fractions of coal.

8.2.3 Side Effect of High Pressure

The application of higher column-making pressures may present many advantages in the rate of penetration tests as illustrated above. Nevertheless, a major concern with the high pressure is that it may cause crushing of coal particles to finer sizes and then possibly alter the coal surface properties.

The possibility of crushing of the coal in the column-making process can be detected in several ways. One possible way is through particle size distribution analysis before and after the column-making process. If any crushing action has occurred, the particle size distribution within the column after re-dispersion would indicate higher yields of fine sizes than prior to the column preparation. The possible shift in size distribution toward finer sizes would suggest the occurrence of the crushing action. The particle size analysis results showed that no apparent shift in size distribution has occurred.

Another way to detect the possible crushing action was to examine directly the pellet surface using Scanning Electron Microscope (SEM) under very high magnification.

The surfaces of columns made under 27.6 MPa were photographed (Figures 6.8.2). The picture magnified 3000

times in Figure 6.8.2, clearly shows that no obvious crushing action has ocurred on the pellet surface. Otherwise, groups of small particles produced from the breakage of larger particles can be seen piled up at some random spots.

The column-making pressure usually used in the present work ranged from 6.9 to 20.7 MPa. It is far below 27.6 MPa as used in the above test. The possible crushing action within a column should be excluded.

8.2.4 Lower Limit of Pressure

The lower limit of column-making pressures was also tested in order to find the lowest pressure feasible for this technique. However, the tests show that there was no clear-cut value. As the pressure was reduced to 3.5 MPa, which is comparable with manual tapping, the column was fragile and needed to be handled with care. When pressure was further decreased down to 2.8 MPa, the column could hardly hold and loosened instantaneously after released from the mould.

In the present work, the column-making pressure, therefore, was chosen in the range from 6.9 to 20.7 MPa. Pressures down to 3.5 and up to 34.5 MPa were also employed

in these experiments in order to study its influence on the column properties and on the rate of penetration.

8.3 PHYSICAL PROPERTIES OF COLUMNS

The columns compacted under high pressures exhibited many distinct properties. The study of these properties may be an integrate part of this technique. Some of these observations may be used in later sections to interpret the results and evaluate the assumptions.

8.3.1 Column Height versus Pressure

The column height is one of the most important parameters in the rate of penetration tests. However its value was inevitably influenced by the column compressing pressure. For the same amount of material, the column height is smaller under higher pressure.

In order to examine the general correlation between column height and pressure, columns of constant weight were pressed under different pressures. Results are shown in Figure 8.3.1. As the pressure increases the column height decreases, but non-linearly. At lower pressures, an increase in pressure can reduce the column height more substantially. As the pressure increases, the influence of pressure on column height diminishes.

Effect of column-making pressure on column packing density (BM-1.3 fract'n)

Figure 8.3.1

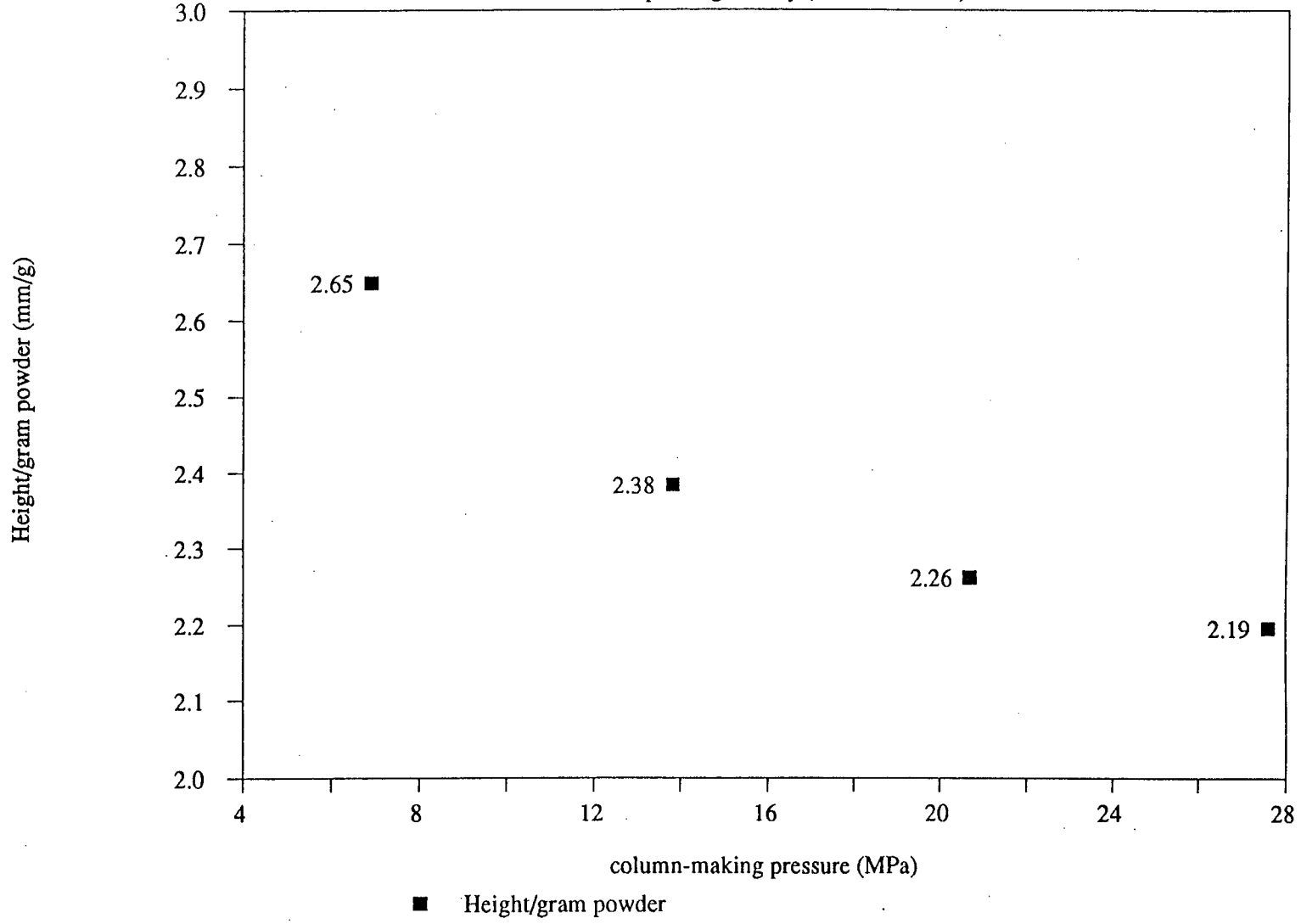

It is worthy of mention that the column height measured at lower compacting pressure is more likely to be scattered because a small random error or disturbance would have larger effect on the interior structure of the column at lower pressure (than at higher pressure). This is one of the reasons why high compressing pressure was preferred for the sake of precision.

As the column-packing pressure reaches a high level (27.6 MPa), a further increase in pressure has little effect on the column height. The tail part of the curve in Figure 8.3.1 therefore tends to level off. Working in this area may possibly have some advantages of being independent of the effect of compressing pressure. Nevertheless, the possibility of changing coal surface properties by destruction becomes more likely for higher pressures and prohibits the use of very high pressure.

8.3.2 Column Height versus Weight

In order to guaranty a constant column packing density, some researchers have packed a constant weight of material into a glass tube; and always kept the column height constant. However this practice could not readily be applied to coal because of the density variation among different coal density fractions. In this work, a constant

Figure 8.3.2 **Column weight vs. its height**

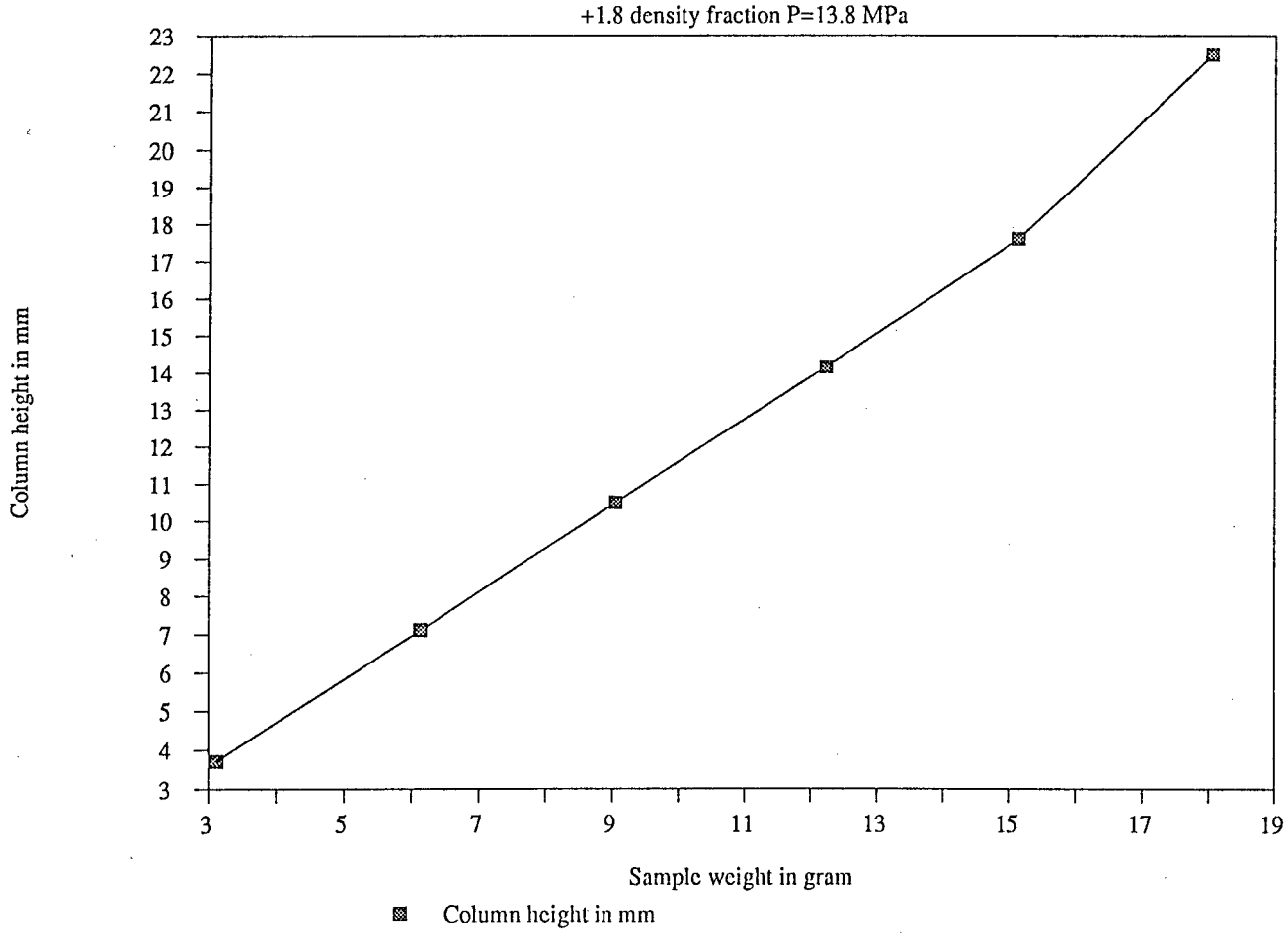

packing density was secured by applying a constant column-making pressure.

Under a constant pressure, a number of columns with different weights were made and their weight accurately measured. As shown in Figure 8.3.2, an acceptable linear relationship between column height and its weight was observed. However, further increase in column weight only makes its height out of proportion and higher than predicted.

It was initially perceived that the height of the column made under constant pressure should be always proportional to the column weight. However in the real column-making process it was not true, because of the existence of the friction forces between the cylindrical wall of the holding mould and the column within it. The friction forces, which will be discussed in detail in the next section, produce a gradient decrease of the pressure through the column and, as a result, may yield a non-linear column height versus weight relationship.

8.3.3 Column Porosity

Although the column-making process is exactly the same as the pellet-making process, the column exhibits quite

different properties because of the substantial difference between their heights. Firstly, the column porosity is not uniform. It changes along its perpendicular axis. Secondly, under the same column-making pressure, the columns with different heights are characterized by different average porosities. Detailed discussion will be given in section 8.4.

8.3.4 Column Expansion

The significance of column expansion after the liquid penetration process was tested. The substantial expansion of the column during penetration affects the measurement of column height and column porosity.

In Table 8.3.1, H_0 is the original column height; H_1 is the column height after penetrated by liquid; dH is the increase in height. The relative column expansion in height is presented in the last column of the table. The columns made from the -1.3 fraction of the Bullmoose coal at different pressures were tested. The results show that the columns made under higher pressures experienced greater expansion than did the columns made under lower pressure. However, the largest average relative expansion was only 0.71 percent and could be neglected.

Swell of columns after penetrated by liquid

Pressure MPa	H0 mm	H1 mm	dH mm	%	Average
	24.55	24.65	0.10	0.41%	
	19.60	19.70	0.10	0.51%	
	17.15	17.35	0.20	1.17%	
P=6.9	13.00	13.00	0.00	0.00%	
	12.80	12.90	0.10	0.78%	
	8.65	8.65	0.00	0.00%	
	6.75	6.75	0.00	0.00%	0.41%
	24.60	24.80	0.20	0.81%	
	20.20	20.40	0.20	0.99%	
	18.10	18.20	0.10	0.55%	
P=13.8	15.85	15.95	0.10	0.63%	
	12.00	12.10	0.10	0.83%	
	8.25	8.25	0.00	0.00%	
	6.30	6.30	0.00	0.00%	0.55%
	24.00	24.30	0.30	1.25%	
	19.75	19.80	0.05	0.25%	
	17.60	17.90	0.30	1.70%	
	15.40	15.50	0.10	0.65%	
P=20.7	12.30	12.35	0.05	0.41%	
	11.50	11.50	0.00	0.00%	
	8.85	8.85	0.00	0.00%	
	7.00	7.10	0.10	1.43%	0.71%

H0 is the original column hight in mm
H1 is the column height (mm) after penetrated by kerosene
dH is the increase in column height (mm)

8.4 The Effect of Friction

When the pressure exerted on the column is high, the force exerted by column on the cylindrical wall of the mould is also significant in the column-making process. The friction force between cylinder wall of the mould and the column of particles can not be neglected. This friction force prevents the propagation of pressure throughout the column, generates a pressure gradient throughout the column, and consequently influences the consistency of column's packing density. The packing density inconsistency could even be visually observed through the change in colour and brightness in the column's axis direction. As demonstrated before, the column-making pressure had a strong influence on the rate of penetration. The existence of pressure gradient may alter the rate of penetration behaviour within a column.

The most direct manifestation of this phenomenon was observed when columns were put upside down and used in the penetration tests. Two sets of columns from the same material were compacted under a constant pressure. The penetration experiments were carried on in two different manners: one set of columns were penetrated in a normal way; but in another set, the columns were placed upside down. The results (Figure 8.4.1) show that two penetration lines with different slopes were obtained.

Change in Rate of Penetration Behavior

Figure 8.4.1 when columns placed upside down

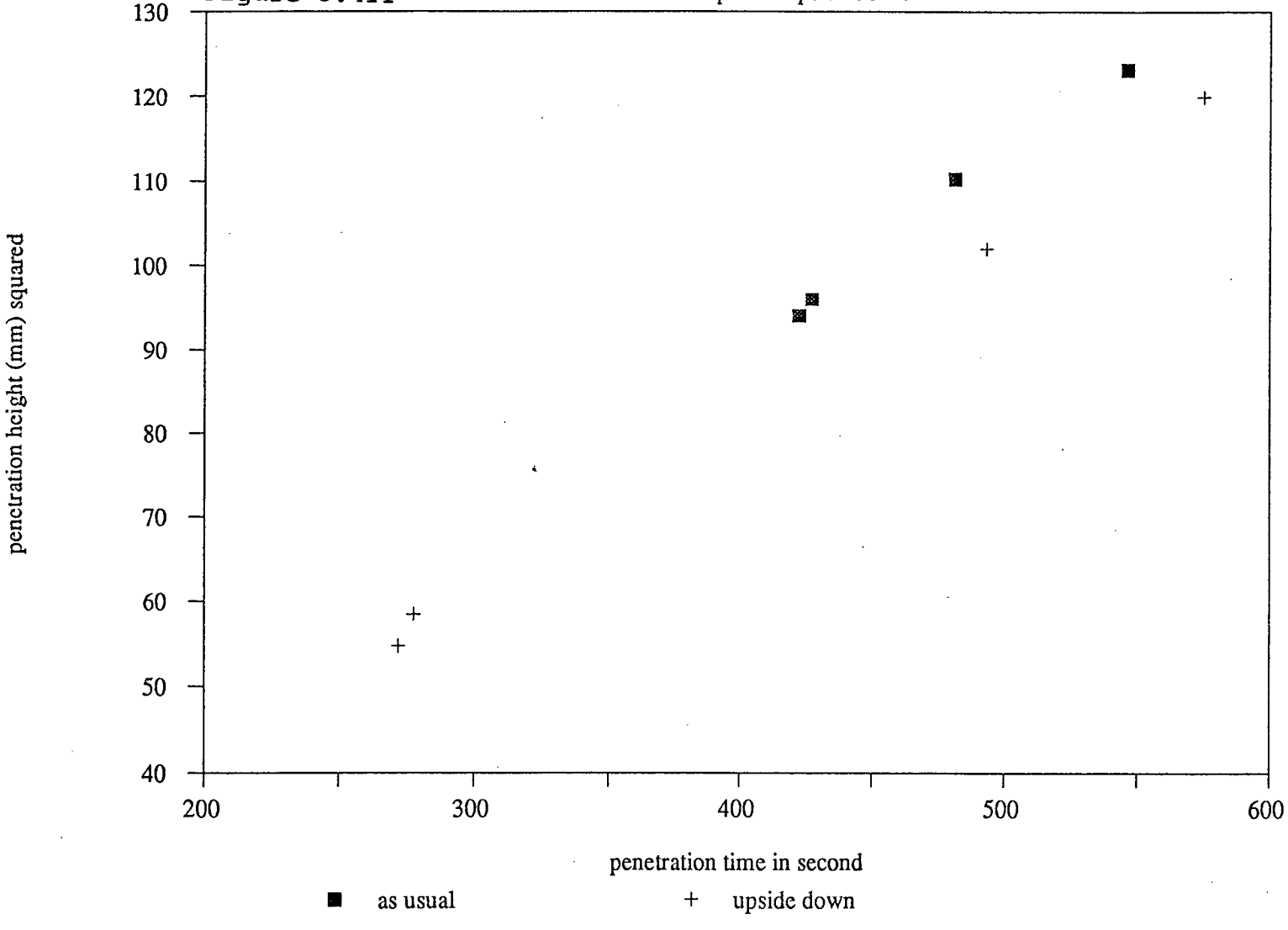

Suppose that in Figure 8.4.2 the friction coefficient is f, the circumference of the column is c (7.98 cm in present work), the pressure at any point within the column is p, a differential equation can be derived

$$dp = -p \cdot c \cdot f \cdot dx \qquad 8.4.2$$

After integrating above equation from x=0 to h, we can get

$$[\ln p]_{P_o}^{p} = [-cfx]_{0}^{h}$$

$$p = P_o \cdot \exp(-cfh) \qquad 8.4.3$$

where P_o is the pressure exerted on the column's bottom (it is kept constant in column-making process). According to the above equation, the pressure decreases from column's bottom, to the column's top surface exponentially.

It has been known that the porosity of a column linearly decreases with column-packing pressure linearly in a relatively narrow range of pressures. That is

$$q = Q - k \cdot p \qquad 8.4.4$$

where q is the column porosity, Q is intercept at q axis and p the pressure exerted on column. By substituting Eq.8.4.3 into Eq.8.4.4, one can get

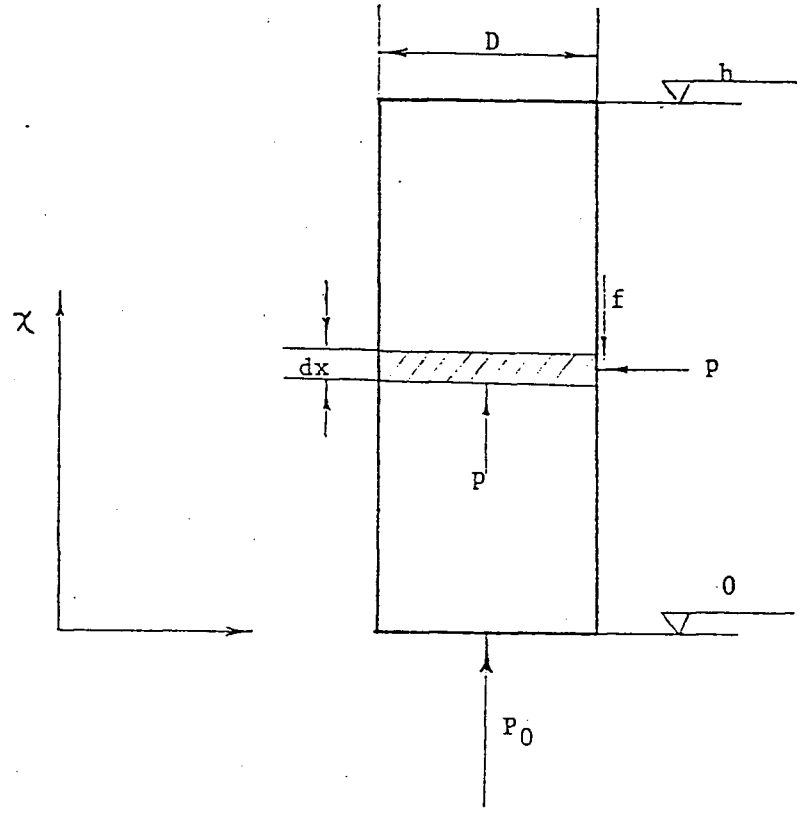

Figure 8.4.2 The forces acting on the column within the mould

P_0 is the pressure (MPa) exerted on the column bottom by the hydraulic press.

p is the pressure (MPa) at a point within the column.

f is the friction coefficient.

$$q = Q - kP_o \cdot \exp(-cfh) \qquad 8.4.5$$

where q is a differential porosity of a very thin layer within the column at h. Apparently the porosity within a column is increasing in x-axis direction toward the top of the column in a pattern given by Eq.8.4.5.

The increase in porosity along column's X-axis suggests an increase in equivalent capillary radius in the same direction. Variation of the equivalent capillary radius within a column can influence the rate of penetration.

There are many ways to test the porosity gradient along X-axis. The most direct way is to chop up some thin layers from a column and to measure their porosity. In practice, however, it is difficult to cut such thin layers from a column and to measure its q value experimentally.

An indirect method was employed here. The basic idea is that if a number of columns with different height were compacted under the same pressure in the absence of the friction force, the porosity for all the columns should be equal. When a porosity gradient is produced within the column in the presence of friction force, the average porosities for columns with different heights should vary. By integrating Eq.8.4.5 from the bottom to the top of the column, one can get the average (or integral) porosity of

the whole column

$$Q_a = \int_0^h q \cdot dx/(h-0) \qquad 8.4.6$$

$$Q_a = Q - \frac{k \cdot P}{c \cdot f \cdot h} \langle 1 - \exp(-cfh) \rangle \qquad 8.4.7$$

where Q_a is the average porosity of the whole column, h is the column height, P is column-making pressure, and c, f, k, and Q are constants. As indicated by Eq.8.4.7, the average porosity, Q_a, of a column made under constant pressure P changes with column height h. This can be readily tested.

The general shape of Eq.8.4.7 was first examined. Q_a was plotted against h by assigning some arbitrary values to the constants in the equation. In Figure 8.4.3, two curves were obtained by assigning two sets of different values to friction coefficient f in Eq.8.4.7. The figure clearly shows that among the columns made under constant pressure P, the average porosity for the taller column will be larger than that for the shorter one. To test this, a set of columns with various weights were compacted under a constant pressure. Their porosities were measured and plotted versus their height in Figures 8.4.4 and 8.4.5. The similarity in the curve shapes between the theoretically predicted and the actually measured porosity versus column height curves reveals the existence of the friction effect.

Theoretical Effect of Column Height On

Figure 8.4.3 The Integral Porosity of the Column

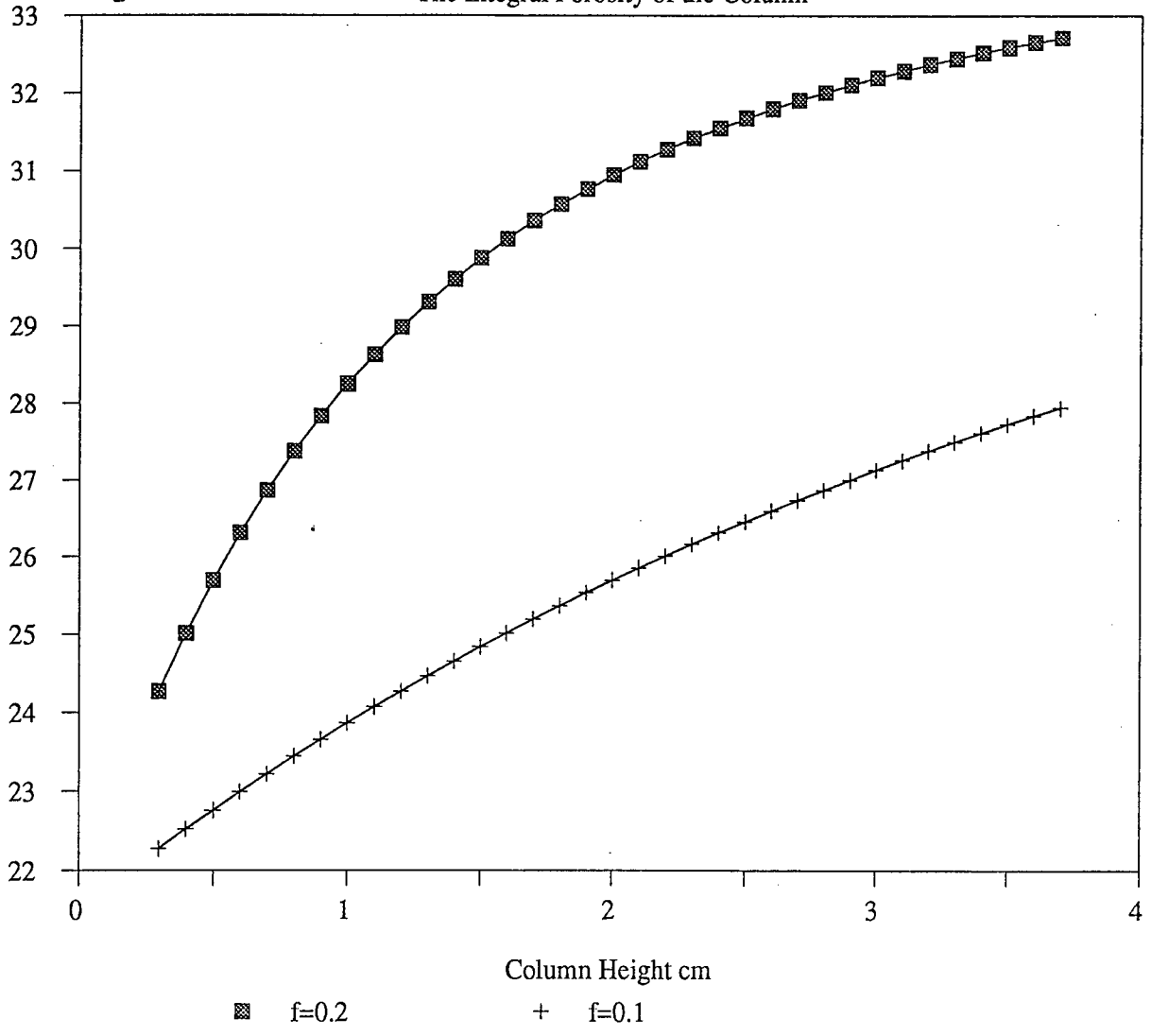

The effect of column height on integral

Figure 8.4.4 porosity avged on four pressure points

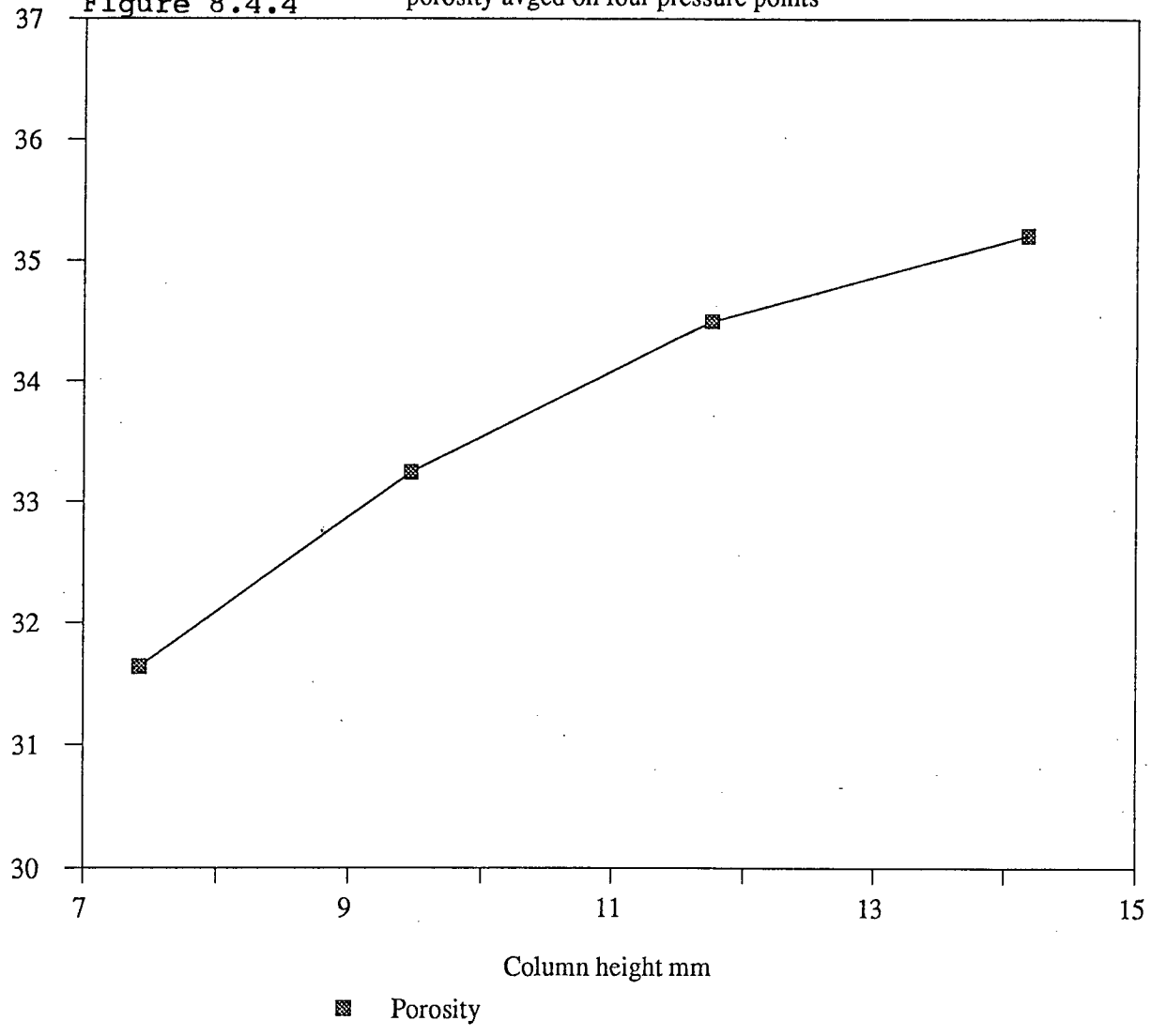

Column Height versus Integral Porosity

Figure 8.4.5 values obtained from actual measurement

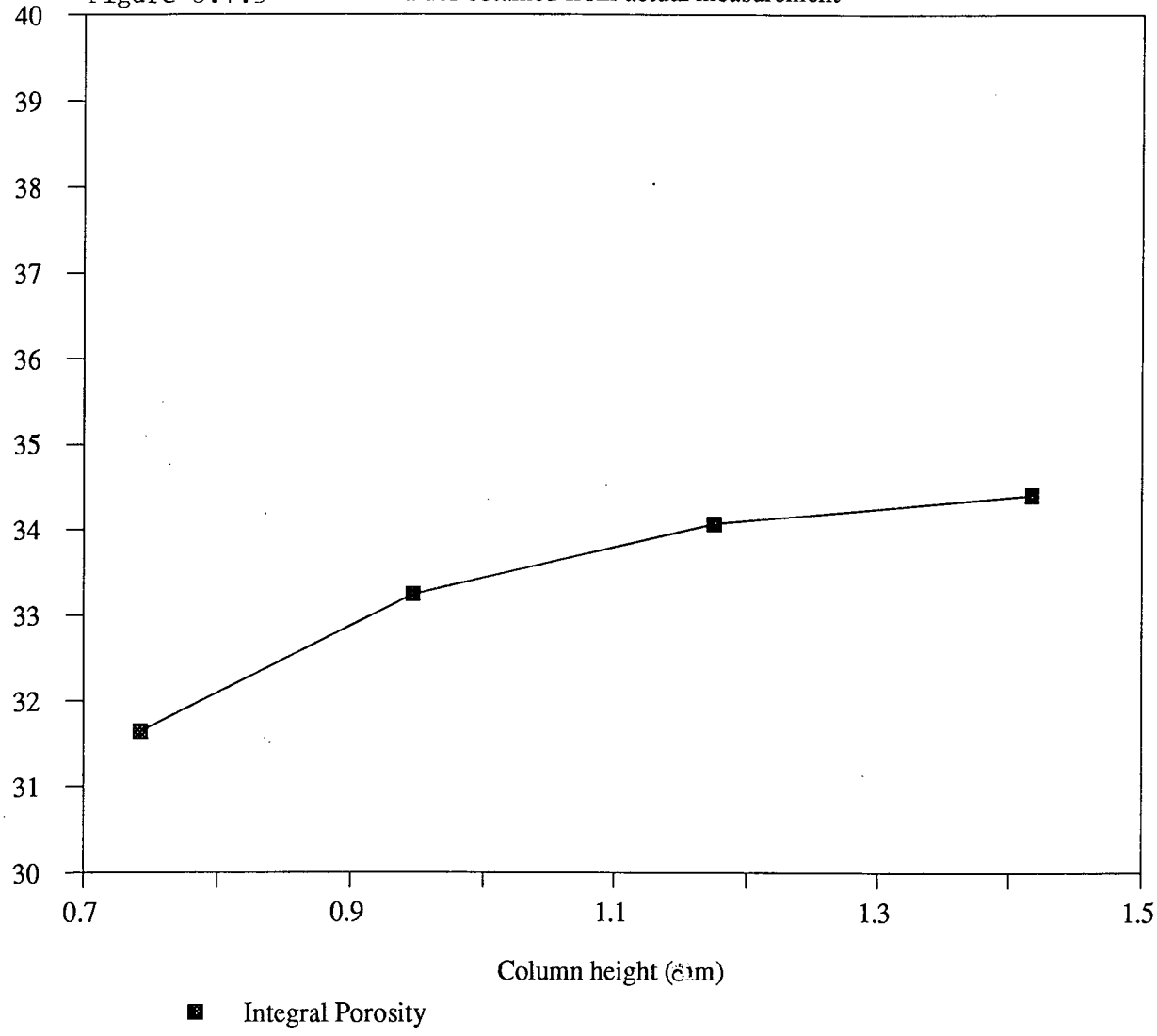

It could thus be concluded that the porosity of a compressed column is not uniform and that there exists a porosity gradient within it; the porosity increases exponentially, according to Eq.8.4.5, from bottom to top of a column. Because an increase of porosity means an increase of tortuosity constant K in Eq.7.2.5, the rate of penetration, $d(h^2)/dt$, should exhibit an increase as the penetration front moves upward. It is to be noticed that gravitational force on the other hand can offset this porosity effect (see Eq.7.2.3). As the penetration front surface moves upward, the term $\Delta\rho gh$ increases linearly and, on the contrary to K, tends to drag the penetration front back. This phenomenon indicates that the height limit for a column made under high pressure is greater than that for a column made by manual tapping.

8.5 CONTACT ANGLE CALCULATIONS

8.5.1 Introduction

As noted previously, the contact angle calculation from the experimental data necessitated the column calibration. The requirement for calibration results from the fact that the tortuosity constant, K, in the Washburn Eq.7.2.5 is unknown and can not be attained by direct measurement, or calculation. Without knowing the K value, the contact angle, θ, can not be determined. For a given packing of column, the tortuosity constant K should be constant, and it can be calculated from Eq.7.2.5 if a reference liquid is chosen for which $\theta=0°$ (complete wetting or spreading).

Since coal wettability ranges very widely from hydrophobicity for low density fractions to hydrophilicity for high density fractions. It is practically impossible to select the liquid for which $\theta=0°$ condition will be always fulfilled. As indicated by Harper <1967> it is risky to assume $\cos\theta=1$ in order to compute the tortuosity constant.

In the following sections, a new approach to compute K and θ values simultaneously will be introduced based on

the proposed assumption.

8.5.2 A New Approach

In the new approach, the absolute values of the tortuosity constant K, and contact angle θ's for different coal density fractions are resolved at the same time from a set of simultaneous equations.

As stressed before, the tortuosity constant K, an equivalent of capillary radius, is purely a geometric property of the packed column. It is only associated with particle size distribution, particle shape, and column packing density. It should be independent of wettability of the material investigated.

Suppose, under idealized conditions, that two different materials are both composed of spherical particles all with identical diameter of, say, 5 microns. If packed under the same pressure, the columns for this two materials should possess the same tortuosity constant, K. This idea may be generalized to apply to materials having similar particle shapes and approximately the same size distributions, e.g. coal powders. According to this assumption, only one calibration is required for a group of materials of different surface wettabilities.

Assume that there are two different materials possessing similar size distributions and similar particle shapes. Two columns are made respectively from the two materials under exactly the same pressure. These two columns should have the same tortuosity constant, K. After penetrating these two columns with the same liquid, one can get

$$d(h^2)/dt = S_1 = K \cdot \gamma_{lv} \cdot \cos\theta_1 / 2\mu \qquad 8.4.8$$

and

$$S_2 = K \cdot \gamma_{lv} \cdot \cos\theta_2 / 2\mu \qquad 8.4.9$$

where S_1 and S_2 are the slopes of the penetration lines for two columns respectively and can be obtained from the penetration test, θ_1 and θ_2 the contact angles on the corresponding materials, γ_{lv} the liquid surface tension, and μ the viscosity of the liquid.

After the column-packing densities are equally changed, by equally changing the column-making pressure, to another tortuosity constant value K', another set of equations can be similarly obtained

$$S_3 = K' \cdot \gamma_{lv} \cdot \cos\theta_1 / 2\mu \qquad 8.4.10$$

and

$$S_4 = K' \cdot \gamma_{lv} \cdot \cos\theta_2 / 2\mu \qquad 8.4.11$$

Thus, a set of four equations with four unknown values, K,

K', θ_1, and θ_2 are obtained. Unfortunately, only three out of the four equations are independent. An indefinite number of solutions instead of one can be obtained. One calibration is needed in order to put a restraint on these solutions. Another useful restraint for the above equations is that contact angle must range from 0 to 90°.

In real applications, efforts were made in the grinding process to keep various density fractions to have the size distributions as similar as possible. Under the precondition of identical size distribution, the column-making pressure becomes the only factor controlling the volumetric packing density of columns. Columns made under the same pressure might be considered possessing the same packing density, which was testified by the porosity measurement, and therefore the same tortuosity constant K.

The intricacy is that the tortuosity constant K is subject to the effect of particle shapes within the column and the particle size distributions can not be exactly the same. Even if the shapes for individual particles may differ, the shapes in general for the different density fractions from the same origin would not show much difference. In addition, for such small particle sizes averaging around ten micrometers, both the shape effect and small distribution deviation will diminish to an insignificant degree under a high column-making pressure.

8.5.3 Numerical Calculations

In applying this approach to the present case, columns for all six different density fractions were made under a set of three different pressures: 6.9, 13.8, and 20.7 MPa, respectively. Corresponding to these pressures, there should be three tortuosity constant K for those columns: K_1, K_2 and K_3. Suppose the contact angles for the six density fractions are θ_1, θ_2, ..., and θ_6. The total number of unknown variables would be nine (K's and θ's).

All the rate of penetration equations for six density fractions and three different pressures were tabulated in Table 8.5.1. In the table, $X_i = \gamma_{lv} \cdot \cos\theta_i / 2\mu$. The slopes of the penetration line, S_i in Table 8.5.1 were obtained from the rate of penetration test. They are given in Table 8.5.2. Among the total eighteen equations in Table 8.5.1, eight are independent, while the number of the unknowns is nine. So the number of solutions is indefinite, and a restrain is required to get one particular solution out of them.

The advantage of employing the redundant equations is that they can encompass more experimental data as much as can be obtained. Though the solutions resolved from the redundant equations may not be fitted in every equation exactly, they can be put in all the equations with the

Table 8.5.1
Rate of penetration equation matrix

Density fractions	P=6.9 MPa K1	P=13.8 MPa K2	P=20.7 MPa K3
-1.3	S11 = K1 X1	S12 = K2 X1	S13 = K3 X1
1.3-1.4	S21 = K1 X2	S22 = K2 X2	S23 = K3 X2
1.4-1.5	S31 = K1 X3	S32 = K2 X3	S33 = K3 X3
1.5-1.6	S41 = K1 X4	S42 = K2 X4	S43 = K3 X4
1.6-1.8	S51 = K1 X5	S52 = K2 X5	S53 = K3 X5
+1.8	S61 = K1 X6	S62 = K2 X6	S63 = K3 X6

Table 8.52
The slopes for different density fractions under various pressures

density fractions	pressure MPa 6.9	13.8	20.7
-1.3	1.17	0.9446	0.8246
1.3-1.4	0.9643	0.829	0.7033
1.4-1.5	0.7544	0.5922	0.499
1.5-1.6	0.6845	0.5308	0.4586
1.6-1.8	0.6028	0.4246	0.3373
+1.8	0.3029	0.2074	0.163

minimum overall deviation. Therefore the solution's reliability is higher.

To solve these equations, simplex search method was employed. A brief description of this method is given below; detailed description of this method can be found in many publications <Spandley etc., 1962, Nelder and Meed, 1965, Mular, 1972>.

The simplex method is a direct search strategy that begins with a n-dimensional general simplex with (n+1) vertices in n-dimensional space (n is the number of unknown variables, in our case n=9). The values of the objective function (here Residual Sum of Squares RSS) are calculated on all vertices of the simplex and compared. The vertex with the highest RSS value is replaced by a new vertex point which is chosen by reflection. Then an adjacent simplex is formed. The above procedure is repeated so the simplex will move on the objective function RSS surface, and is forced to adapt itself to the 'local landscape'. On a long inclined surface, the simplex will elongate down by expansion. Upon approaching the bottom of the basin, the simplex will contract in the neighborhood until a minimum RSS is reached. An illustrative two dimensional simplex search process is shown in Figure 8.5.1.

The utilization of simplex search method is only made

possible by using computer because of the tremendous amount of iterative computation involved. The computer program written in FORTRAN and its flowsheet are given in Appendix one. In the program, the number of search variables was nine. C(1) to C(3) represent K_1 to K_3 and C(4) to C(9) correspond to X_1 to X_6 respectively. The values of C(I) could be arbitrarily given. They should finally converge at the same point.

The computed results are presented in Table 8.5.3. In the Table, T3 and T are the values of program objective function to be minimized. As expected, the tortuosity constant K becomes smaller with an increase in column-making pressure. In the lower part of the table, in the second column are the measured rate of penetration values; in the third column are the values calculated according to the corresponding equations in Table 8.5.1.

In Table 8.5.1, there are eight independent equations and nine unknowns, there should be indefinite number of solutions for the equations. Only one set of the solutions is presented in Table 8.5.3. By multiplying all the K values by a coefficient N, and at the same time dividing all the X values by the same coefficient, N, one can obtain

K's $1.53Nx10^{-5}$, $1.18Nx10^{-5}$, $0.98Nx10^{-5}$ 8.4.12

Xi's 797.97/N, 676.39/N, 499.58/N, 453.09/N,

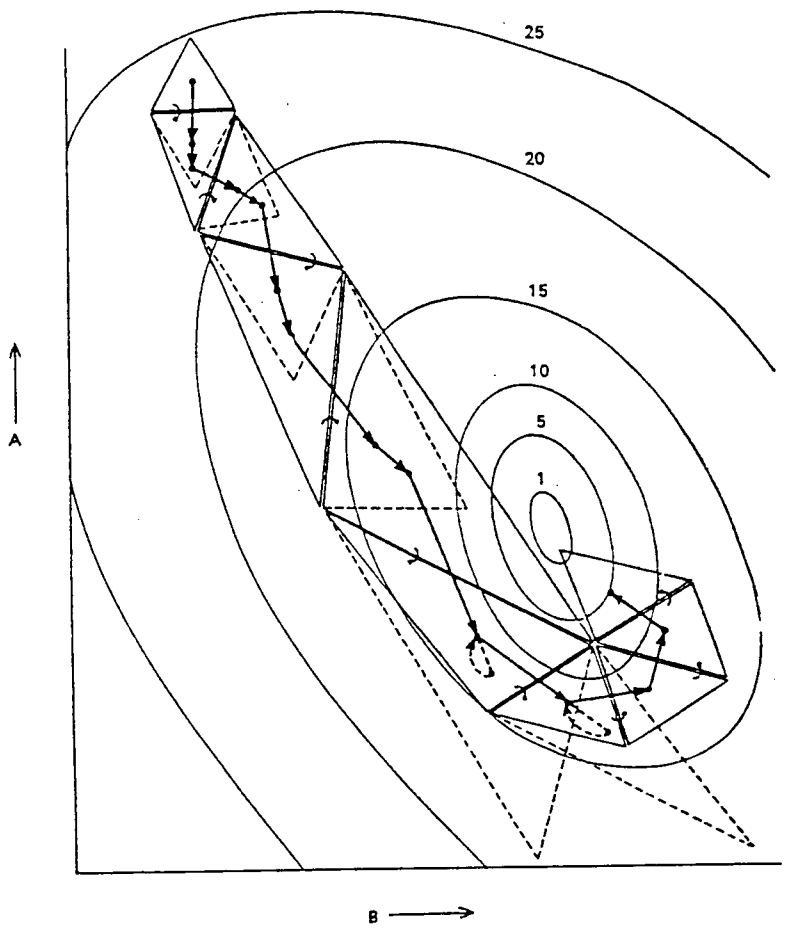

Figure 8.5.1 An illustration of the two dimensional simplex search process

Table 8.5.3 A General Contact Angle And Tortuosity Constant Calculation Results

CYCL. TIMES
501

T3= T=
0.26980E-05 0.26980E-05

THE TORTUOSITY CONSTANTS K1, K2, K3
0.000027065 0.000020889 0.000017361

THE X VALUES FOR SIX DENSITY FRACTIONS
452.40 383.25 283.22 256.83 205.37 100.58

CONTACT ANGLES ON SIX DENSITY RFACTIONS
55.45 61.28 69.20 71.22 75.08 82.76

	SLOPE VALUES			
DENSITY	MEASURED	CALCULATED	DIFFERENCE	RELATIVE%
		P = 6.9 MPa		
-1.3	0.01170	0.01226	-0.00056	-4.78038
1.3-1.4	0.00964	0.01038	-0.00074	-7.65562
1.4-1.5	0.00754	0.00767	-0.00012	-1.63480
1.5-1.6	0.00685	0.00695	-0.00011	-1.54287
1.6-1.8	0.00603	0.00556	0.00046	7.70454
+1.8	0.00303	0.00273	0.00030	10.03356
		P = 13.8 MPa		
-1.3	0.00945	0.00946	-0.00001	-0.09892
1.3-1.4	0.00829	0.00801	0.00028	3.41586
1.4-1.5	0.00592	0.00591	0.00001	0.14100
1.5-1.6	0.00531	0.00536	-0.00005	-0.99584
1.6-1.8	0.00425	0.00429	-0.00005	-1.06134
+1.8	0.00207	0.00210	-0.00003	-1.34038
		P = 20.7 MPa		
-1.3	0.00825	0.00786	0.00039	4.71980
1.3-1.4	0.00703	0.00665	0.00038	5.40061
1.4-1.5	0.00499	0.00491	0.00008	1.52551
1.5-1.6	0.00459	0.00445	0.00013	2.86652
1.6-1.8	0.00337	0.00357	-0.00019	-5.71031
+1.8	0.00163	0.00175	-0.00012	-7.14510

Above are the general solutions of equations in Table 8.5.1. Mathematically, N can be any real value. However, one of the restraints in real situation is that the contact angle of kerosene on coal can not be less than 0° and greater than 90° (If greater than 90°, kerosene will not penetrate). Therefore, the N value is limited in the range from 1.13 to 2.0.

Once the exact N value is obtained, all the K's and θ's can be calculated. In present work, this was done with quartz. Quartz, on which water was known to have a zero contact angle, was ground in mortar to the same size range as coal powder. The quartz powder was pressed under pressure of 12.7 MPa into columns. Exactly the same experimental procedure as that for coal was followed. The tortuosity constant for the quartz column was easily calculated from Eq.7.2.5

$$K = 2S \cdot \mu/\gamma$$

where μ is viscosity of water, γ is the surface tension of water.

The tortuosity constant K for quartz column made under pressure of 12.7 MPa was found to be 1.451×10^{-5}. This value was also considered, according to the assumption, to be the K value for all coal columns made under 12.7 MPa.

That is, $1.18N \times 10^{-5} = 1.451 \times 10^{-5}$, and N=1.23. After substituting N=1.23 into the general solutions in Eqs.8.4.12 and 8.4.13, one can get the final contact angle values as shown in Table 8.5.4.

The contact angles, as discussed above, were calculated through indirect calibration. According to the assumption made previously in this section, the tortuosity constant of a column is only dependent on particle shapes, size distributions and its packing density. The tortuosity constant K will be same for all columns of different materials with approximately the same size distributions and shapes if they are compacted under the same pressure.

This implies how to find the correlation between the column tortuosity constant and particle size distribution. Once the correlation is defined, tortuosity constant can be obtained simply from particle size distribution.

8.5.4 Evaluation

The assumption that the columns made of different materials, but under the same pressures, have the same tortuosity constant K, needed to be verified. There are many ways of doing this. Cross examination in which the validity of this assumption is simply tested by repeating the same

Table 8.5.4 The Final Contact Angle And Tortuosity Constant Calculation Results

CYCL. TIMES
5001

T3= T=
0.13141E-06 0.13141E-06

THE TORTUOSITY CONSTANTS K1, K2, K3
0.000016662 0.000012852 0.000010691

THE X VALUES FOR SIX DENSITY FRACTIONS
734.14 622.91 459.85 417.30 333.77 163.49

CONTACT ANGLES ON SIX DENSITY RFACTIONS
23.02 38.66 54.80 58.46 65.26 78.17

DENSITY	SLOPE VALUES MEASURED	CALCULATED	DIFFERENCE	RELATIVE%
		P = 6.9 MPa		
-1.3	0.01170	0.01223	-0.00053	-4.55185
1.3-1.4	0.00964	0.01038	-0.00074	-7.63957
1.4-1.5	0.00754	0.00766	-0.00012	-1.56433
1.5-1.6	0.00685	0.00695	-0.00011	-1.60030
1.6-1.8	0.00603	0.00556	0.00047	7.72557
+1.8	0.00303	0.00272	0.00030	10.06571
		P = 13.8 MPa		
-1.3	0.00945	0.00943	0.00001	0.11730
1.3-1.4	0.00829	0.00801	0.00028	3.42823
1.4-1.5	0.00592	0.00591	0.00001	0.20814
1.5-1.6	0.00531	0.00536	-0.00006	-1.05509
1.6-1.8	0.00425	0.00429	-0.00004	-1.04044
+1.8	0.00207	0.00210	-0.00003	-1.30631
		P = 20.7 MPa		
+1.3	0.00825	0.00785	0.00040	4.82406
1.3-1.4	0.00703	0.00666	0.00037	5.31168
1.4-1.5	0.00499	0.00492	0.00007	1.48661
1.5-1.6	0.00459	0.00446	0.00012	2.70571
1.6-1.8	0.00337	0.00357	-0.00020	-5.80134
+1.8	0.00163	0.00175	-0.00012	-7.22349

rate of penetration test with different kinds of liquids is probably the simplest. If the assumption is true, the tortuosity constants, K's, will keep unchanged for all different liquids tested. Because of the large number of repeated tests, this method was not, at present, used.

By taking a look at the relationship between column packing density and column-making pressure in Figure 8.3.1, one can find that a very similar relationship exists between tortuosity constant and column-making pressure in Table 8.5.4. This gives a clue that there must be a certain linear relation between the column-packing density and tortuosity constant. As expected, the tortuosity constant data in Table 8.5.4 plotted against the packing density data in Figure 8.3.1 gives, as expected, a very good linear relation (Figure 8.5.2).

Because column-packing density and column porosity are both based on the same concept, it can be concluded that there is a linear relationship between column porosity and tortuosity constant K. This is an important correlation. It will make possible in future to obtain K values from the measurement of column packing densities or column porosities. Attention should be paid to the fact that the above assumption is made based on the non-porous solid particles. As discussed in section 6.7, there are two different types of porosities: the inner-particle porosity

Tortuosity Const. vs. Packing Density

Figure 8.5.2

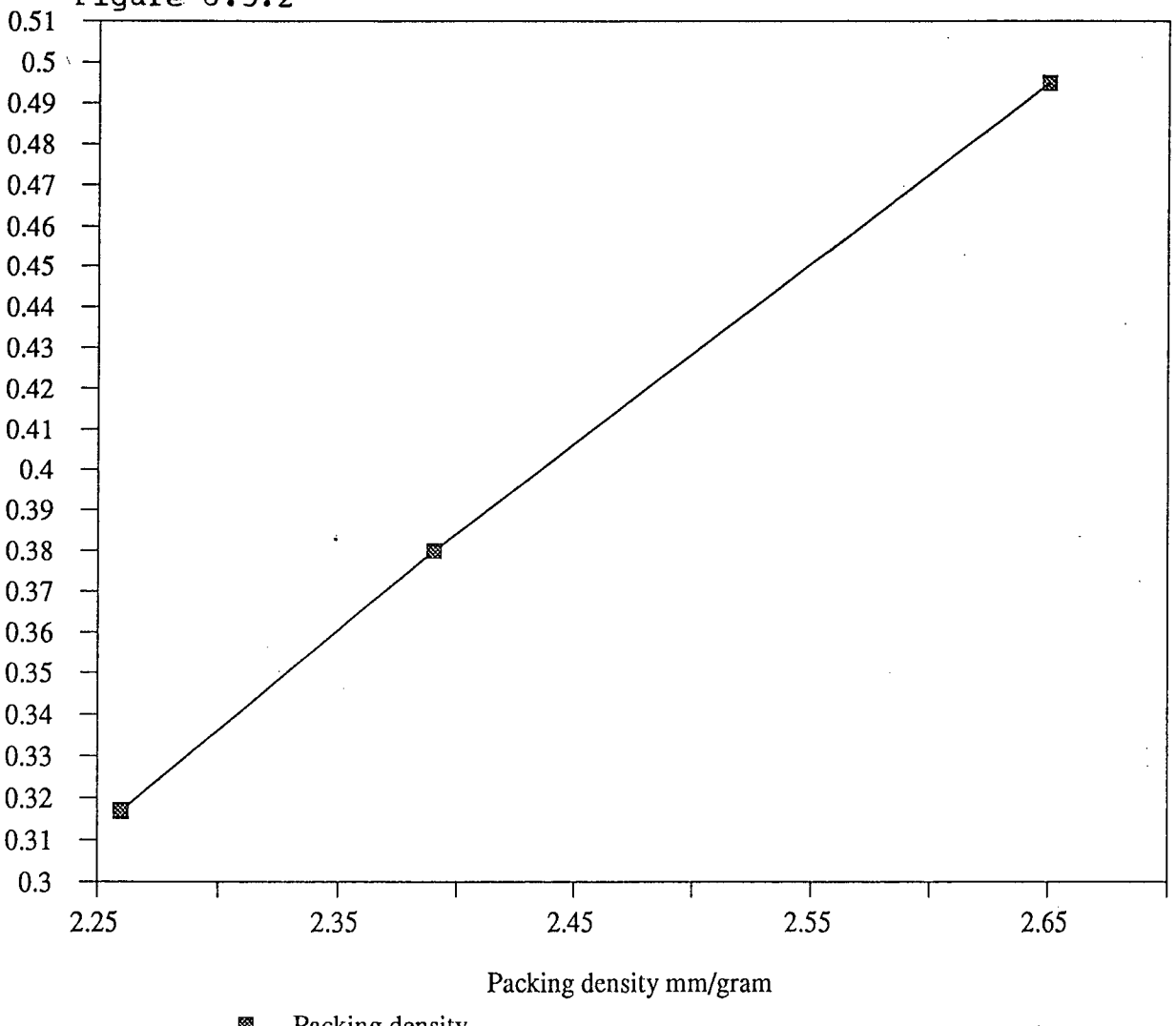

and inter-particle porosity. Correspondingly, there are two different types of capillary tubes: the inner-particle and inter-particle capillary tubes. The radii of inner-particle capillary tubes are much more smaller than that of inter-particle capillary tubes. The rate of penetration through a compacted column is mainly controlled by the inter-particle capillaries. The porosity of the material does not have a prominent effect on the rate of penetration.

8.6 SUMMARY AND DISCUSSION

The rate of penetration technique is based on the Washburn equation which states that the squared liquid penetration height is linearly proportional to the penetration time. The contact angle can be calculated from the slope of this linear relationship.

In the conventional procedure, the tested fine particles are placed in a glass tube 0.8 cm in diameter. The tube is manually tapped to ensure a uniform packing. The tube is calibrated on its external surface for the penetration height reading. This method suffers from poor reproducibility and not very good experimental accuracy.

The method was modified in the present work. The specimen mounting press was employed to compress coal powder into a highly compacted column (or pillar). When released from the mounting press, the coal column holding does not fall apart and is strong enough to resist the experimental handling. The diameter of the column is 2.54 cm, and the height ranges from 0.5 to 3 cm. Kerosene was utilized as a penetration liquid.

The column height was accurately measured with vernier. Because the column diameter is quite large, the

time is read when half of the column top surface is wetted. Thus for each column, only one pair of data is obtained. For each coal sample, four to six columns with different heights were prepared and penetrated to get the same number of experimental points.

The experiments revealed that the Washburn equation is still applicable to the highly compacted column. The linearity of the penetration line, which is represented by R squared, can be as high as 0.9992 to 1.000 for columns made under pressure of 20.7 MPa. The accuracy is also very high. The standard deviations of the slope values are only 0.0003 and 0.013 for the slope values of 0.163 and 0.8246, respectively (see Tables 8.2.4 and 8.5.2).

The column-making pressure has a positive effect on experimental reproducibility and accuracy. Results for a -1.3 density fraction of Bullmoose coal (Table 8.2.4) indicate that when a column-making pressure increases from 6.9 to 20.7 MPa, the standard deviation of the slope value decreases from 0.059 to 0.013, and the R squared value increases from 0.9930 to 0.9992.

It is possible that coal particles can be crushed under the influence of the high column-making pressure. However, examination under Scanning Electron Microscope showed that the crushing of coal particles under pressure of

up to 27.6 MPa is negligible. The applied pressures to make columns did not exceed 20.7 MPa. The minimum pressure required to make strong enough columns cannot be lower than 2.8 MPa.

For a certain amount of coal, the height of the column decreases appreciably with pressure. Further increase in pressure beyond 20 MPa has only a slight effect on the height (Figure 8.3.1) because particles in the column have already reached a very close packing.

At a constant column-making pressure, the column height increases with the column weight linearly. However, as the weight increases to a certain value (16 grams for +1.8 density fraction in Figure 8.3.2), the column height will be out of proportion and greater than predicted. This is because of the frictional forces which exist between the column and mounting press mold in the column-making process.

In the liquid penetration process, columns experience some swelling. The columns made under higher pressure experience a greater expansion than do the columns made under lower pressure. The relative column height increase after liquid penetration is 0.41% for columns made at pressure of 6.9 MPa, and 0.71% for columns made at 20.7 MPa. The expansion is very small and can be ignored.

Following determination of the penetration rate (slope) values from the test, the Washburn equation (Eq. 7.2.5) is employed to calculate the contact angles of kerosene on the fine coal particles. The tortuosity constant K which appears in the equation is, however, unknown. Conventionally, the second liquid which perfectly wets particles is used to obtain K in a parallel experiment. Having K, the contact angle can be calculated. This practice is not readily applicable to coal because coal is extremely heterogeneous and its wettability is widely distributed. No liquid can be found to have a zero contact angle on coal.

In the present work, an assumption was made that for the materials with the same particle size distribution, and shape, their columns, if made under the same pressure, possess the same tortuosity constant. Under this assumption, the columns for different coal density fractions also have the same tortuosity constant. Washburn equation's matrix for different density fractions of coal, and at different pressures is given in Table 8.5.1, and the simplex search program was used to solve this matrix. The contact angle values of kerosene on different density fractions of the Bullmoose coal were calculated as shown in Table 8.5.4.

One of the advantages of this technique is that the total surface area penetrated by liquid within a unit height of the column is much greater than that in a conventional

method. Therefore, it is more statistically representative. In addition, the column height was lowered to a range of 0.5 to 2 cm compared to the conventional range of 4 to 10 cm. Therefore, the penetration process was subjected, to a much less extent, to the effect of gravitational force.

The work needed to be done in future is to find the relationship between the tortuosity constant and various parameters such as particle shape and size distribution, column porosity, and packing density. In addition, the applicability of this technique to different combinations of liquids and materials should also be tested.

The quantitative comparison of the contact angle obtained for the same coal by the "column" method on the one hand, and by the "pellet" method on the other, is impossible because of the dependence of the contact angles on drop size. In addition, kerosene was used in the former method, and water in the latter one.

Since in the direct method, only those particles which form the pellet surface participate in the measurement, while all the particles in the column take part in affecting the penetration rate, the rate of penetration technique is statistically more reliable. The standard deviation of the contact angle values measured on the pellets ranges from 2.06 to 3.71 degrees corresponding to

the angle value of about 120 degrees. The relative measurement error is 1.7 - 3.1%. While the standard deviation of the slope values measured on the columns is 0.0003 to 0.013 corresponding to the slope values of 0.163 to 0.8246. The relative measurement error is 0.2 - 1.6%. Clearly, the measurement accuracy in the rate of penetration technique is higher.

CHAPTER 9

CONCLUSIONS

The direct contact angle measurements

a. On a heterogeneous coal surface, the contact angle measured by constructing a tangent to the drop profile at the three-phase contact line and the contact angle calculated through the whole drop profile are different. The former one reflects the contact angle on the higher surface energy area, while the latter one represents the average contact angle on the overall heterogeneous surface. The directly measured angle value is, on the average, five degrees lower than the one calculated from the same drop profile (Figure 6.2.1).

b. The contact angle on the pellet surface was found to depend on the drop size and the way the size of the drop was manipulated. The contact angle of a liquid on the solid does not necessarily increases with the size of the drop. It can also decrease when the drop size is enlarged by incremental additions.

c. The surface of a compressed coal pellet is glossy and macroscopically flat. However, the pellet is microscopically very porous both inside and on its surface. The surface porosity is characterized by the fractional area of pores. While the pellet bulk porosity can be experimentally measured, the surface porosity cannot. Under the assumption made in Section 6.8, the fractional area of pores is equal, in value, to the pellet bulk porosity. The pellet porosity is composed of two portions: intra-particle porosity which is the porosity inside an individual particle, and inter-particle porosity which is the porosity between particles; it is controlled by particle size, shape, and pellet-making pressure (Figures 6.7.1 and 6.7.2).

d. The contact angle measured directly on the surface of a compressed coal pellet is an apparent contact angle determined by solid and air. The pellet-making pressure influences the apparent contact angles via the fractional area of air pores on the pellet surface. This effect can be quantitatively corrected using the Cassie-Baxter equation to transform the apparent contact angle into the real angle value on the solid. For example in Figure 6.9.3, the contact angle values measured on the pellet surfaces of a -1.3 density fraction of the Line Creek coal range from 109 to 133

degrees depending on the pellet-making pressure. After correction, the contact angle value become 84.2 degrees.

e. It was found that a pellet-making pressure of lower than 27.6 MPa cannot result in the perceivable crushing of coal particles and, therefore, does not release new surfaces (and does not influence the applicability of this technique).

f. The reproducibility of the contact angle measured directly on the coal pellets as given by the standard deviation of the angle values ranges from 2.06 to 3.71 degrees. The deviation mainly resulted from the heterogeneity of the coal pellet surface. In the contact angle measurements on finely polished coal surfaces carried out by Vargha-Butler et al. <Vargha-Butler, Kashi, Hamza, and Neumann, 1986>, the confidence limit of the contact angle ranges from 0.5 to 4.2 degrees.

The rate of penetration method

a. The Washburn equation is well applicable to the highly compacted column made of fine coal. This is demonstrated by the linearity of the rate of

penetration relationship. The R squared (coefficient of multiple determination) values fall between 0.9992 and 1.0000. The linearity is very high.

b. It was found that when working with fine coal particles, the modified rate of penetration method gave better accuracy and reproducibility than that of the original method. The standard deviation of the penetration slope values ranges from 0.0003 to 0.013 corresponding to 0.163 to 0.8246 of the slope values.

c. The experimental accuracy and reproducibility also depend on the flatness of the penetration front within the column. The liquid penetration front in the highly compacted column was found very flat. The ruggedness which is the vertical distance between the highest point and the lowest point is lower than 0.06 cm for the columns 2.54 cm in diameter.

d. A column made under higher pressure experiences a greater swelling after penetration. The swelling for all the columns, however, was found to be so small (less than 0.71% relative), that it could be neglected.

e. The pressure is the most important factor in affecting the column properties and the penetration process. The physical properties of the column become more uniform

and reproducible under higher pressure. As the pressure increases, the penetration rate becomes smaller for the same solid-liquid system.

f. The tortuosity constant of a column is independent of the solid surface properties. Its value is given by particle shapes and size distribution, and by column-making pressure. For different materials possessing similar particle shapes and size distributions, the column tortuosity constants are only controlled by column-making pressure, provided that there is no particle deformation under the pressure applied. At identical column-making pressures, all these columns are characterized by the same tortuosity constants.

REFERENCES

Adam, N.K., and Jessop, G., (1925) "Angles of Contact and Polarity of Solid Surfaces", J. Chem. Soc., Vol.127, p.1863.

Adam, N.K., (1964) "The Chemical Structure of Solid Surfaces as Deduced From Contact Angle", Contact Angle - Wettability and Adhesion Advances in Chemistry Series 43, American Chemical Society, Washington, D.C. p.52.

Adams-Viola, M., Botsaris, G.D., and Glazman, Y.M., (1981) "An investigation of the hydrophilic/oleophilic nature of various coals", Colloids and Surfaces, Vol.3, p.159.

Baker, H.R., Shafrin, E.G., Zisman, W.A., (1952) "The adsorption of hydrophobic monolayers of carboxylic acids", J. Phys. Chem., Vol.56, p.405.

Bashforth, F. and Adams, J.C., (1892) "An Attempt to Test the Theory of Capillary Action", Cambridge Univ. Press and Deighton Bell & Co., Cambridge, 1892.

Berkowitz, N., (1985) The Chemistry of Coal - Coal Science and Technology 7, Elsevier Science Publishers, New York.

Bigelow, W.C., Pickett, D.L., and Zisman, W.A., (1946) "Oleophobic monolayers I. film adsorbed from solution in non-polar liquids", J. Colloid Sci., Vol.1, p.513.

Blake, P., and Ralston, J., (1985) "Controlled methylation of quartz particles", Colloid and Surfaces, Vol.15, p.101.

Blake, T.D., and Kitchener, J.A., (1972) "Stability of Aqueous Films on Hydrophobic Methylated Silica", J. Chem. Soc. Faraday Trans., I, Vol.68, p.1435.

Boyce, E., Schurch, S., Rotenberg, Y., and Neumann, A.W., (1984) "The measurement of surface and interfacial tension by the axisymmetric drop technique", Colloid and Surfaces, Vol.9, p.307

Bracke, M., De Bisschop, F., and Joos, P.,(1988) "Contact Angle Hysteresis due to Surface Roughness", Progr. in Colloid & Polym Sci., Vol.76, p.251.

Bruil, H.G., and van Aartsen, J.J., (1979) "The determination of Contact Angles of Aqueous Surfactant Solutions on Powder", Colloid and Polymer Sci., Vol.252, No.1, p.32.

Bartell, L.S., and Ruch, R.J., (1956) "The wetting of incomplete monomolecular layers", J. Phys. Chem., Vol.60, p.1231.

Cassie, A.B.D., and Baxter, S., (1944) "Wetting of Porous Surfaces", Trans. Faraday Soc., Vol.40, pp.546.

Cassie, A.B.D., (1948) Discussions Faraday Soc., 3, 11.

Cochrane, H., Hendriksen, B.A., Pearce, D.R., and Rudham, R., (1967) "Heat of Immersion γ- and β-alumina", in Wetting S.C.I. Monograph No.25., p.370.

Crawford, R., Koopal, L.K., and Ralston, J., (1987) "Contact Angles On Particles and Plates", Colloid and Surfaces,

Crowl, V.T., and Wooldridge, D.W.S, (1967) "A Method For the Measurement of Adhesion Tension of Liquids in Contact With Powders", Wetting -- S.C.I. Monograph No.25, Gordon and Breach Science Publishers, New York.

Derjaguin, B.V. and Dukhin, S.S., (1961) "Theory of flotation of small and medium size particles", Trans. Inst. Mining and Metallurgy, Vol.70, p.221.

Dettre, R.H., and Johnson, Jr., R.E.,(1964) "Contact angle hysteresis III. study of and idealized heterogeneous surface", J. Phys. Chem., Vol.68, p.1744.

Donahue, D.J., and Bartell, F.E., (1952) "The Boundary Tension at Water-Organic Liquid Interfaces", J. Phys. Chem., Vol.56, p.480.

Eick, J.D., Good, R.J., and Neumann, A.W., (1975) "Thermodynamics of Contact Angles I. Heterogeneous Solid Surfaces", J. Colloid and Interface Sci., Vol.53, p.235.

Eigeles, M.A., and Volva, M.L., (1960) "Kinetic Investigation of Effect of Contact Time, Temperature, and Surface Condition on the Adhesion of Bubble to Mineral Surfaces", Proceeding, 5th International Mineral Processing Congress, IMM, London, p.271.

Ely, D.D., and Pepper, D.C., (1946) "A dynamical determination of adhesion tension", Trans. Faraday Soc., Vol.42, p.697.

Fisher, L.R., and Lark, P.D., (1980) "The Effect of Adsorbed Water Vapour on Liquid Flow in Pyrex Glass Capillary Tubes", J. Colloid and Interface Sci., Vol.76, p.1.

Fox, H.W, and Zisman, W.A., (1950) "The spreading of liquid on low energy surfaces I. polytetrafluoroethylene", J. Colloid Sci., Vol.5, p.514.

Fuerstenau, D.W., and Williams, M., (1987) "Characterization of the lyophobicity of particles by film flotation", Colloid and Surfaces, Vol.22, p.87.

Fuerstenau, D.W., Yang, G.C.C., and Laskowski, J.S., (1986) "Oxidation Phenomena in Coal Flotation Part I", Coal Preparation, (J.S.Laskowski ed.), Vol.4, p.161.

Garshva, S., Contreras, S., and Goldfarb, J.,(1978) "Hydrophobic characterization of powder - some criteria and experimental evidence" Colloid and Polymer Sci., Vol.256, p.241.

Gaudin, A.M., (1957) Flotation, 2nd Ed., McGraw Hill, New York.

Gibbs, J.W., (1928) The Collected Works of J.Willard Gibbs, Vol.1, Thermodynamics, Yale University Press, New Heaven.

Glanville, J.O., Wightman, J.P., (1980) "Wetting of Powdered Coals by Alkanol-Water Solutions and Other Liquids", Fuel, Vol.59, p.557.

Good, R.J., (1973) "The Rate of Penetration of a Fluid Into a Porous Body Initially Devoid of Adsorbed Material", J. Colloid and Interface Sci., Vol.42, p.3.

Good, R.J., and Lin, N.J., (1976) "Rate of Penetration of a Porous Body", J. Colloid and Interface Sci., Vol.54, p.52.

Good, R.J., and Lin, N.J., (1976) in Proceedings of the 50th Colloid and Interface Science Symposium, Colloid and Interface Sci., (M.Kerker, Ed.), Vol.3, Academic Press, New York.

Good, R.J., (1979) "Contact Angle And Surface Free Energy of Solids", Surface And Colloid Sci., Vol.11, Plenum Press, New York.

Good, R.J., and Koo, M.N., (1979) "The Effect of Drop Size on Contact Angle", J. Colloid and Interface Sci., Vol.71, p.2.

Gutierrez-Rodrigues, J.A., Purcell Jr., R.J., and Aplan,

F.F., (1984) "Estimating the Hydrophobicity of Coal" Colloids and surfaces, Vol.12, p.1.

Gutierrez-Rodrigues, J.A., and Aplan, F.F., (1984) "The effect of oxygen on the hydrophobicity and floatability of coal", Colloid and Surfaces, Vol.12, p.27.

Harper, H.R., (1967) "Discussion", Wetting, S.C.I. Monograph No.25, Soc. Chem. Ind., London, p.209.

Hartland, S., and Paynter, H.M., (1981) J. Colloid Interface Sci., Vol.82, p.269.

Herzberg, W.J., and Marian, J.E., (1970) "Relationship Between Contact Angle and Drop Size", J. Colloid and Interface Sci., Vol.33, p.1.

Hornsby, T.D., and Leja, J., (1980) "Critical Surface Tension and Selective Separation of Inherently Hydrophobic Solids", Colloids and Surfaces, Vol.1, p.425.

Hornsby, T.D., and Leja, J., (1983) "Critical Surface Tension of Floatability", Colloid and Surfaces, Vol.1, p.339.

Hornsby, T.D., and Leja, J., (1984) "A Technique for Evaluating Floatability of Coal Fines, Using Methanol Solutions", Coal Preparation, (J.Laskowski, ed.), Vol.1, p.1.

Horsley, R.M., and Smith, H.G., (1951) "Principles of Coal Flotation", Fuel, Vol.30, p.54.

Huh, C., and Mason, S.G., (1974) "The Flotation of Axisymmetric Particles at Horizontal Liquid Interfaces", J. Colloid and Interface Sci., Vol.47, No.2, p.271.

Huh, C., and Mason, S.G., (1977) "Effect of Surface Roughness on Wetting (Theoretical)", J. Colloid and Interface Sci., Vol.60, p.11

Iskra, J., and Laskowski, J., (1967) "New Possibilities For Investigating Air-Oxidation of Coal Surface at Low Temperatures", Fuel, 46(1), p.5.

Jameson, G.J., Nam, S., and Young, M.M., (1977) "Physical Factors Affecting Recovery Rate in Flotation", Miner. Sci. Eng., Vol.9, No.3, p.103.

Jin, R., Ye, Y., Miller, J.D., and Hu, J.S., (1987) "Characterization of Coal Hydrophobicity by Contact Angle, Bubble Attachment Time and FTIR Spectroscopy",

116th AIME Annual Meeting, Preprint No.87-146, Denver, Colorado.

Johnson, Jr.,R.E. and Dettre, R.H., (1964) "Contact Angle Hysteresis I. Study of an Idealized Rough Surface", Contact Angle -- Wetting and Adhesion, American Chemical Society, Washington, D.C., p.112.

Johnson, Jr., R.E. and Dettre, R.H., (1964) "Contact angle hysteresis", J. Phys. Chem., Vol.68, p.1744.

Jonson, Jr. R.J., and Dettre, R.H., (1969) "Wettability and Contact Angles", Surface and Colloid Sci., Vol.2, (E.Matijevic and F.R.Eirich, eds.), Plenum Press, New York.

Kelebek, S., (1980) "Surface Chemistry of Coal Flotation Systems", M.Eng. Thesis.

Kelebek, S., and Smith, G.W., (1985) "Selective Flotation of Inherently Hydrophobic Minerals by Controlling the Air/Solution Interfacial Tension", J. Inst. Mineral Process., Vol.14, p.275.

Kelebek, S., and Smith, G.W., (1987) "Wetting Behaviour, Polar Characteristics and Flotation of Inherently Hydrophobic Minerals", Trans. Inst. Mining and Metall. (sec. C), Vol.96, p.103.

Keller, Jr. D.V., and Burry, W., (1987) "An investigation of a separation process involving liquid-water-coal system", Colloid and Surfaces, Vol.22, p.37.

Kneen, E., and Benton, W.W., (1937) "A simplified technique for determination of contact angles and its application to studies on wetting", J. Phys. Chem., Vol.41, p.1195.

Kossen, N.W.F., and Heertjes, P.M., (1965) Chem. Eng. Sci., Vol.20, p.593.

Laskowski, J.S., (1965) "The Flotation of Naturally Hydrophobic Minerals in Solutions With a Raised Concentration of Inorganic Salts", Colliery Guardian, Sept. 17, 1965, p.361.

Laskowski, J.S., and Kitchener, J.A.,(1969) " The hydrophilic-hydrophobic transition on silica", J. Colloid and Interface Sci., Vol.29, p.670.

Laskowski, J.S., and Iskra, J., (1970) "Role of Capillary Effects in Bubble-Particle Collision in Flotation", Trans. Inst. Min. Metall. (sec. C), Vol.79, p.6.

Laskowski, J.S., (1974) "Particle-bubble attachment in

flotation", Minerals Sci. and Engineering, Vol.6, No.4, p.223.

Laskowski, J.S., (1986) "Flotation of Difficult-to-float Coals", 10th International Coal Preparation Congress, Canada.

Leja, J., and Poling, G.W., (1960) "On the interpretation of contact angle", in Proceeding of the International Mineral Processing Congress, Inst. Mining & Metallurgy, London.

Lekki, J., and Laskowski, J., (1970) "On the Dynamic Effect of Frother-Collector Joint Action in Flotation", Trans. Inst. Min. Metall. (Sec. C), Vol.83, No.3, p.174.

Levine, O., and Zisman, W.A., (1954) "Hydrophobic Monolayer and Their Adsorption From Aqueous Solutions", Monomolecular Layers, American Assoc. Advance Sci., Washington, D.C.

Mack, G.L., (1936) "The Determination of Contact Angle from Measurements of the Dimensions of Small Bubbles and Drops I. The spheroidal Segment Method for Acute Angles" J. Phys. Chem., Vol.40, p.159.

Malcolm, J.D., and Paynter, H.M., (1981) "Simultaneous determinations of contact angle and interfacial tension from sessile drop measurement", J. Colloid Interface Sci., Vol.82, p.269.

Mraw, S.C., De Neufville, J.P., Freund, H., Baset, Z., Gorbaty, M.L., and Wright, F.J., (1983) "The Science of Mineral Matter in Coal", Coal Science, (Gorbaty, M.L., Larsen, J.W., and Wender, I., Eds.), Vol.2, p.1.

Neumann, A.W., Renzow, D., Reumuth, H., and Richter, I.E., (1971) Fortschr. Kolloide Polym., Vol.55, p.49.

Neumann, A.W., and Good, R.J., (1972) "Thermodynamics of Contact Angles I. Heterogeneous Solid Surfaces", J. Colloid & Interface Sci., Vol.38, p.341.

Neumann, A.W., and Good, R.J., (1979) "Techniques of Measuring Contact Angles", Surface and Colloid Sci., (R.J.Good and R.R Stromberg eds.), Vol.11, Plenum Press, New York.

Oliver, J.F., Huh, C., and Mason, S.G., (1980) An Experimental Study of Some Effects of Solid Surface Roughness on Wetting", Colloids and Surfaces, Vol.1, p.79.

Paddy, J.F. (Ed.), (1978) Wetting, Spreading, And Adhesion,

Academic Press, London.

Painter, P.C., Starsinic, M., Squires, E., and Davis, A.A., (1983) "Concerning the 1600 cm^{-1} region in the i.r. spectrum of coal", Fuel, Vol.62, p.742.

Parekh, B.K., and Aplan, F.F., (1978) "The Critical Surface Tension of Wetting of Coal" Recent Development in Separation Science, Vol.4 (N.N. Li, ed.), CRC Press, West Palm Beach, Fla., p.107.

Pease, D.C., (1950) "Sliding of drops from surface of different roughness", J. Colloid Sci. Vol.5, p.349.

Reay, D., and Ratcliff, G.A., (1973) "Removal of Fine Particles From Water by Dispersed Air Flotation: Effect of Bubble Size and Particle Size on Collection Efficiency", Can. J. Chem. Eng., Vol.51, p.178.

Rotenberg, Y., Boruvka, L., and Nuemann, A.W., (1983) "Determination of Surface Tension and Contact Angle from the Shapes of Axisymmetric Fluid Interfaces", J. Colloid and Interface Sci., Vol.93, No.1, p.169.

Shafrin, E.G., and Zisman, W.A., (1952) "The spreading of liquid on low energy surfaces IV. monolayer coatings on platinum", J Colloid Sci., Vol.7, p.166.

Shuttleworth, R., and Bailey, G.L.J., (1948) Discuss Faraday Soc., Vol.3, p.16.

Stach, E., (1982) Stach's Text Book of Coal Petrology, 3rd ed., Gebruder Borntraeger, Berlin.

Studerbaker, M.L., and Snow, C.W., (1955) "The Influence of Ultimate Composition Upon the Wettability of Carbon Blakes", J. Phys. Chem., Ithaca, Vol.59, p.973.

Sun, S.C., (1954) "Hypothesis for Different Floatabilities of Coals, Carbons and Hydro-carbon Minerals", Trans. AIME, Vol.199, p.67.

Sven-Nillson, (1934) "Effect of Contact Time Between Mineral and Air on Flotation", Kolloid Z., Vol.69, p.230

Szekely, J., Neumann, A.W., and Chuang, Y.K., (1971) "The Rate of Capillary Penetration and the Application of the Washburn Equation", J. Colloid and Interface Sci., Vol.35, No.2, p.273.

Taylor, J.A.G., (1967) "The Dependence of Heats of Immersion of Inorganic Oxides on the Surface Parameters", in Wetting S.C.I. Monograph No.25, p.380.

Tomlinson, J.S., and Fleming, M.G., (1963) "Flotation Rate Studies", in Proc. 6th Int. Miner. Process. Cong., (A.Roberts ed.), Cannes, p.563.

Vargha-Butler, E.I., Kashi, M., Hamaza, H.A., and Nuemann, A.W., (1986) "Direct Contact Angle Measurements on Polished Sections of Coal", Coal Preparation, (J.Laskowski, ed.) Vol.3, p.53.

Vargha-Butler, E.I., Absolom, D.R., Nuemann, A.W., and Hamza, H.A., (1989) "Characterization of Coal by Contact Angle and Surface Tension Measurements", Interfacial Phenomena in Coal Technology, (G.D.Botsaris and Y.M.Glazman eds.), Marcel Dekker, Inc., New York.

Walker, Jr., P.L., Petersen, E.E., and Wright, C.C., (1952) "Surface active agent phenomena in dust abatement" Industrial and Engng. Chem., Vol.44, No.10, p.2389.

Washburn, E.W., (1921) "The dynamics of capillary flow", Phys. Rev., Vol.17, p.374.

Wenzel, R.N., (1936) "Resistance of Solid Surfaces to Wetting by Water", Industrial Engng. Chem., Vol.28, p.288.

White, L.R., (1982) "Capillary Rise in Powder", J. Colloid and Interface Sci., Vol.90, p.2.

Winans, R.E., and Crelling, J.C., (1984) "Chemistry and Characterization of Coal Macerals: Overview", Chemistry and Characterization of Coal Macerals, American Chemical Society, Washington, D.C.

Wiser, W., (1975) Preprints Fuel Division Am. Chem. Soc. Meeting, Vol.20, No.2, p.122.

Yarar, B., and Leja, J., (1982) "Flotation of Weathered Coal Fines From Western Canada", IX International Coal Preparation Congress, New Dehli.

Ye, Y., Jin, R., and Miller, J.D., (1986) "Thermal Treatment of Low-rank Coal and Its Relationship to Flotation Response", in Proceeding of the 14th Biennial Lignite Symposium on Technology and Utilization of Low-rank Coal.

Yoon, R.H. and Sabey, J.B., (1989) "Coal Flotation in Inorganic Salt Solution", Interfacial Phenomena in Coal Technology - Surfactant Sci. Series, Vol.32, (G.D.Botsaris and Y.M.Glazman, eds.), Marcel Dekker, Inc. New York.

Yordan, J.L., and Yoon, R.H., (1986) "Induction Time Measurements for the Quartz-amine Flotation System", SME-AIME Annual Meeting, New Orleans, Louisiana, Preprint p.86.

Yordan, J.L., and Yoon, R.H., (1988) Interfacial Phenomena in Biotechnology and Materials Processing, (Y.A.Attia, B.M.Moudgil and S.Chander, eds.), Elservier Science Publisher.

Young, T., (1855) Miscellaneous Works, (G.Peacock, Ed.), Vol.1, J.Murray, London

Yuh, S.J., and Wolf, E.E., (1983) "FTIR studies of potassium catalyst-treated gasified coal chars and carbons", Fuel, Vol.62, p.252.

Yuh, S.J., and Wolf, E.E., (1984) "Kinetic and FT-i.r. studies of the sodium-catalyzed steam gasification of coal chars", Fuel, Vol.63, p.1065.

Zettlemoyer, A.C., and Chessick, J.J., (1964) "Wettability by Heat of Immersion", Contact Angle - Wettability and Adhesion, (R.F.Could ed.), American Chem. Soc., Washington, D.C., p.88.

Zettlemoyer, A.C., (1965) "Immersional Wetting of Solid Surface", Ind. and Engng. Chem., Vol.57, No.2, p.27.

Zisman, W.A., (1964) "Relation of Equilibrium Contact Angle to Liquid and Solid Constitution", Contact Angle - Wettability and Adhesion, American Chemical Society Applied Publication, Washington, D.C.

APPENDIX 1 A FLOWSHEET FOR SIMPLEX SEARCH PROGRAM

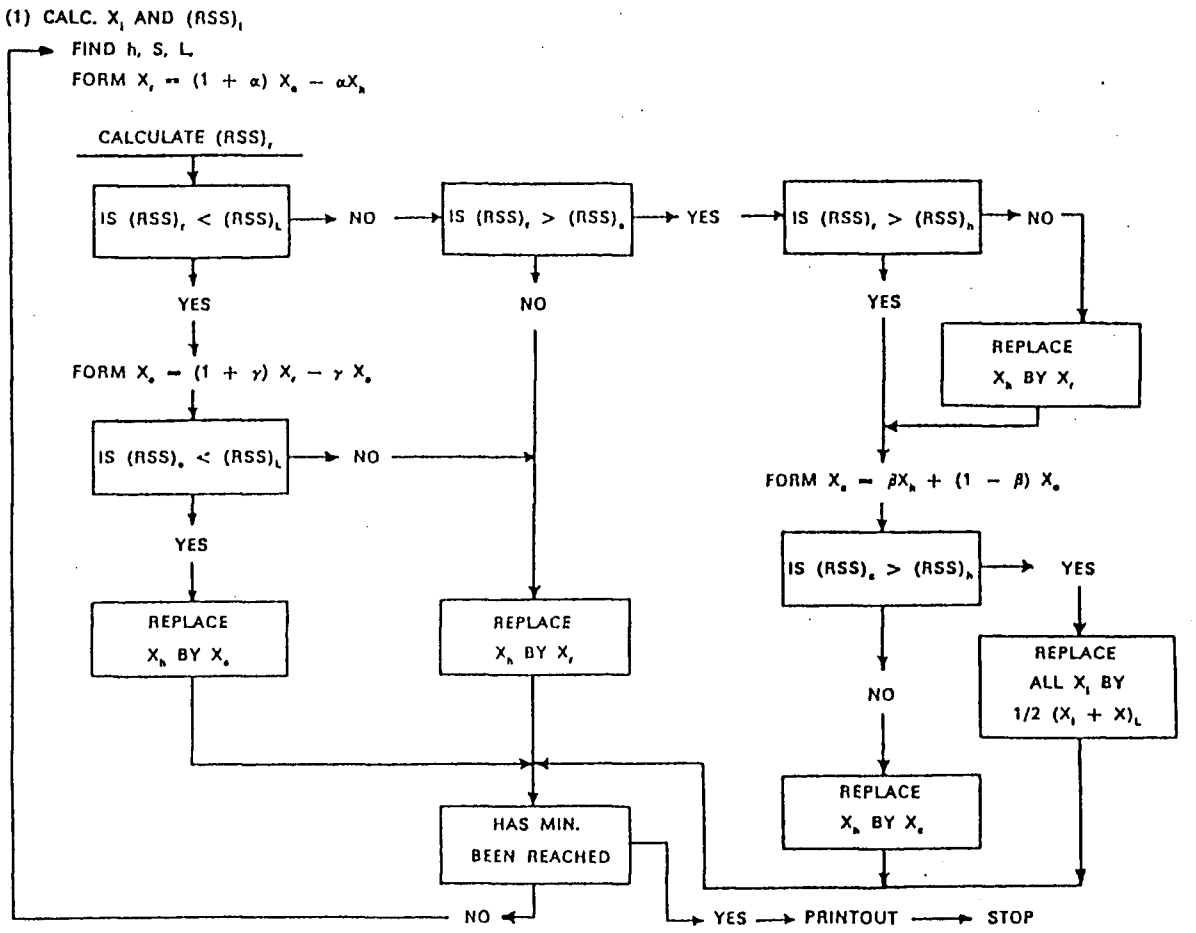

APPENDIX 2 Contact Angle Calculation Program

```
*****************************************************************
*                                                               *
*                                                               *
*              CONTACT ANGLE CALCULATION PROGRAM                *
*                                                               *
*                                                               *
*****************************************************************


*  This is a program writen in  FORTRAN for the contact angle
*  result calculation. It uses simplex optimization technique
*  to search the best values of unknown variables in the  set
*  of redundant equations.


*                     TABLE OF PARAMETERS


*    N -- the number of search variables
*    Z9 -- the subroutine computation cycle times
*    RSS and Y(I) -- the Residule Sum of Squares  I=1 to N+1
*    H -- the point on the simplex where RSS is the highest
*    S -- the point on the simplex where RSS is the second
*         highest
*    L -- the point on the simplex where RSS is the lowest
*    A -- the reflection coefficient
*    V -- the expansion coefficient
*    B -- the contraction coefficient
*    SL(I,J) -- SLope values actually measured.
*    SP(I,J) -- Slope values Predicted accoding to the equations
*           I -- the number of density fractions
*           J -- the number of column-making pressures used
*    X(I,J) -- the simplex matrix -- I=1 to N+1 and J=1 to N
*    GAMA -- the liquid surface tension
*    MU -- liquid viscosity
*    COS -- a transit variable
```

```
      INTEGER N, Z9, H, L, S
      REAL T,T1,T2,T3,C2,RSS,A,V,B, GAMA,MU,COS, N2
      DIMENSION D(9),C(9),X(10,9),Z(9),Y(10),Q(9),
     +          SL(6,3),SP(6,3),THETA(6)
      OPEN (UNIT=12, FILE='SLOPE.DAT', STATUS='OLD')
      OPEN (UNIT=13, FILE='ANGLE.DAT', STATUS='NEW')
      READ (12, *) (SL(I,1), I=1, 6)
      READ (12, *) (SL(I,2), I=1, 6)
      READ (12, *) (SL(I,3), I=1, 6)


      GAMA=27.36
      MU=0.01715


      N=9
      A=1.
      V=2.
      B=.5



*****************************************************************
*   Set up initial simplex -- Calculate and set up the start  *
*         values of search variables    C(I)  I=1 TO 9        *
*****************************************************************


      N2=1.1340000032
      N2=2.
      C(1)=0.000013535*N2
      C(2)=0.000010450*N2
      C(3)=0.000008691*N2
      C(4)=903.04/N2
      C(5)=767.68/N2
      C(6)=564.63/N2
      C(7)=513.84/N2
      C(8)=410.68/N2
      C(9)=200.88/N2
      DO 30 J=1,N
      D(J)=0.1*C(J)
30    CONTINUE
      DO 31 J=1, N
      DO 32 I=1, N+1
      X(I, J)=C(J)-(2./(J+1))*D(J)
      IF(I.EQ.(J+1)) GO TO 33
32    CONTINUE
33    X(I, J)=C(J)+((2./(J+1))*D(J))*J
      DO 34 I=J+2, N+1
      X(I, J)=C(J)
```

```
34      CONTINUE
31      CONTINUE



*****************************************************************
*      Calculate the standard error of objective function       *
*****************************************************************


        Z9=0
        T3=1.E9


*  Calculate the residual sum of (RSS)i

101     DO 70 K=1, N+1
        H=K
        CALL SUBRSS(N, X, H, RSS, Z9, SL, SP)
        Y(K)=RSS
70      CONTINUE


*  To find out the H, L, S

91      CALL SUBLHS(Y, N, H, L, S, RSSH, RSSL, RSSS)
        T1=0.
        T2=0.
        DO 92 I=1, N+1
        T1=T1+Y(I)
92      CONTINUE
        DO 93 I=1, N+1
        T2=T2+(Y(I)-T1/(N+1))**2
93      CONTINUE
        T=SQRT(T2/N)



*****************************************************************
*     Judge minimum or cycle mnumber being rearched or not      *
*****************************************************************


        IF (T.LT.1.E-10.OR.Z9.GT.500) GO TO 81
        IF (T.GT.T3) GO TO 41
        T3=T
```

```
*****************************************************************
*                    Reflection    Xr=(1+A)Xo-AXh                 *
*****************************************************************

41      DO 43 J=1, N
        P=0
        DO 42 I=1, N+1
        IF(I.EQ.H) GO TO 42
        P=P+X(I, J)/N
42      CONTINUE
        Q(J)=X(H, J)
        Z(J)=(1.+A)*P-A*X(H, J)
        X(H, J)=Z(J)
        D(J)=P
43      CONTINUE


 *  Calculate (RSS)r

        CALL SUBRSS(N, X, H, RSS, Z9, SL, SP)
        R=RSS
        IF(RSS.LT.Y(L)) GO TO 71
        IF(RSS.LT.Y(S)) GO TO 91
        IF(RSS.LT.Y(H)) THEN
        Y(H)=RSS
        GO TO 51
        ELSE
        DO 88 J=1, N
        X(H, J)=Q(J)
88      CONTINUE
        ENDIF



*****************************************************************
*       Contration   Xc=BXh+(1-B)*Xo, Replacement of Xh by Xc   *
*****************************************************************


51      J=0
        DO 52 J=1, N
        Q(J)=X(H, J)
        X(H, J)=B*X(H, J)+(1.-B)*D(J)
52      CONTINUE


*   Calculate (RSS)c
```

```
      CALL SUBRSS(N, X, H, RSS, Z9, SL, SP)
      IF(RSS.GT.Y(H)) GO TO 55
      Y(H)=RSS
      GO TO 91



**********************************************************************
*                    Reduce the size of simplex                      *
**********************************************************************

55    I=0
      J=0
      DO 57 J=1, N
      X(H, J)=Q(J)
      DO 56 I=1, N+1
      X(I, J)=(X(I, J)+X(L, J))/2
56    CONTINUE
57    CONTINUE
      GO TO 101


*  Replace Xh by Xr

25    J=0
      DO 26 J=1, N
      X(H, J)=Z(J)
26    CONTINUE
      Y(H)=R
      GO TO 91



**********************************************************************
*Expansion, Xe=(1+v)*Z(1, J)-v*D(1, J), replacement of Xh by Xe*
**********************************************************************


71    J=0
      DO 72 J=1, N
      X(H, J)=(1.+V)*Z(J)-V*D(J)
72    CONTINUE


*  Calculate (RSS)e

      CALL SUBRSS(N, X, H, RSS, Z9, SL, SP)
      IF(RSS.GT.Y(L)) GOTO 25
      Y(H)=RSS
      GO TO 91
```

```
*****************************************************************
*                      Contact Angle Calculation                *
*                  d(HxH)/dT = K.Gama.Cos(Theta)/(2.Mu)         *
*****************************************************************

81      COS=GAMA/2./MU
        DO 5 I=1, 6
        THETA(I)=X(L,I+3)/COS
        IF(THETA(I).LE.1.0) THEN
        THETA(I)=ACOS(THETA(I))*180./3.1416
        ELSE
        THETA(I)=0.0
        ENDIF
5       CONTINUE



*****************************************************************
*                        Print out the result                   *
*****************************************************************


        PRINT *
        WRITE(13, 78)
78      FORMAT(5X, 5HCYCL., 1X, 5HTIMES)
        WRITE(13, 77) Z9
77      FORMAT(5X, I5)
        WRITE(13, *)
        WRITE(13, 2)
2       FORMAT(5X, 3HT3=, 16X, 2HT=)
        WRITE(13, 3) T3, T
3       FORMAT(5X, 2E13.5)
        WRITE(13, *)


        WRITE(13, 124)
124     FORMAT(5X, 35HTHE TORTUOSITY CONSTANTS K1, K2, K3)
        WRITE(13, 120) (X(L,I), I=1,3)
120     FORMAT(5X, 3F16.9)
        WRITE(13, *)


        WRITE(13, 125)
125     FORMAT(5X, 38HTHE X VALUES FOR SIX DENSITY FRACTIONS)
        WRITE(13, 126) (X(L,I), I=4, 9)
126     FORMAT(5X, 6F9.2)
        WRITE(13, *)
```

```
      WRITE(13, 129)
129   FORMAT(5X, 39HCONTACT ANGLES ON SIX DENSITY RFACTIONS)
      WRITE(13,128) (THETA(I), I=1, 6)
128   FORMAT(5X, 6F9.2)
      WRITE(13, *)


      WRITE(13, 127)
127   FORMAT(7X, 8HMEASURED, 4X, 10HCALCULATED, 3X,
     +       10HDIFFERENCE, 5X, 9HRELATIVE%)
      WRITE(13, *)
      DO 123 J=1, 3
      DO 122 I=1, 6
      WRITE(13, 121) SL(I,J), SP(I,J), SL(I,J)-SP(I,J),
     +        (SL(I,J)-SP(I,J))/SL(I,J)*100.
121   FORMAT(1X, 4F13.5)
122   CONTINUE
      WRITE(13, *)
      WRITE(13, *)
123   CONTINUE
      STOP
      END
```

```
**********************************************************************
*                          SUBROUTINE I                              *
*        This subroutine is used for calculating (RSS)               *
**********************************************************************


      SUBROUTINE SUBRSS(N, X, H, RSS, Z9, SL, SP)
      INTEGER  H, Z9, I, J
      REAL C2, RSS, X(N+1, N), SL(6,3), SP(6,3)


*   Calculate the predicted values

      DO 2 J=1, 3
      DO 4 I=1, 6
      SP(I,J)=X(H,J)*X(H,3+I)
4     CONTINUE
2     CONTINUE


*   Calculate the residual sum of squares
```

```
      C2=0
      DO 6 J=1, 3
      DO 8 I=1, 6
      C2=C2+(SL(I,J)-SP(I,J))**2/SL(I,J)**2
8     CONTINUE
6     CONTINUE
      RSS=C2
      Z9=Z9+1
      RETURN
      END



*****************************************************************
*                          SUBROUTINE II                        *
*          The subroutine for finding out   H, L, S             *
*****************************************************************

      SUBROUTINE SUBLHS(Y, N, H, L, S, RSSH, RSSL, RSSS )
      REAL Y(N+1), RSSH, RSSL, RSSS
      INTEGER L, H, S
      H=1
      S=1
      L=1
      DO 21 I=2, N+1
      IF(Y(I).GT.Y(H)) THEN
      H=I
      ELSE
      IF(Y(I).LT.Y(L)) THEN
      L=I
      ELSE
      ENDIF
      ENDIF
21    CONTINUE
      RSSH=Y(H)
      RSSL=Y(L)
      Y(H)=0.
      DO 23 I=2, N+1
      IF(Y(I).GT.Y(S)) THEN
      S=I
      ELSE
      ENDIF
23    CONTINUE
      Y(H)=RSSH
      RETURN
      END
```